

POLITECNICO DI TORINO

in collaborazione con

CRANFIELD UNIVERSITY



Dipartimento di ingegneria strutturale, edile e geotecnica

TESI DI LAUREA MAGISTRALE IN INGEGNERIA CIVILE

“Damage localisation in pultruded materials based on
experimental modal analysis”

Relatori:

Prof. Rosario Ceravolo

Ing. Luca Zanotti Fragonara

Candidato:

Pier Paolo Cosentino

Anno accademico 2017/2018

INDEX

1	Introduction	1
2	Literature review.....	2
2.1	Structural pultruded materials	2
2.2	Experimental modal analysis.....	4
2.3	Modal Identification	4
2.3.1	General analytical formulation of identification methods.....	5
2.3.2	Identification methods with unknown input.....	7
2.3.2.1	Eigensystem Realization Algorithm (ERA).....	7
3	Methods	11
3.1	Curvature method	11
3.1.1	Analytical Model	11
3.1.2	Analysys of results	13
3.1.3	Numerical result	14
3.2	Treed Gaussian Process (TGP).....	20
3.2.1	Gaussian Process (GP)	20
3.2.2	Crack Detection	22
3.2.3	Algorithm TGP	23
3.3	Piecewise Cubic Hermite Interpolating Polynimial (pchip).....	25
4	Finite Element Model	27
5	Results	30
5.1	Dynamic tests	30
5.1.1	Data processing	31
5.1.2	Identification: ERA method.....	33
5.1.3	Mode Shapes	35
5.1.4	Curvature mode shapes.....	37

5.2	FEM.....	38
5.2.1	Pre-processor	38
5.2.2	Post-Processor	41
5.3	Curvature method on analytic models	52
5.4	Treed Gaussian Process	59
5.4.1	Analytical data.....	59
5.4.2	Experimental data.....	69
6	Conclusion.....	73
	Bibliografia.....	74
	Ansys code.....	76

INDEX OF FIGURES

Fig. 1 Pultrusion process [Wikipedia].	2
Fig. 2 Pultruded material profiles.	3
Fig. 3 Cantilever beam model. (a) Finite element model; (b) cross-section of the cantilever [6].	12
Fig. 4 Simply supported beam model. (a) Finite element model; (b) cross-section of the simply supported beam [6].	12
Fig. 5 Displacement mode shapes for intact cantilever [6].	14
Fig. 6 Curvature mode shapes for the intact cantilever [6].	15
Fig. 7 Absolute difference between the curvature mode shapes for the intact and the damaged cantilever [6].	16
Fig. 8 Absolute difference between displacement mode shapes for the intact and the damaged cantilever [6].	16
Fig. 9 Example of pchip and spline interpolation on sample points [MatLab manual].	25
Fig. 10 Example of pchip and spline interpolation on oscillatory sample points [MatLab manual].	26
Fig. 11 Shell281 [ANSYS manual].	27
Fig. 12 Accelerometer and impact hammer positioning in y direction.	30
Fig. 13 Accelerometer and impact hammer positioning in x direction.	30
Fig. 14 Photos 1 of the experiment in the laboratory	31
Fig. 15 Photos 2 of the experiment in the laboratory	31
Fig. 16 Original signals, before the cut-off.	32
Fig. 17 Signals after the cut-off.	32
Fig. 18 Fourier transform of signals.	32
Fig. 19 Stabilisation diagram: Frequency – Model order.	33
Fig. 20 Stabilisation diagram: Frequency – Damping	34
Fig. 21 First mode shape of experimental data.	35
Fig. 22 Second mode shape of experimental data.	36
Fig. 23 Third mode shape of experimental data.	36
Fig. 24 Fourth mode shape of experimental data.	36
Fig. 25 Experimental curvature mode shape.	37
Fig. 26 Model of intact beam from Ansys.	40

Fig. 27 Damaged beam from Ansys.	40
Fig. 28 Intact beam: mode shape 1 from Ansys.	41
Fig. 29 Intact beam: mode shape 2 from Ansy.	42
Fig. 30 Intact beam: mode shape 3 from Ansys.	42
Fig. 31 Intact beam: mode shape 4 from Ansys.	43
Fig. 32 Damaged beam with crack of 1 mm: mode shape 1 from Ansys.	43
Fig. 33 Damaged beam with crack of 1 mm: mode shape 2 from Ansys.	44
Fig. 34 Damaged beam with crack of 1 mm: mode shape 3 from Ansys.	44
Fig. 35 Damaged beam with crack of 1 mm: mode shape 4 from Ansys.	45
Fig. 36 Damaged beam with crack of 10 mm: mode shape 1 from Ansys.	45
Fig. 37 Damaged beam with crack of 10 mm: mode shape 2 from Ansys.	46
Fig. 38 Damaged beam with crack of 10 mm: mode shape 3 from Ansys.	46
Fig. 39 Damaged beam with crack of 10 mm: mode shape 4 from Ansys.	47
Fig. 40 Damaged beam with crack of 25 mm: mode shape 1 from Ansys.	47
Fig. 41 Damaged beam with crack of 25 mm: mode shape 2 from Ansys.	48
Fig. 42 Damaged beam with crack of 25 mm: mode shape 3 from Ansys.	48
Fig. 43 Damaged beam with crack of 25 mm: mode shape 4 from Ansys.	49
Fig. 44 Damaged beam with crack of 50 mm: mode shape 1 from Ansys.	49
Fig. 45 Damaged beam with crack of 50 mm: mode shape 2 from Ansys.	50
Fig. 46 Damaged beam with crack of 50 mm: mode shape 3 from Ansys.	50
Fig. 47 Damaged beam with crack of 50 mm: mode shape 4 from Ansys.	51
Fig. 48 Curvature Mode Shapes: intact beam.	52
Fig. 49 Curvature Mode Shapes: damaged beam with crack of 1 mm.	53
Fig. 50 Curvature Mode Shapes: damaged beam with crack of 10 mm.	53
Fig. 51 Curvature Mode Shapes: damaged beam with crack of 25 mm.	54
Fig. 52 Curvature Mode Shapes: damaged beam with crack of 50 mm.	54
Fig. 53 Plot 3D: differences in curvatures for cracked beam model with crack of 1 mm. ...	55
Fig. 54 Differences in curvatures for cracked beam model with crack of 1 mm.	55
Fig. 55 Plot 3D: differences in curvatures for cracked beam model with crack of 10 mm. ...	56
Fig. 56 Differences in curvatures for cracked beam model with crack of 10 mm.	56
Fig. 57 Plot 3D: differences in curvatures for cracked beam model with crack of 25 mm. ...	57
Fig. 58 Differences in curvatures for cracked beam model with crack of 25 mm.	57
Fig. 59 Plot 3D: differences in curvatures for cracked beam model with crack of 50 mm. ...	58
Fig. 60 Differences in curvatures for cracked beam model with crack of 1 mm.	58

Fig. 61 Cycle – Crack detection, Crack 1 mm, mode-shape1-std1.	60
Fig. 62 Cycle – Crack detection, Crack 1 mm, mode-shape1-std3.	61
Fig. 63 First result of 50 cycles; Crack 1 mm;	61
Fig. 64 First result of 50 cycles; Crack 1 mm;	61
Fig. 65 Cycle – Crack detection, Crack 1 mm,	62
Fig. 66 Cycle – Crack detection, Crack 1 mm,	62
Fig. 67 First result of 50 cycles; Crack 1 mm;	62
Fig. 68 First result of 50 cycles; Crack 1 mm;	62
Fig. 69 Cycle – Crack detection, Crack 1 mm,	63
Fig. 70 Cycle – Crack detection, Crack 1 mm,	63
Fig. 71 First result of 50 cycles; Crack 1 mm;	63
Fig. 72 First result of 50 cycles; Crack 1 mm;	63
Fig. 73 Cycle – Crack detection, Crack 1 mm,	64
Fig. 74 Cycle – Crack detection, Crack 1 mm,	64
Fig. 75 First result of 50 cycles; Crack 1 mm;	64
Fig. 76 First result of 50 cycles; Crack 1 mm;	64
Fig. 77 Cycle – Crack detection, Crack 50 mm,	65
Fig. 78 Cycle – Crack detection, Crack 50 mm,	65
Fig. 79 First result of 50 cycles; Crack 50 mm;	65
Fig. 80 First result of 50 cycles; Crack 50 mm; mode-shape1-std3.....	65
Fig. 81 Cycle – Crack detection, Crack 50 mm,	66
Fig. 82 Cycle – Crack detection, Crack 50 mm,	66
Fig. 83 First result of 50 cycles; Crack 50 mm;	66
Fig. 84 First result of 50 cycles; Crack 50 mm;	66
Fig. 85 Cycle – Crack detection, Crack 50 mm,	67
Fig. 86 Cycle – Crack detection, Crack 50 mm,	67
Fig. 87 First result of 50 cycles; Crack 50 mm;	67
Fig. 88 First result of 50 cycles; Crack 50 mm;	67
Fig. 89 Cycle – Crack detection, Crack 50 mm,	68
Fig. 90 Cycle – Crack detection, Crack 50 mm,	68
Fig. 91 First result of 50 cycles; Crack 50 mm;	68
Fig. 92 First result of 50 cycles; Crack 50 mm;	68
Fig. 93 Experimental mode shapes using pchip interpolation.....	69
Fig. 94 Experimental curvature mode shapes using pchip interpolation.....	70

Fig. 95 First result of 50 cycles; Experimental data:.....	70
Fig. 96 Cycle – Crack detection, experimental data:.....	70
Fig. 97 Cycle – Crack detection, experimental data:.....	71
Fig. 98 First result of 50 cycles; Experimental data:.....	71
Fig. 99 First result of 50 cycles; Experimental data:.....	71
Fig. 100 Cycle – Crack detection, experimental data:.....	71
Fig. 101 Cycle – Crack detection, experimental data:.....	72
Fig. 102 First result of 50 cycles; Experimental data:.....	72

INDEX OF TABLES

Table 1 Mechanical and physical properties of pultruded GFRP material.....	3
Table 2 Natural frequencies for the intact cantilever and the cantilever damaged [6].....	14
Table 3 MAC values for the intact and damaged displacement mode shapes for the cantilever [6].	15
Table 4 COMAC values for the intact and the damaged displacement mode shape for the cantilever [6].....	15
Table 5 Natural frequencies for the intact and damaged simply supported beam [6].....	17
Table 6 Curvature (or displacement) mode shapes for the simply supported beam [6].....	17
Table 7 Absolute difference between the curvature mode shapes for the intact and the damaged simply supported beam [6].....	18
Table 8 Absolute difference between the displacement mode shapes for the intact and the damaged simply supported beam [6].....	18
Table 9 Identification matrix form.	35
Table 10 Information on parameters.	38
Table 11 Structural detail: example of triangular crack.	39
Table 12 Material properties input data.....	39
Table 13 Standard deviation values.....	59
Table 14 Summary table of modal analyses.....	60

1 INTRODUCTION

The damage localisation has always been a topic of interest in the area of research, especially in recent decades, as well as the use of innovative materials in the world of civil construction. In this thesis, the two topics are covered together using different methodologies.

The object of the work is a simply supported beam made of pultruded material, i.e. resin and fibre of glass, on which dynamic tests are carried out by exciting the structure with a hammer and recording the displacements by means of sensors. After the distances between the accelerometers and the impact positions of the hammer have been determined, the test is carried out. Once all the information has been acquired, data processing is performed, obtaining frequencies and modal shapes for the first four modes of vibrating. Modal shapes are in turn analysed using the Treed Gaussian Process (TGP) to identify and locate the crack.

The TGP is a statistical method based on the regression of Gaussian processes. Gaussian Processes (GP) are the extension from the distribution of scalar values to functions; in other words, through Gaussian Processes a function is obtained in which every point represents a probability function. The TGPs use Gaussian Processes, but interpolation is not done on the whole domain; the latter is divided into two parts, obtaining two interpolating functions. At the next step each individual part of the domain could be divided into two other parts and so on. The points that divide the domain are points in which there is a local variation of the function. In this case, will be due to the presence of a crack.

Parallel to the experimental data, four models of cracked beams are created by means of FEM on which dynamic parameters and modal shapes are determined. This is done as a support, to compare the results with the experimental ones. The FEM models differ according to the size of the crack: 1, 10, 25 and 50 millimetres. The position of the crack is inserted at the position of 3.65 m from the origin of the beam; this choice is completely arbitrary. Once the modal analysis is performed, the first four modal shapes are analyzed through Treed Gaussian Process. To locate the crack, on FEM models, the "curvature method" is also applied: it identifies the position of the crack making a difference between the curvatures of the cracked and intact model.

The objective of the work is to understand whether a TGP analysis can detect a possible crack position on the real beam.

2 LITERATURE REVIEW

2.1 Structural pultruded materials

Pultruded materials consist of the combination of two different materials: glass fibers and polymer resin (GFRP Glass Fiber Reinforced Polymers). To create this kind of composite material, the glass fibers are impregnated with polymer resin and they are pulled through a heated die where polymerization takes place. Then the reinforcement is pulled through a bath. When the material comes out of the oven, it is transported up to a cutting area where it is appropriately cut by blades that size it [1]. Pultrusion process can be simplified in the following diagram:

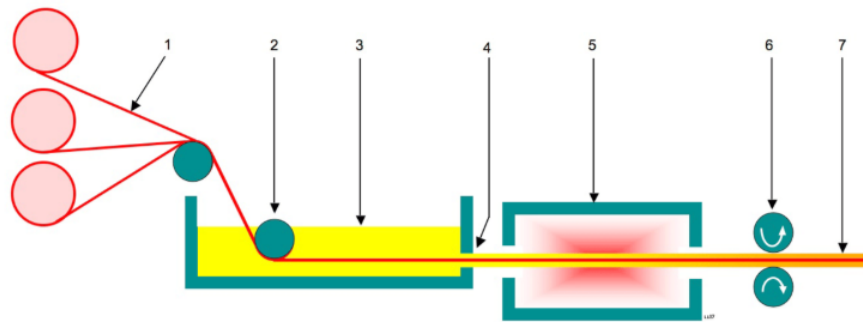


Fig. 1 Pultrusion process [Wikipedia].

The first who used the pultrusion process was B. Goldsworthy in 1951. The use of fiber-reinforced composites is rapidly spreading because of their advantages in strength and lightness. In particular, the strength and stiffness is given by the fibers while the resin protects the fibers and distributes the stresses [2].

Currently, the structural elements of GFRP are finding application in civil engineering works to strengthen the existing constructions but also for build new all GFRP structures. In the second case a very light structures can be obtained, for instance pedestrian bridge. Usually pultruded Glass Fiber Reinforced Polymer are used alongside conventional material such as concrete, aluminium and steel [3].

Pultruded material has a low density of 1734 kg/m^3 that is under $\frac{1}{4}$ of steel one. Although the shapes of these GFRP materials are similar to steel sections, as shown in figure:

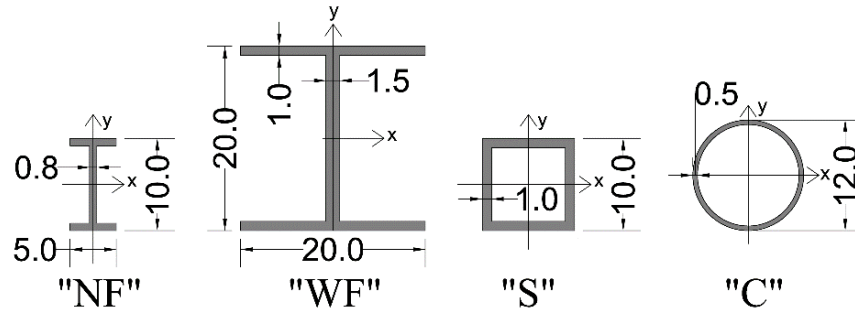


Fig. 2 Pultred material profiles.

Longitudinal tensile strength, in the direction of fibers, is 350 MPa that is comparable with structural steel. The longitudinal tensile modulus of elasticity, in the direction of fibers, is 28.5 GPa while in perpendicular direction of fibers is 8.5 GPa. All other parameters are listed in the following table:

Properties	Test method	Notation	Mean value
Longitudinal tensile modulus of elasticity	ASTM D638	$E_z = E_L$	28.5 (GPa)
Transverse tensile modulus of elasticity	ASTM D638	$E_y = E_x = E_T$	8.5 (Gpa)
Transverse shear modulus of elasticity	EN 13706-2 (full scale)	$G_{yx} = G_L$	3.5 (Gpa)
In-plane shear modulus of elasticity		$G_{xz} = G_{yz} = G_T$	2.5 (Gpa)
Longitudinal Poisson's ratio	ASTM D3039	$\nu_{zx} = \nu_{zy} = \nu_L$	0.25
Transversal Poisson's ratio	ASTM D3039	$\nu_{xy} = \nu_{yx} = \nu_T$	0.12
Longitudinal tensile strength	ASTM D638	$\sigma_{zt} = \sigma_{Lt}$	350 (Mpa)
Transverse tensile strength	ASTM D638	$\sigma_{xt} = \sigma_{yt} = \sigma_{Tt}$	70 (Mpa)
Longitudinal compressive strength	ASTM D695	$\sigma_{zc} = \sigma_{Lc}$	413 (Mpa)
Transverse compressive strength	ASTM D695	$\sigma_{xc} = \sigma_{yc} = \sigma_{Tc}$	80 (Mpa)
Shear strength	ASTM D2344	$\tau_{xy} = \tau_{xz} = \tau_{yz}$	40 (Mpa)
Density	ASTM D792	γ	1734 kg/m ³
Fibers percentage	ASTM D2584	V_f	45%

Table 1 Mechanical and physical properties of pultred GFRP material.

The isotropy is defined by the relationships $E_X=E_Y$, $\nu_{XY}=\nu_{YX}$ and $G_{ZX}=G_{ZY}$.

2.2 Experimental modal analysis

Modal analysis is a method that allows to determinate the dynamic characteristics of a system through the analysis of experimental data. Data can be displacements, velocities, accelerations measured on the structure. This approach is called 'modal analysis' and it revolves around two basic concept: linearity and time invariance of the structure [4]. The modal parameters to solve the problem are frequency, damping and mode shape. Naturally, the mechanical behaviour of a structure depends on its inertial and stiffness characteristics that govern the response of the system, caused by an external force. Through some transformations, we pass from the spatial model to the "phase-space". This is done because the representation in the phase-space is convenient to use the modal identification techniques. It is important to emphasise that the measure are not carried out with continuity over time but they are carried out at intervals of time. Therefore, during the test a sampling time must be defined.

2.3 Modal Identification

There are different types of modal identification methods; they can be classified according to different criteria:

- **DOMAIN**

This classification may be subdivided into three types: time domain, frequency domain and time-frequency domain. The time domain method works well when the structure has a high number of modes or the frequency range of interest is limited. The frequency domain method, instead, works well when the structure has a limited number of modes or the frequency range of interest is wide. The third type is a combination of the two previous ones and it is used to analyse non-stationary signals.

- **ANALYTICAL PROCESS**

In this classification we can distinguish: direct and indirect methods. In the first one, the identification is based on matrices determination that define the spatial model. Therefore, mass matrix, stiffness matrix and damping matrix are considered. It is a classical eigenvalue problem. In the second one, the identification of frequency response functions (FRF) is based on a modal model. That is on the evaluation of modal parameters: natural frequencies, damping and mode shape.

- **NUMBER OF MODE-SHAPES**

This criterion consist of the number of modal-shapes the have been analysed. It can be “SDOF” single degree of freedom or “MDOF” multi degree of freedom.

- INPUT AND OUTPUT

This criterion is linked to the operations of the experimental phase. It depends on the number of frequency response functions (FRF) available. Usually you have data for each sensor placed on the structure and therefore you have a function for each point monitored. In the light of this, four methods can be distinguished:

- SISO, single input – single output;
- SIMO, single input – multi output;
- MIMO, multi input – multi output;
- MISO, multi input – single output.

- TYPE OF EXCITATION

The excitation can be of two types: known (artificial excitation) or unknown. Artificial excitations can be: free oscillations and those induced by the use of a shaker; while the unknown ones can be: environmental noise, wind actions and mechanical vibrations due to vehicles.

2.3.1 General analytical formulation of identification methods

In order to illustrate the general approach of identification of the systems, a SISO system (single input – multiple output) is considered. Considering an input signal $u(t)$ and an output signal $y(t)$ where $t = (0, 1, \dots, N - 1)$, the discrete time system can be represented as follows:

$$y(t) = G(z)u(t) + v(t) \quad (1)$$

The $G(z)u(t)$ represent the convolution between two response functions $g(t)$ due to input signal $u(t)$, namely:

$$G(z)u(t) = \sum_{k=0}^{\infty} g(k)u(t - k) \quad (2)$$

The function $v(t)$ represents the error due to the instrument and noise.

$G(z)$ represent the transfer function of the system and it is defined as follows:

$$G(z) = \sum_{k=0}^{\infty} g(t) z^{-t} \quad (3)$$

Where z is the displacement

$$z^{-t}y(t) = y(t - 1) \quad (4)$$

This is a parametric approach linked to the determination of a set of parameters that describe $G(z)$ function.

It is possible to generalise the formula (1) to create a parametric model:

$$A(z)y(t) = \frac{B(z)}{F(z)}u(t) + \frac{C(z)}{D(z)}e(t) \quad (5)$$

Where the terms $A(z)$, $B(z)$, $C(z)$, $D(z)$ and $F(z)$ are polynomials. They are depend on displacement:

$$A(z) = 1 + a_1z^{-1} + \dots + \alpha_{n_a}z^{-n_a} \quad (6)$$

n_a is the polynomial order of $A(z)$.

Other similar equations can be written for the other polynomials using respectively n_b , n_c , n_d , n_e and n_f . $e(t)$ can be assumed as white noise and equal to $v(t)$. Based on the value of the coefficients it is possible to obtain different models:

- ARX, $n_c = n_d = 0$;
- ARMAX, $n_d = n_f = 0$;
- OE (output error), $n_a = n_c = n_d = 0$;
- BOX-JENKINS, $n_a = 0$.

Until now, the analytical formulation was based on a transfer function. It is possible to perform another formulation in the phase space by modifying the relation (5):

$$x(t + 1) = Ax(t) + Bu(t) \quad (7)$$

$$y(t) = Cx(t) + Du(t) + v(t) \quad (8)$$

Where A , B , C , and D are matrices containing constants. The equation (7) can be rewritten as follows:

$$zx(t) = Ax(t) + Bu(t) \quad (9)$$

by resolving you get:

$$x(t) = (zI - A)^{-1}Bu(t) \quad (10)$$

By replacing in the (8), the following is obtained:

$$y(t) = [C(zI - A)^{-1}D]u(t) + v(t) \quad (11)$$

In this case the transfer function is linked A, B, C, and D matrices through the following expression:

$$S(z) = C[zI - A]^{-1}B + D \quad (12)$$

In conclusion, the identification of systems corresponds to determining the matrices of constants.

2.3.2 Identification methods with unknown input

Most of the techniques with unknown input operate in the time domain and provide the modal parameters of the system starting from the structural response. Two methods must be distinguished: *not-parametric identification* and *parametric identification*. The first, estimate an impulse response function (for instance, ERA method), the second estimate the best parameters that are close to the experimental ones.

2.3.2.1 Eigensystem Realization Algorithm (ERA)

Eigensystem Realization Algorithm is a method designed by Juang and Pappa and it solves Multi Input Multi Output (MIMO) systems [5].

The first step of the method is to pass from the time domain to the phase domain; the dynamic equilibrium equations for a viscous damping MDOF system are:

$$[M]\{\ddot{x}(t)\} + [C]\{\dot{x}(t)\} + [K]\{x(t)\} = \{f(x(t), t)\} \quad (13)$$

Defining $u(t)$ the vector:

$$\{u(t)\} = \begin{Bmatrix} \{x(t)\} \\ \{\dot{x}(t)\} \end{Bmatrix} \quad (14)$$

the problem can be brought to the linear case:

$$[A'] = \begin{bmatrix} [0] & [I] \\ -[M]^{-1}[K] & -[M]^{-1}[C] \end{bmatrix} \quad (15)$$

$$\{f(x, t)\} = [F]\{\delta(t)\} \quad (16)$$

$$[B'] = \begin{bmatrix} [0] \\ -[M]^{-1}[F] \end{bmatrix} \quad (17)$$

Where $\{\delta(t)\}$ is an input vector relates to q points of stress; $[F]$ is the coefficients matrix of input signals. The system can be represented by writing equation (1a prima) in the phase space:

$$\{\dot{u}(t)\} = [A']\{u(t)\} + [B']\{\delta(t)\} \quad (18)$$

It is possible to establish a relationship between $\{u(t)\}$ and $\{x(t)\}$ (responses measured in p points) through the transform matrix $[R]$:

$$\{x(t)\} = [R]\{u(t)\} \quad (19)$$

The solution (18) is expressed by:

$$\{u(t)\} = e^{[A'](t-t_0)}\{u(t_0)\} + \int_0^{\Delta t} e^{[A']\tau'}[B']\{\delta(k\Delta t)\}dt \quad (20)$$

For each instant of time t ; where t_0 is the starting time. To provide a discrete representation of formulation (20) the following intervals must be considered: $0, \Delta t, \dots, k\Delta t$. Assuming that the input remains constant in the range $(k\Delta t, (k+1)\Delta t)$ and $\tau = (k+1)\Delta t - \tau$, is obtained:

$$\{u((k+1)\Delta t)\} = e^{[A']\Delta t}\{u(k\Delta t)\} - \int_0^{\Delta t} e^{[A']\tau'}[B']\{\delta(k\Delta t)\}dt \quad (21)$$

For simplicity, it is possible to introduce the following notations:

$$[A] = e^{[A']\Delta t} \quad (22)$$

$$[B] = - \int_0^{\Delta t} e^{[A']\tau'}[B'] \quad (23)$$

$$\{u(k+1)\} = \{u((k+1)\Delta t)\} \quad (24)$$

$$\{\delta(k)\} = \{\delta(k\Delta t)\} \quad (25)$$

The equation (21), for a discrete system, becomes:

$$\{u(k+1)\} = [a]\{u(k)\} + [B]\{\delta(k)\} \quad k = 0, 1, 2, \dots \quad (26)$$

So, formula (19) becomes:

$$\{x(k)\} = [R]\{u(k)\} \quad (27)$$

If all points (q) of stress are taken into account:

$$[X(k)] = [R] \quad [A]^{k+1} \quad [B] \quad (28)$$

$(p \times q) \quad (p \times 2N) \quad (2N \times 2N) \quad (2N \times q)$

Where:

p is the number of measured responses ($\{x(t)\}$) and q is the numbers of stress point.

All the matrices $[X(k)]$ are called “*parameters of Markov*” and are used to compose the *Hankel matrix*:

$$[H(k-1)] = \begin{bmatrix} [X(k)] & [X(k+1)] & \dots & [X(k+j)] \\ [X(k+1)] & [X(k+2)] & \dots & [X(k+j+1)] \\ \dots & \dots & \dots & \dots \\ [X(k+i)] & [X(k+i+1)] & \dots & [X(k+j+i)] \end{bmatrix} \quad (29)$$

With $i = 1, \dots, r-1$ and $j = 1, \dots, s-1$. Where r and s are numbers that satisfy the conditions $pr > N$ and $qs > N$. These conditions are necessary to have a sufficient amount of data to carry out the *Singular Value Decomposition* (SVD).

One of the advantages of ERA is that only the significant responses can be placed within the Hankel matrix. So you can use only those with low noise. This process involves the determination of matrices: $[R]$, $[A]$, and $[B]$.

There is an infinite number of combinations to satisfy the formula (28). The objective is to obtain a formulation with the minimum degree in order to represent adequately the dynamic behaviour of the structure. This is possible by using the SVD.

First, you have to find the $[H]'$ matrix so that the following report is respected:

$$[W][H]'[Q] = [I] \quad (30)$$

It is possible rewrite the relation (28) for values of $k \geq 0$;

$$[X(k+1)] = [R][A]^k[B] \quad (31)$$

If you use the identity:

$$[X(k+1)] = [E_p]^T[H(k)][E_q] \quad (32)$$

and

$$[E_p]^T = [[I] \ [0] \dots \ [0]] \quad (33)$$

$$[E_q] = \begin{bmatrix} [I] \\ [0] \\ \vdots \\ [0] \end{bmatrix} \quad (34)$$

it can be demonstrated that:

$$[X(k+1)] = [[E_p]^T [U_{2N}] [\varepsilon_{2N}]^{\frac{1}{2}}] \cdot [\varepsilon_{2N}]^{-\frac{1}{2}} [U_{2N}]^T [[Q][A]^k [W] \cdot \\ \cdot [[V_{2N}] [\varepsilon_{2N}]^{\frac{1}{2}}] \cdot [[\varepsilon_{2N}]^{\frac{1}{2}} [V_{2N}]^T [E_q]] \quad (35)$$

It is possible obtain the modal parameters once the transformation from discrete to continuous system has been carried out. The eigenvalues and eigenvalues are taken from matrix $[A]$:

$$[A]\{\Psi_u\} = \lambda\{\Psi_u\} \quad (36)$$

The mode shapes can be obtained by multiplying the eigenvalue matrix by the transformation matrix $[R]$:

$$\{\Psi_u\} = [R]\{\Psi_u\} \quad (37)$$

Frequencies and damping are evaluated by eigenvalues of the matrix $[A]$.

It is important to note that this method needs to be checked because the noise contained in the signal generates computational modes alongside the real ones.

3 METHODS

3.1 Curvature method

This method allows us to detect a crack using the change of modal shapes. Other methods based on frequency change can easily detect the presence of damage but not the position. This is because two cracks in two different positions can generate the same frequency variation. So it is not possible to know where the crack is. The curvature method instead detects the position of the damage through the changes of the curvature mode shapes because these changes take place in the region of the damage.

Modal Assurance Criterion (MAC) [7] and Co-ordinate Modal Assurance Criterion (COMAC) [8] are used to compare the mode shapes. MAC indicates the overall difference between two set of mode shapes. COMAC indicates the correlation between two mode shapes at a selected measurement point of a structure.

Curvature at a section is equal to:

$$v'' = M/(EI) \quad (38)$$

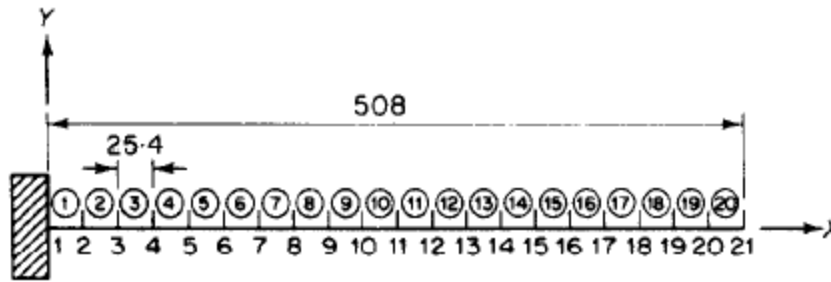
Where M is the bending moment at a section, E is the modulus of elasticity and I is the moment of inertia.

If the structure is damaged or cracked the value of EI will be reduced at the cracked section while the magnitude of curvature at that section will increase.

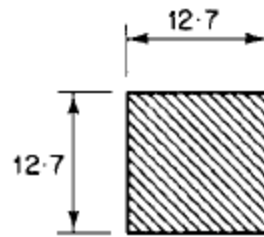
If the value of EI decreases, the change in curvature increases so the greater the damage, the more noticeable the change of curvature will be.

3.1.1 Analytical Model

Cantilever beam and supported beam models with uniform square cross-section were used to show this method. The geometric parameters are shown in the figures 3 and 4.

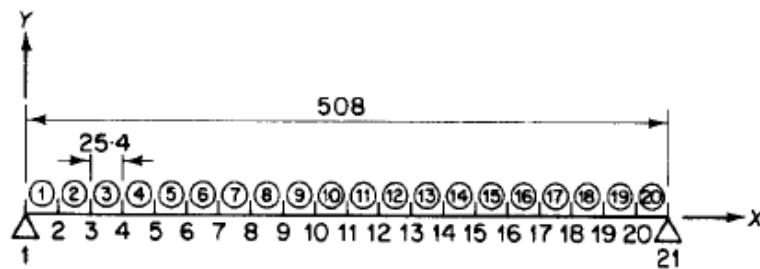


(a)

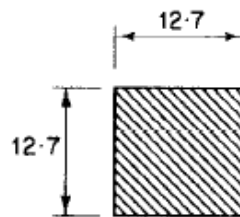


(b)

Fig. 3 Cantilever beam model. (a) Finite element model; (b) cross-section of the cantilever [6].



(a)



(b)

Fig. 4 Simply supported beam model. (a) Finite element model; (b) cross-section of the simply supported beam [6].

The cantilever beam model was chosen because the curvature and the displacements have different forms. Instead, the simply supported beam model was chosen because the curvature and displacements are the same. Two other cases can be distinguished:

- *Intact*: all elements have the same properties.

- *Cracked*: element 13 is damaged, has a reduced value (by 50%) of the modulus of elasticity E .

In both cases, 20 two-dimensional beam elements of the same length were used. Adams and Cawley assumed that damage in a structure effects only the stiffness matrix and not the inertia matrix in the eigenvalue problem formulation [9]. The eigenvalue problem for the *intact case* can be written as follows:

$$(K - \lambda_j M)x_j = 0 \quad (39)$$

and for the *cracked case* as:

$$(K' - \lambda'_j M)x'_j = 0 \quad (40)$$

where:

- K is the stiffness matrix of the intact case;
- K' is the stiffness matrix of the cracked case;
- λ_j is the j -th eigenvalue of the intact case;
- λ'_j is the j -th eigenvalue of the cracked case;
- x_j is the j -th displacement eigenvector of the intact case;
- x'_j is the j -th displacement eigenvector of the cracked case;

3.1.2 Analysys of results

The only degree of freedom that has been considered in the analysis is the translation degree of freedom along the Y axis because in the experimental work the rotations measurement are difficult. The mode shapes were orthonormalized against the inertia matrix:

$$x_j^T M x_j = 1 \quad (41)$$

The curvatures were determined from the displacements v through the following relationship:

$$v_i'' = (v_{i+1} - 2v_i + v_{i-1})/h^2 \quad (42)$$

where h is the length of each element.

Once the curvatures were calculated MAC and COMAC were applied for the intact and damaged curvature mode shapes.

3.1.3 Numerical result

- CANTILEVER BEAM MODEL

In the following table is possible to see the first five natural frequencies of the two cases: intact and damaged (element 13) cantilever.

Mode no.	Natural frequency (Hz)		Percentage change in frequency
	Intact	Damaged	
1	39·631	39·463	0·42
2	247·110	237·181	4·02
3	687·663	665·472	3·23
4	1336·898	1331·641	0·39
5	2188·828	2108·587	3·67

Table 2 Natural frequencies for the intact cantilever and the cantilever damaged [6].

From the results it can be concluded that the natural frequencies decrease if the structure is damaged. From the percentage change in frequency it is noted that there is a damage in the structure but to know the position it is necessary to make further analysis.

The following graph shows the first five displacement mode shapes for the intact cantilever.

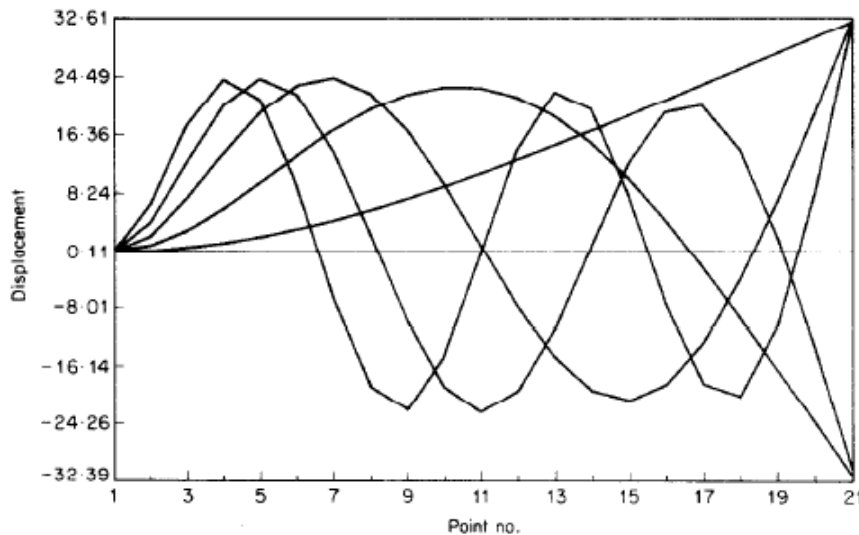


Fig. 5 Displacement mode shapes for intact cantilever [6].

The tables below show the Modal Assurance Criterion (MAC) and Co-ordinate Modale Assurance Criterion (COMAC) values for the intact and damaged displacement mode shapes.

Damaged cantilever	Intact cantilever				
	1	2	3	4	5
1	1.00	0.01	0.01	0.01	0.01
2	0.01	1.00	0.00	0.01	0.01
3	0.01	0.01	1.00	0.01	0.01
4	0.01	0.01	0.01	1.00	0.00
5	0.01	0.01	0.00	0.01	1.00

Table 3 MAC values for the intact and damaged displacement mode shapes for the cantilever [6].

Point no.	COMAC values	Point no.	COMAC values
1	1.00	12	1.00
2	1.00	13	1.00
3	1.00	14	1.00
4	1.00	15	1.00
5	1.00	16	1.00
6	1.00	17	1.00
7	1.00	18	1.00
8	1.00	19	1.00
9	1.00	20	1.00
10	1.00	21	1.00
11	1.00		

Table 4 COMAC values for the intact and the damaged displacement mode shape for the cantilever [6].

All numbers 1 on the diagonal (Table 3) indicate that the modal shapes of the intact case and the damaged case are almost identical. The following figure shows the curvatures:

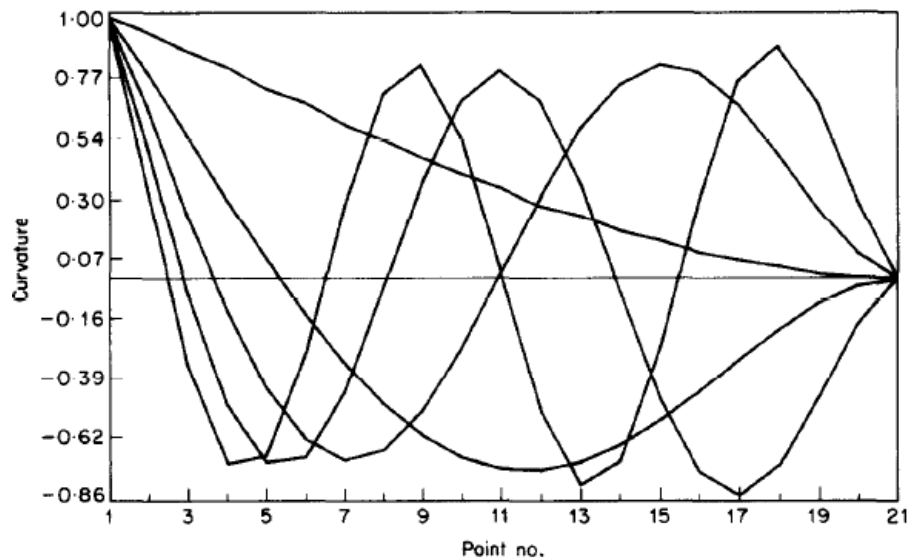


Fig. 6 Curvature mode shapes for the intact cantilever [6].

Once the curvature mode shapes and displacement mode shapes were known, the absolute differences, between intact and damaged cantilever, were calculated:

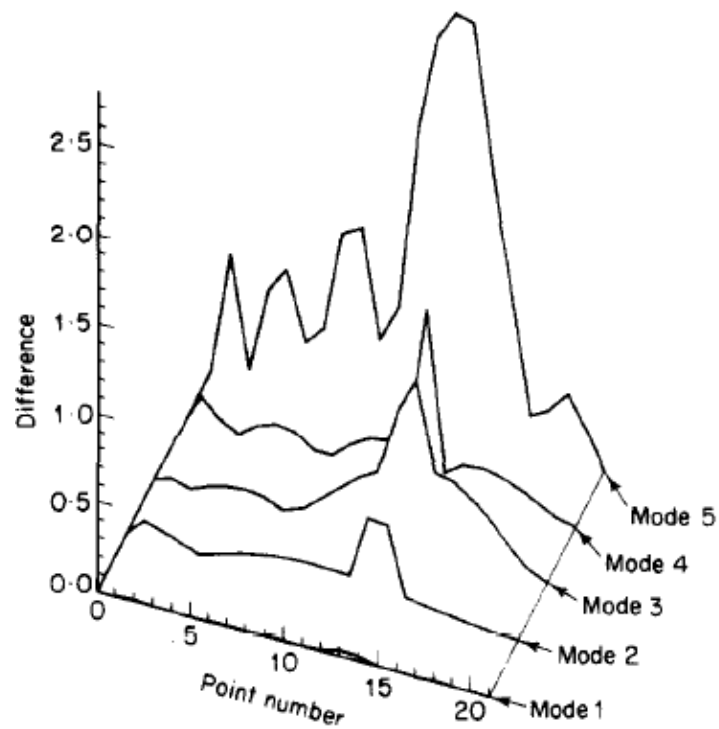


Fig. 7 Absolute difference between the curvature mode shapes for the intact and the damaged cantilever [6].

For each curvature mode, the maximum difference occurs in the damage zone.

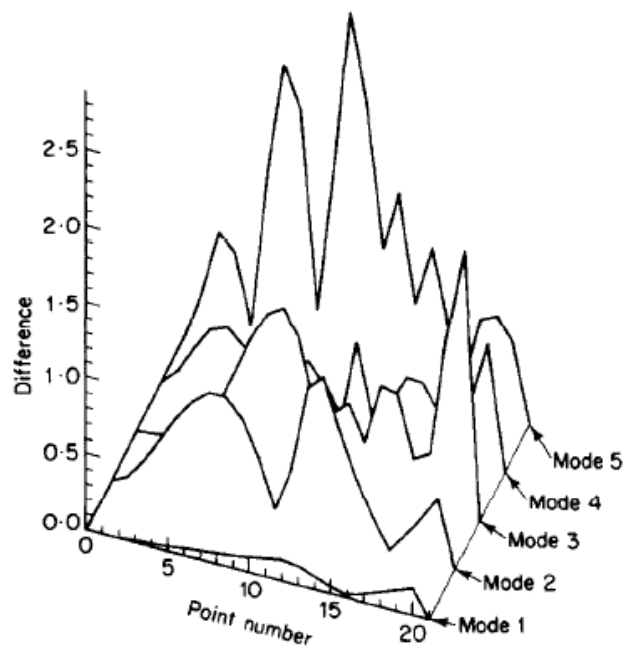


Fig. 8 Absolute difference between displacement mode shapes for the intact and the damaged cantilever [6].

The changes in the displacement mode shapes are not localized to the damage region, so this information is not useful to localise the damage area.

- SIMPLY SUPPORTED BEAM MODEL

In the following table is possible to see the first five natural frequencies of the two cases: intact and damaged (element 13) simply supported beam.

Mode no.	Natural frequency (Hz)		Percentage change in frequency
	Intact	Damaged	
1	111.327	106.857	4.02
2	444.228	434.274	2.24
3	995.420	987.643	0.78
4	1759.279	1690.227	3.93
5	2727.609	2702.741	0.91

Table 5 Natural frequencies for the intact and damaged simply supported beam [6].

From the results it can be concluded that the natural frequencies decrease if the structure is damaged.

The following graph shows the first five curvature mode shapes for the simply supported beam, which are in the same form as displacements.

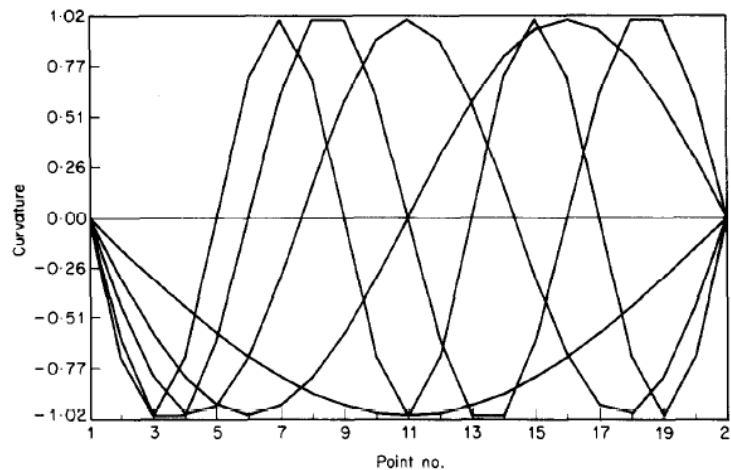


Table 6 Curvature (or displacement) mode shapes for the simply supported beam [6].

Once the curvature mode shapes and displacement mode shapes were known, the absolute differences, between intact and damaged cantilever, were calculated:

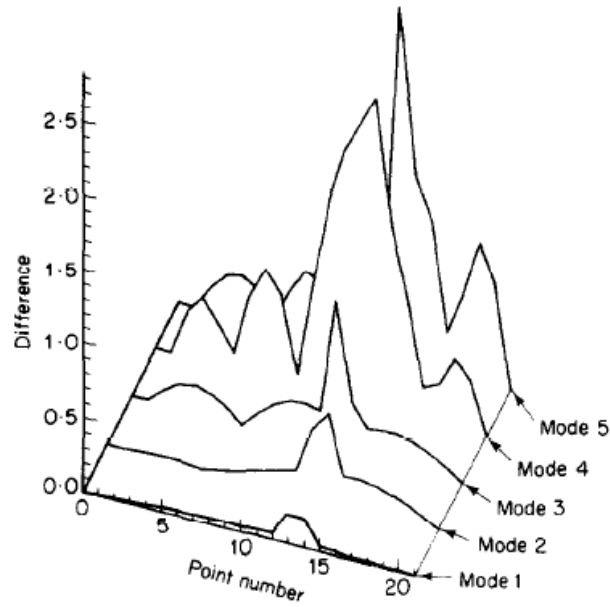


Table 7 Absolute difference between the curvature mode shapes for the intact and the damaged simply supported beam [6].

For each curvature mode, the maximum difference again occurs in the damage zone.

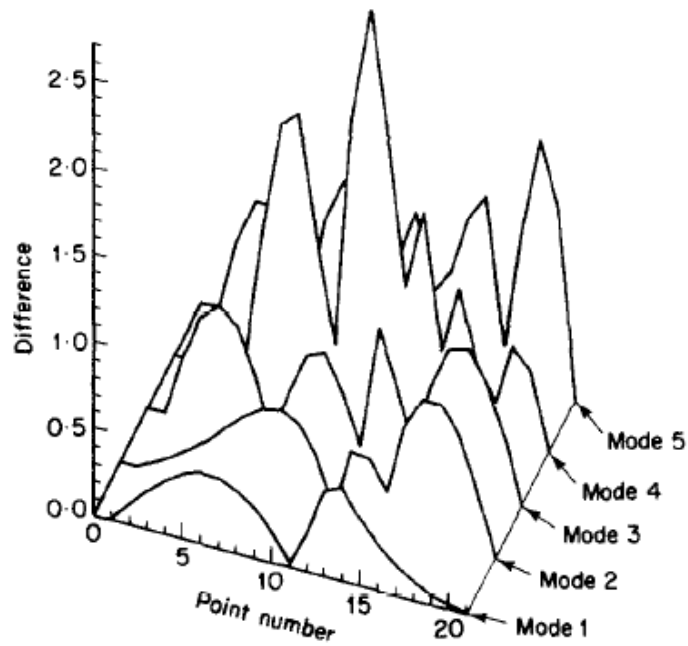


Table 8 Absolute difference between the displacement mode shapes for the intact and the damaged simply supported beam [6].

Also in this case, the changes in the displacement mode shapes are not localized to the damage region.

In conclusion, seeing the numerical results for the cantilever beam model and the simply supported beam model, the curvature mode shapes is a useful method to identify the damage area.

3.2 Treed Gaussian Process (TGP)

This is a specific method in detecting cracks in a structure through mode shapes and the approach is based on Gaussian process (GP) regression. For the use of GP it is required that the beam is uniformly smooth and this assumption is valid only for the undamaged section of the beam. If, on the other hand, a crack is present, it induces a discontinuity. The idea was to allow a spatial switch point in the GP covariance, which allowed different characteristics near a point and on either side of the point [10]. After creating this function, it is possible to determine the position of the crack by maximizing the probability of the data (of the mode shape) by varying the position of the switching point. In the Gaussian process regression it is used a covariance Kernel which characterises the smoothness of the structure being modelled.

3.2.1 Gaussian Process (GP)

The Gaussian processes are a Gaussian distribution of functions that return a Gaussian probability distribution. Gaussian processes are statistically based (Bayesian) and are able to automatically return the time interval for predictions. In practice, a series of preliminary assumptions are made about the function to be modelled, and then the data is processed to update and evaluate a posterior distribution over functions.

The GP algorithm implementation is shown as follows.

Let us consider n input points $\{x_1, \dots, x_n\}$, the prior beliefs about the corresponding outputs can be represented by a multivariate normal distribution, the mean of which is least squares regression fit through the training data:

$$E[f(x)|\beta] = m(x) = h(x)^T \beta \quad (43)$$

Where:

- $h(x)^T$ is a regression function of x ;
- β is a vector of coefficients.

The covariance between output points is given as:

$$\text{cov}[f(x), f(x') | \sigma_f^2, \sigma_n^2, L] = k(x, x') \quad (44)$$

Where:

- σ_f^2 is a scaling factor;
- σ_n^2 is a noise variance;
- L is a diagonal matrix of inverse length-scales;

L matrix represent the roughness of the output with respect to the individual input parameters. The constant are the *hyperparameter* of the problem. The covariance function usually used is as follows:

$$k(x, x') = \sigma_f^2 \exp[-(x - x')^T L (x - x')] + \sigma_n^2 \delta \quad (45)$$

Where $\delta = 1$ if $x = x'$.

If the matrix L is restricted to the form δ_{ij}/l^2 the convariance is isotropic:

$$k(x, x') = \sigma_f^2 \exp\left(-\frac{1}{2l^2} \|x - x'\|^2\right) + \sigma_n^2 \delta \quad (46)$$

These equations complete the prior specification of the problem; the *posterior distribution* is then found by conditioning the prior distribution on the training data y . One of the properties of GP is that the density of a number of outputs from the process is multivariate normal. It is possible to evaluate this function only in some sampled points: training points and forecasts. f indicates the function values at the X training points and f^* indicates the function value at a new x^* training point. It is therefore obtained:

$$\begin{pmatrix} f \\ f^* \end{pmatrix} \sim N\left(0, \begin{bmatrix} K(X, X) & K(X, x^*) \\ K(x^*, X) & K(x^*, x^*) \end{bmatrix}\right) \quad (47)$$

Where a zero-mean prior has been for simplicity; $K(X, X)$ is a matrix where i, j^{th} element corresponds to $k(x_i, x_j)$. In the same way, $K(X, x^*)$ is a vector where i^{th} element corresponds to $k(x_i, x^*)$ and $K(x^*, X)$ is the transpose of the same.

To compare the observed target data y with the f function, a Gaussian noise model can be assumed:

$$y \sim N(f, \sigma_n^2 I) \quad (48)$$

Where I is the identity matrix.

Since is not interested in the variable f , it can be integrated out from equation (47):

$$p(y) = \int p(y|f)p(f)df \quad (49)$$

The equation (47) can be rewritten:

$$\begin{pmatrix} y \\ y^* \end{pmatrix} \sim N \left(0, \begin{bmatrix} K(X, X) + \sigma_n^2 I & K(X, x^*) \\ K(x^*, X) & K(x^*, x^*) + \sigma_n^2 I \end{bmatrix} \right) \quad (50)$$

To use this expression, it is necessary to move from a joint distribution $p(y, y^*)$ to a conditional distribution $p(y^*|y)$. Using standard results for conditional proprieties of a Gaussian, it is possible to write:

$$y^* \sim N(m^*(x^*), k^*(x^*, x^*)) \quad (51)$$

Where

$$m^*(x^*) = k(x^*, X)[K(X, X) + \sigma_n^2 I]^{-1}y \quad (52)$$

is the *posterior mean* of the GP, and

$$k^*(x^*, x') = k(x^*, x') - [K(x^*, X) + \sigma_n^2 I]^{-1}K(X, x') \quad (53)$$

Is the *posterior variance*.

Thus GP model provides a posterior distribution for the unknown quantity y^* . The mean from equation (51) can be used for a regression problem as a “best estimate”, and the variance can be used to define confidence intervals.

The last factor to calculate and optimize is the hyperparameter; this can be done by using an evidence framework [11]. These parameters can be found by maximizing the following function:

$$f(\vartheta) = \frac{1}{2}y^T [K(X, X) + \sigma_n^2 I]^{-1}y - \frac{1}{2} \log |K(X, X) + \sigma_n^2 I| \quad (54)$$

Which is the *log marginal likelihood* and is equal to the log of the evidence, up to some constant.

3.2.2 Crack Detection

One approach to adapting the GP model is to specify a covariance function that can change its behavior in different regions of the beam. It is possible to perform a covariance function, assuming the beam is fissured at position $x = a$.

$$k(x_i, x_k) = f(x) = \begin{cases} k_1(x_i x_j) + k_2(x_i x_j), & x_i < a, x_j < a \\ k_1(x_i x_j) + k_2(x_i x_j), & x_i > a, x_j > a \\ k_1(x_i x_j) & otherwise \end{cases} \quad (55)$$

This approach was used in [12] where k_1 was taken as a polynomial kernel,

$$k_1(x_i x_j) = \sigma_f^2 (1 + x_i x_j)^N + \sigma_n^2 \delta_{1j} \quad (56)$$

and k_2 was an SE kernel as defined in equation (46). σ_f^2 and σ_n^2 are hyperparameter associated with the signal and noise variances, and N is a hyperparameter controlling the polynomial order.

Now all the elements are available to detect cracks using GP regression. The only unknown factor is the parameter of the position of the cracks, which is changed in order to maximize the probability of the data.

3.2.3 Algorithm TGP

In this algorithm it is important to divide the space of the independent variables into fields where there is a smooth response behaviour, then create low order regression models for each region. The problem will be solved with linear least-squares model if partitioning is carried out manually. In Treed Gaussian Process method, the partitions are determined by the data as part of the modelling problem, so the problem becomes highly non-linear and the least-squares model is no longer usable. The algorithm is therefore based on rigorous concepts of probability theory; In Bayesian *Classification and Regression Trees* (CART) a probability distribution on all tree structures and all coefficients is proposed [13]. In the original formulation made by Chipman, all regression models were linear; later Gramcy proposed the use of GP models, thus creating the TGP [14].

As the Gramcy algorithm is very complex, it is possible to illustrate a variant developed by O'Hagan based on Bayesian probability that integrates the hyper-parameters σ_f^2 and β by eliminating them from the problem of optimization. The result is a Student *t-process*, conditional on L and the training data:

$$[f(x)|y, L] \sim t_n - (m^*(x), \hat{\sigma}_f^2 k^*(x, x)) \quad (57)$$

In which,

$$(m^*(x) = h(x)^T \hat{\beta} + k(x)^T K^{-1}(y - H\hat{\beta})) \quad (58)$$

$$k^*(x, x') = k(x, x') - k(x)^T K^{-1} k(x') + (h(x) - k(x)K^{-1}H)(H^T K^{-1}H)(h(x') - k(x')K^{-1}H)^T \quad (59)$$

$$k(x)^T = k(x, x_1), \dots, k(x, x_n) \quad (60)$$

$$H^T = (h(x_1), \dots, h(x_n)) \quad (61)$$

$$K = \begin{pmatrix} 1 & k(x_1, x_2) & \dots & k(x_1, x_n) \\ k(x_2, x_1) & 1 & \dots & \vdots \\ \vdots & \vdots & \ddots & \vdots \\ k(x_n, x_1) & \dots & \dots & 1 \end{pmatrix} \quad (62)$$

$$\hat{\beta} = (H^T K^{-1} H)^T H^T K^{-1} y \quad (63)$$

$$\hat{\sigma}_f^2 = \frac{y^T (K^{-1} - K^{-1} H (H^T K^{-1} H) H^T K^{-1}) y}{n - d - 3} \quad (64)$$

$$y = (f(x_1), \dots, f(x_n))^T \quad (65)$$

The quality of the model is highly dependent on the number and distribution of training data points in the input space and on the values of the hyper-parameters.

It can be demonstrated that the $\hat{\beta}$ and $\hat{\sigma}_f^2$ values (mentioned above) coincide with the values derived from the least-squares model. The diagonal matrix of the L roughness parameters is evaluated by estimating the maximum probability or by means of the Markov Chain Monte Carlo (MCMC); this estimate is the longest and most complex part from a computational point of view.

The calculations for the TGP were performed on the R software using the TGP package written by Gramcy.

3.3 Piecewise Cubic Hermite Interpolating Polynomial (pchip)

PCHIP is a function implemented in the MatLab toolbox that performs a cubic interpolation of data through a third-order polynomial $P(x)$.

The polynomial $P(x)$ is characterized by four local coefficients $[a, b, c, d]$ that are chosen at each interval $[x_1, x_2]$; it has the following form:

$$P(x) = a(x - x_1)^3 + b(x - x_1)^2 + c(x - x_1) + d \quad (66)$$

Below there are a graphic examples of interpolation using the pchip and spline functions.

EXAMPLE1

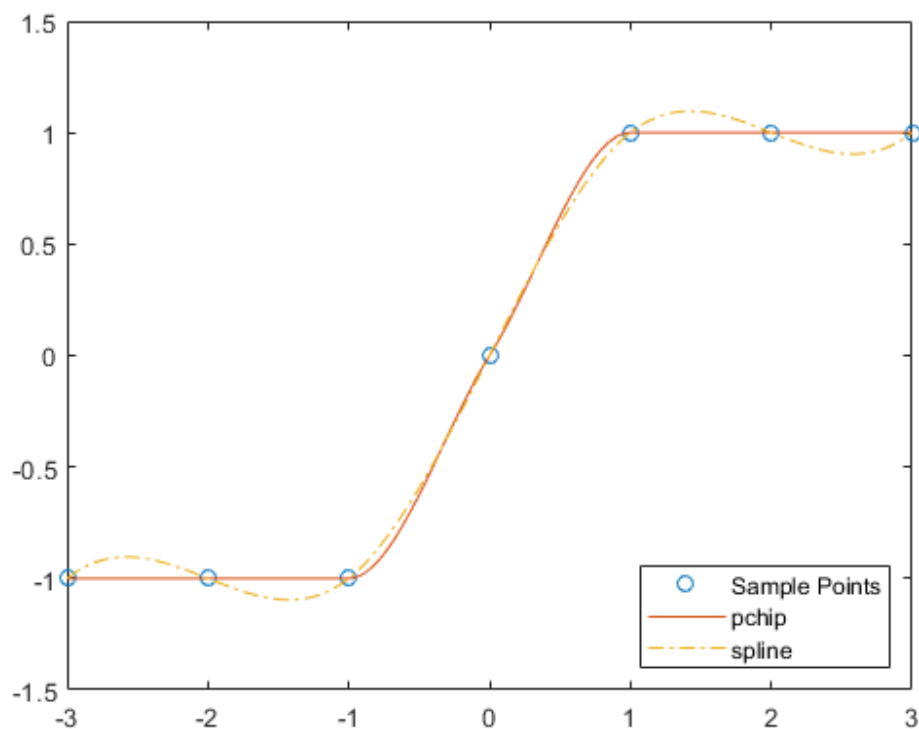


Fig. 9 Example of pchip and spline interpolation on sample points [MatLab manual].

EXAMPLE 2

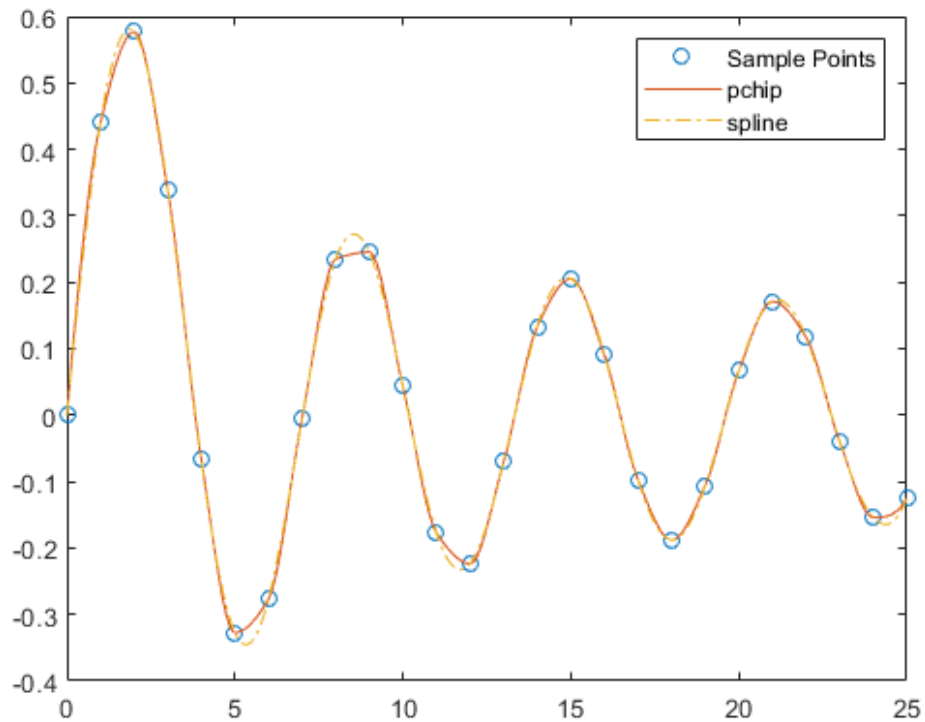


Fig. 10 Example of pchip and spline interpolation on oscillatory sample points [MatLab manual].

In the first example, pchip is a better interpolation of data because it does not oscillate freely between sampling points. In the second case, the sampled points refer to an oscillatory function, and the pchip interpolation loses information where the curvature is high.

'pchip' properties [MatLab manual]

- The Hermite cubic polynomial is used on specified derivative points (slope) for each interval $x_k \leq x \leq x_{k+1}$.
- $P(x_j) = y_j$ and the first derivative of P is continuous. The second derivative is probably not continuous so jumps at the x_j are possible.
- The slopes at the x_j are chosen in such a way that $P(x)$ preserves the shape of the data and respects monotonicity.

For this study, it was therefore decided to use the pchip function because there were few sampling points and very slight oscillations.

4 FINITE ELEMENT MODEL

The finite element method (FEM) is a numerical process that solves problems of differential equations at partial derivatives.

Geometric modelling has been defined in order to physically and mathematically represent the reality of the structure under examination. The finite element method is used to derive approximate solutions of problems defined by differential equations through a system of algebraic equations. This method subdivides the components into one-dimensional, two-dimensional and solid elements capable of representing the structural behaviour. The main function is to discretize the structure by creating a mesh made from elements of coded form.

The finite element software described in this chapter is ANSYS®, which includes the following steps:

- **Geometry Construction;**

With regard to the geometry construction, there are three ways to operate:

1. Exporting the geometry from another software;
2. Creating geometry through the ANSYS interface;
3. Creating the geometry through command codes (modality used).

- **Defining the Element Type;**

ANSYS has many types of elements to represent and discretize reality; the element that was used in the thesis work is called: *SHELL281*.

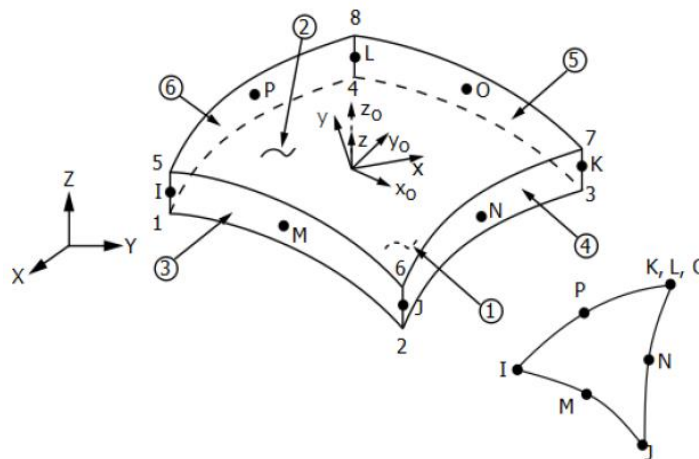


Fig. 11 Shell281 [ANSYS manual].

This type of element is usually used to analyse thin or not very thick shells and is characterized by 8 nodes; each node has 6 degrees of freedom: three translational and three rotational. These degrees of freedom are valid in the hypothetical case in which the element in question performs the function of "shell"; if on the other hand it performs a membrane behaviour, the rotational components are neglected. It is usually used for linear applications, large rotation and/or large deformation.

- **Attributes material properties;**

For the materials to be assigned, ANSYS has a large library with standard values for different types. In the present case, an elastic model was used; for this model ANSYS offers three alternatives:

- Isotropic

where the parameters to be written as input are: elastic modulus (EX) and major Poisson's ratio (PRXY).

- Orthotropic (modality used)

where the parameters to be written as input are: elastic modules (EX,EY,EZ), Poisson's ratios (PRXY, PRYZ, PRXZ) and shear modules (GXY, GYX, GXZ).

- Anisotropic

where the parameters to be written as input are the elements of Anisotropic Elastic Matrix.

- **Define mesh;**

The definition of the mesh is a very important phase because in function of its dimension, different solutions can be achieved. Of course, the smaller the mesh, the more accurate the results will be , but the computational time will increase.

- **Boundary conditions;**

In this section are inserted and conditions of constraint: fixed points, free or yielding.

- **Analysis;**

The types of analysis that are implemented in Ansys are:

- Static;

- Modal (modality used);

- Harmonic;

- Transient;

- Spectrum;
- Eigen Buckling
- Substructuring
- **Post Processing;**
Here is possible to view the results after the resolution.

5 RESULTS

This chapter shows graphs whose results are generated by the hammer in position B7 and with accelerometers in the Y direction; in the appendix, it is possible to find all the other graphs regarding the accelerometers in the X direction and all other impact-hammer positions.

5.1 Dynamic tests

The dynamic tests on the beam of “H” profile were carried out in the laboratory using accelerometers and an opposed hammer. First, the positions of the accelerometers to be placed along the beam were defined. The following image shows the beam geometries, the accelerometer positioning (A1, A2, ..., A8) and the impact-hammer positioning (B0, B1, ..., B7) in both the x and y directions.

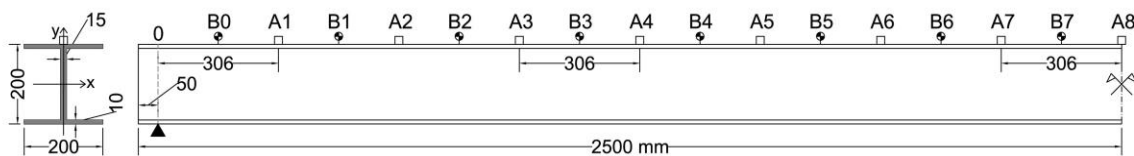


Fig. 12 Accelerometer and impact hammer positioning in y direction.

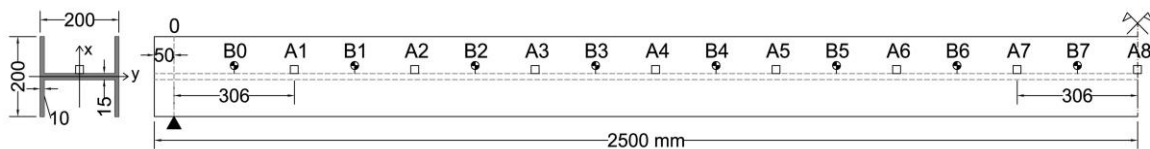


Fig. 13 Accelerometer and impact hammer positioning in x direction.

The beam was studied using the static scheme of the simply supported beam and was made by placing the beam on two cylindrical section supports. The excitation pulse to the beam was generated using a Dytran5850 hammer; the structural responses due to the excitation of the hammer were captured by the BBN, model 507Lf, accelerometers (15 total), which have a mass of 10g and record data in the frequency range of 0.10 to 12 kHz.

Both hammer and sensor are piezoelectric sensing elements with a cylindrical shear stress configuration with an integrated charge pre-amplifier and are connected to a data acquisition system via high stability coaxial cables that minimize the environmental influence on the test result.



Fig. 14 Photos 1 of the experiment in the laboratory



Fig. 15 Photos 2 of the experiment in the laboratory

Fifteen hammers were made at different positions, from B0 to B15, both in the X and Y directions, resulting in a total of 16 data for the accelerometers in the X direction and 16 data for the accelerometers in the Y direction. In X direction 62500 samples were recorded with a sampling frequency of 38147 while in Y direction 16,384 samples with a sampling frequency of 10,000.

All information was then processed on the MatLab® software.

5.1.1 Data processing

The first operation was to correct the data matrix because the first part of the signals had cut-offs due to the high frequencies generated by the hammer. This happened because the frequency generated by the hammer at that time exceeded the permissible frequency range of the accelerometers. Thus, the information prior to the cut-off has been deleted. This is shown in the image below with all 15 accelerometer responses.

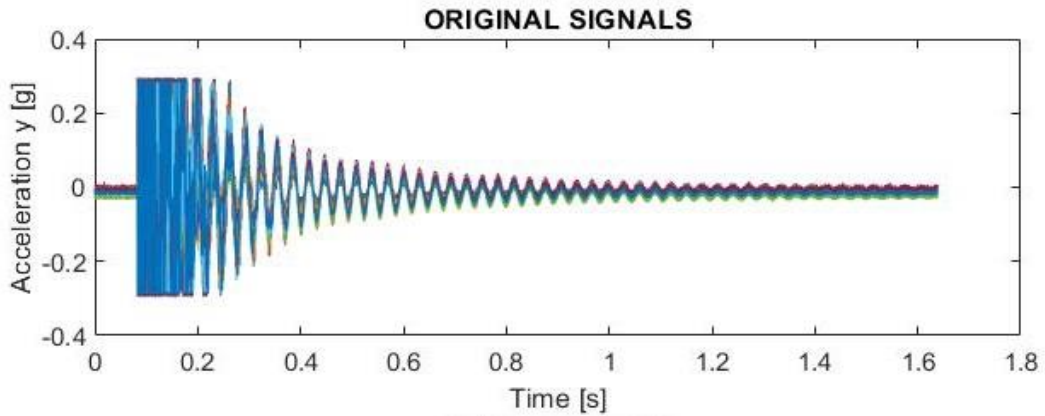


Fig. 16 Original signals, before the cut-off.

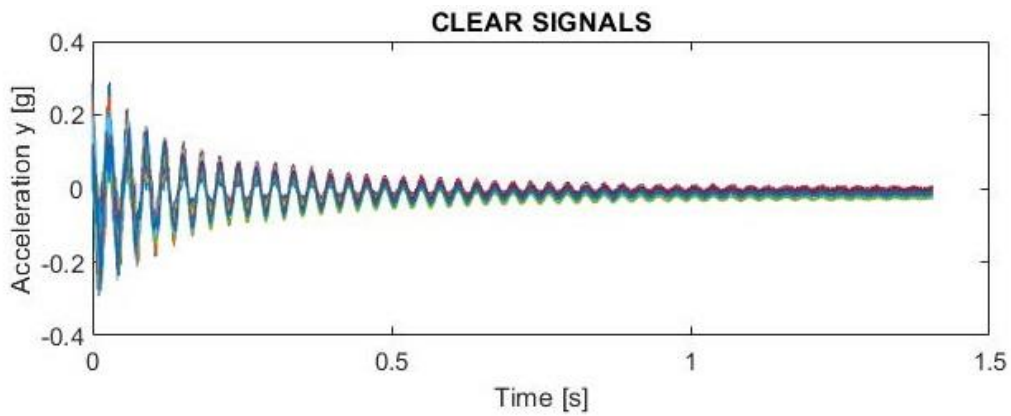


Fig. 17 Signals after the cut-off.

Once the data had been corrected, a *filter* was applied to eliminate the very low frequencies, below 1Hz, and the very high frequencies, above 150 Hz. Subsequently, the time domain was moved to the frequency domain by applying the *Fourier transform* to the different signals.

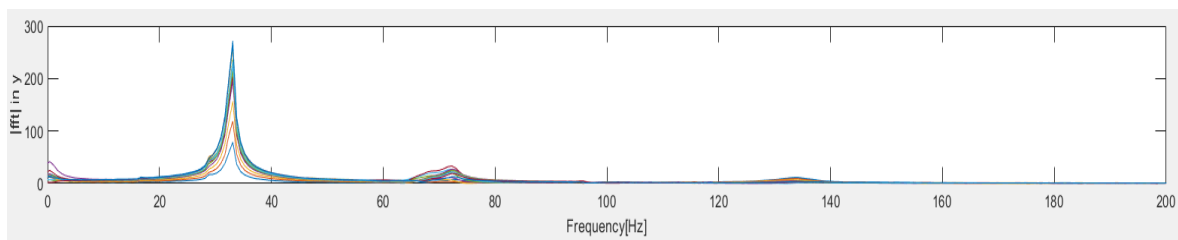


Fig. 18 Fourier transform of signals.

From the graph there are clearly peaks where the frequencies of the modal shapes correspond.

Mode shapes have been obtained using the *ERA method* described in Chapter 2.3.2.1.

5.1.2 Identification: ERA method.

This algorithm has been implemented on Matlab and allows executing experimental modal analysis.

The input parameters that have been inserted inside the algorithm are:

- Signal;
- Signal sampling frequency
- Minimum and maximum order of the algorithm, in this case 10 and 100;

The output are:

- Stabilization diagram showing the model order of the algorithm as a function of the natural frequencies of the structure;
- Stabilization graph showing the damping of the structure as a function of natural frequencies of the structure;
- Identification matrix in which frequencies, damping and eigvalue are present.

The first output from the algorithm is the following:

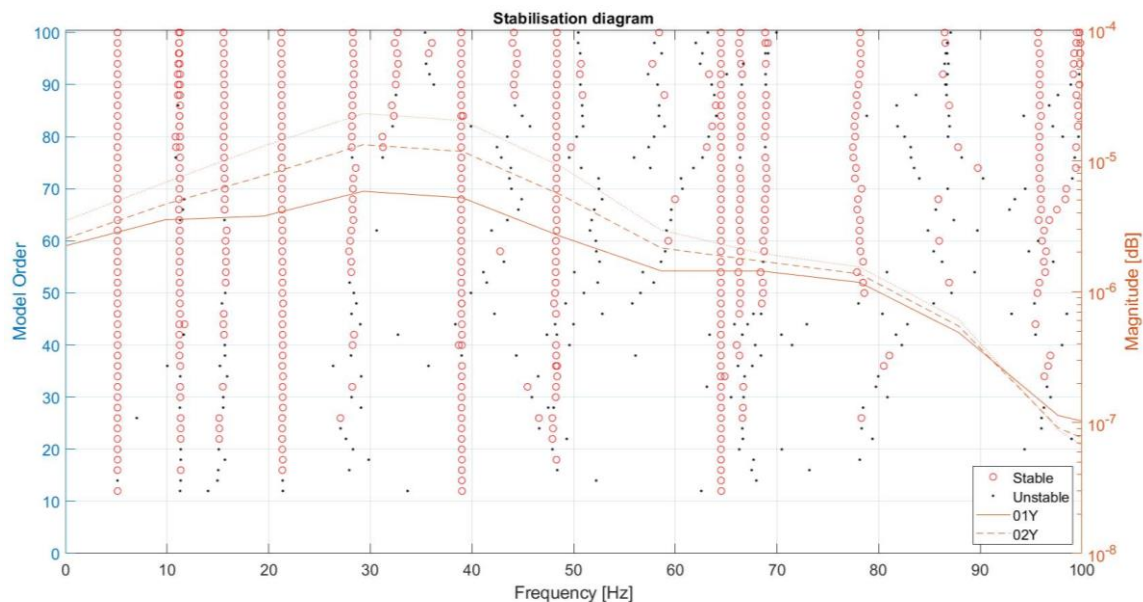


Fig. 19 Stabilisation diagram: Frequency – Model order.

The above image is the stabilization diagram for the frequencies and order of the model; on the axis of the abscissae there is the frequency scale in Hz while on the ordinates there is

the order of the system that has been made to vary from 10 to 100 with a step of 2. The larger the order, the greater the refinement of the calculation, but with orders too high computational frequencies are generated that do not represent a real behavior of the structure. The red circles and black dots indicate the results of the calculation and the difference in representation is in the *stability* of the solution.

The input parameters used to evaluate the *stability* are:

- Maximum frequency variation: 1%;
- Maximum damping variation: 10%;
- Minimum MAC: 0.98.

If, as the order increases, a coherence with the results is maintained, the identified frequency is defined as stable and it is represented with a red circle, vice versa with a black dot. An important point to underline is that the obtained frequencies must be verified in order to not confuse the real frequencies with the computational ones.

The second output from the algorithm is the following:

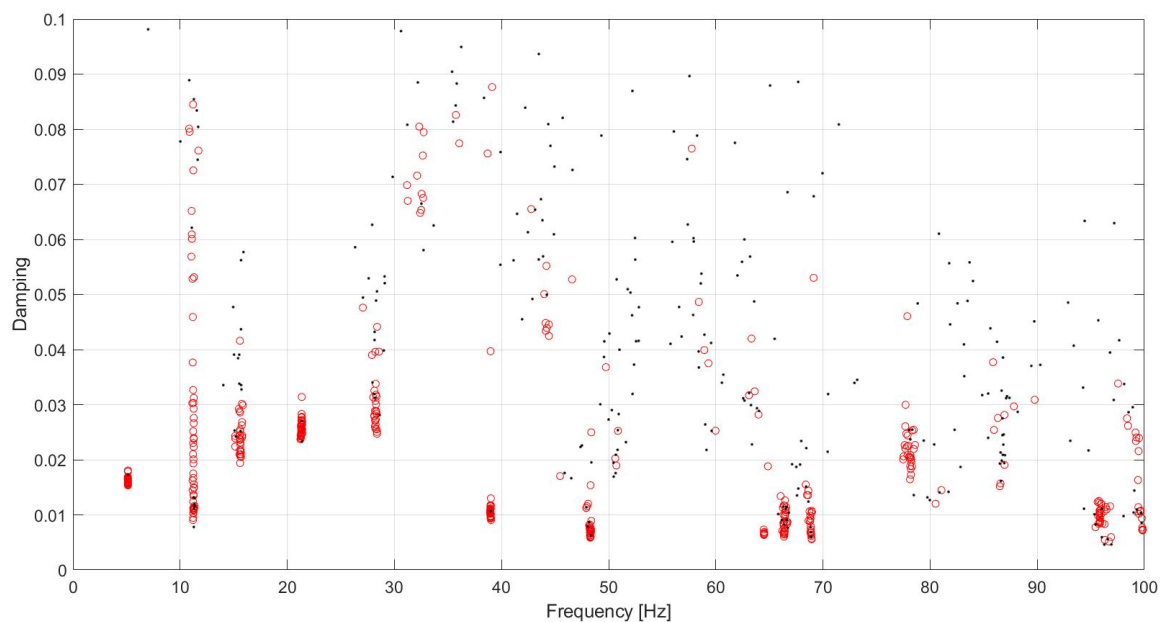


Fig. 20 Stabilisation diagram: Frequency – Damping.

In this case we have the frequencies on the abscissae and the damping on the ordinates. In addition, in this case, the same applies as before with regard to the symbolism (circles and points); the solution is represented in the form of a *cluster*. If there is a higher concentration of red circles, it means that the frequency value belongs to the structure.

The third and last output concerns the identification matrix: a vector containing matrices; these matrices differ from each other according to the model order with which they have been calculated. Having chosen a minimum order of 10 and a maximum order of 100, with a step of 2, we will have a total of 45 matrixes.

The matrix shall be presented in the following manner:

Frequency	F_1	F_2	...	F_i
Damping	D_1	D_2	...	D_i
Sensor 1	Eigvalue 1	Eigvalue 2	...	Eigvalue i
Sensor 2				
...				
Sensor 15				

Table 9 Identification matrix form.

The first line is related to the frequencies, the second to the damping, from the third to the end there are the modal displacement values.

5.1.3 Mode Shapes

In order to have control over the results and to try to understand what kind of modes correspond to the frequencies found, we passed to the representation of eigvalues.

If the order of the most appropriate system (the most stable) has been carefully chosen, the eigvalues present in the identification matrix will be the correct ones to be displayed. The first four mode shapes are as follows:

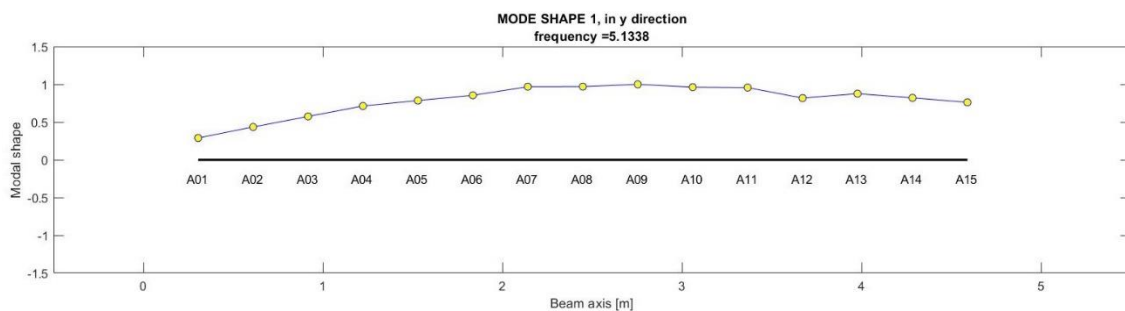


Fig. 21 First mode shape of experimental data.

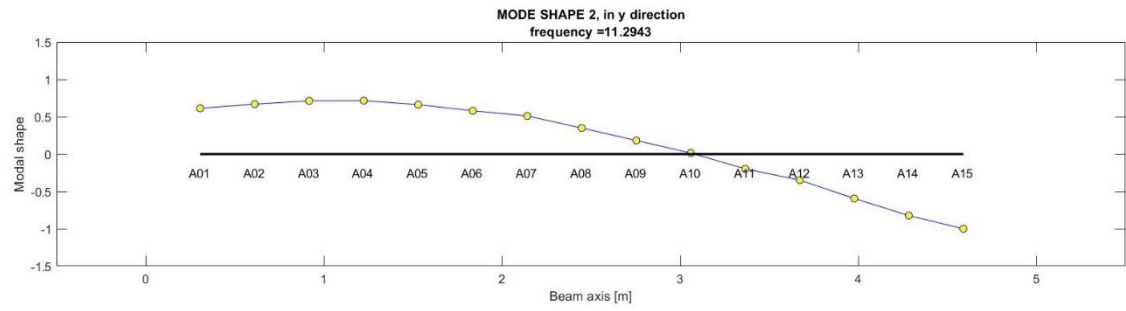


Fig. 22 Second mode shape of experimental data.

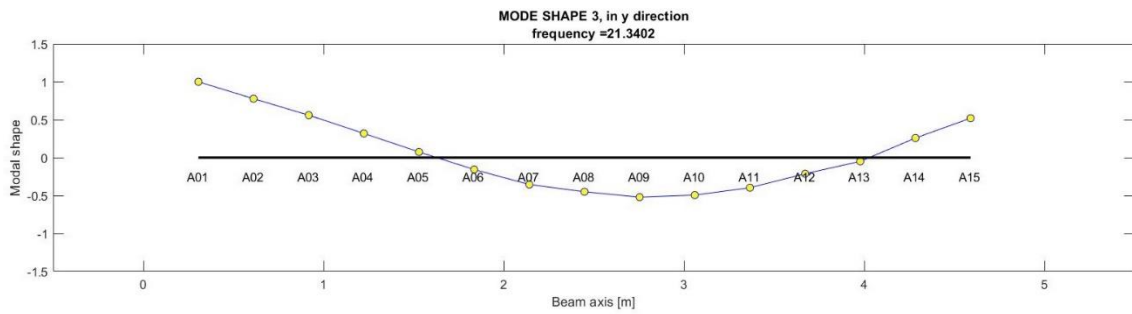


Fig. 23 Third mode shape of experimental data.

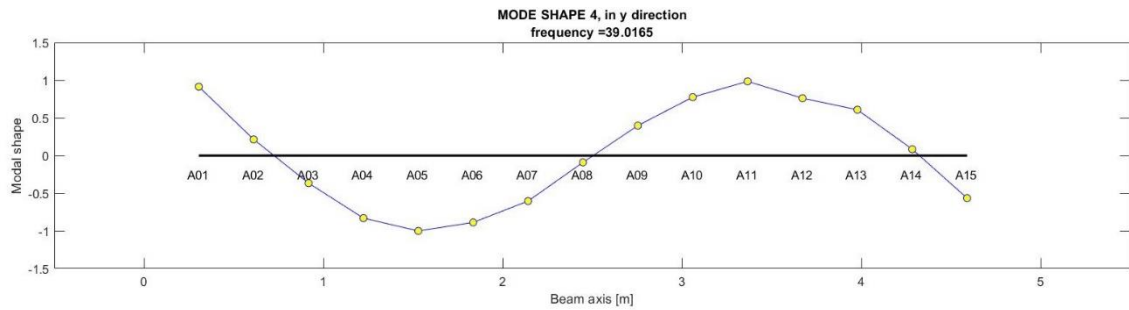


Fig. 24 Fourth mode shape of experimental data.

5.1.4 Curvature mode shapes

The calculation of the curvatures has been carried out starting from the mode shapes obtained in 5.1.3. The analytical formulation (number 42) has been expressed in the paragraph (3.2.2) on the method of curvatures.

The curvatures corresponding to the experimental modal shapes are shown below.

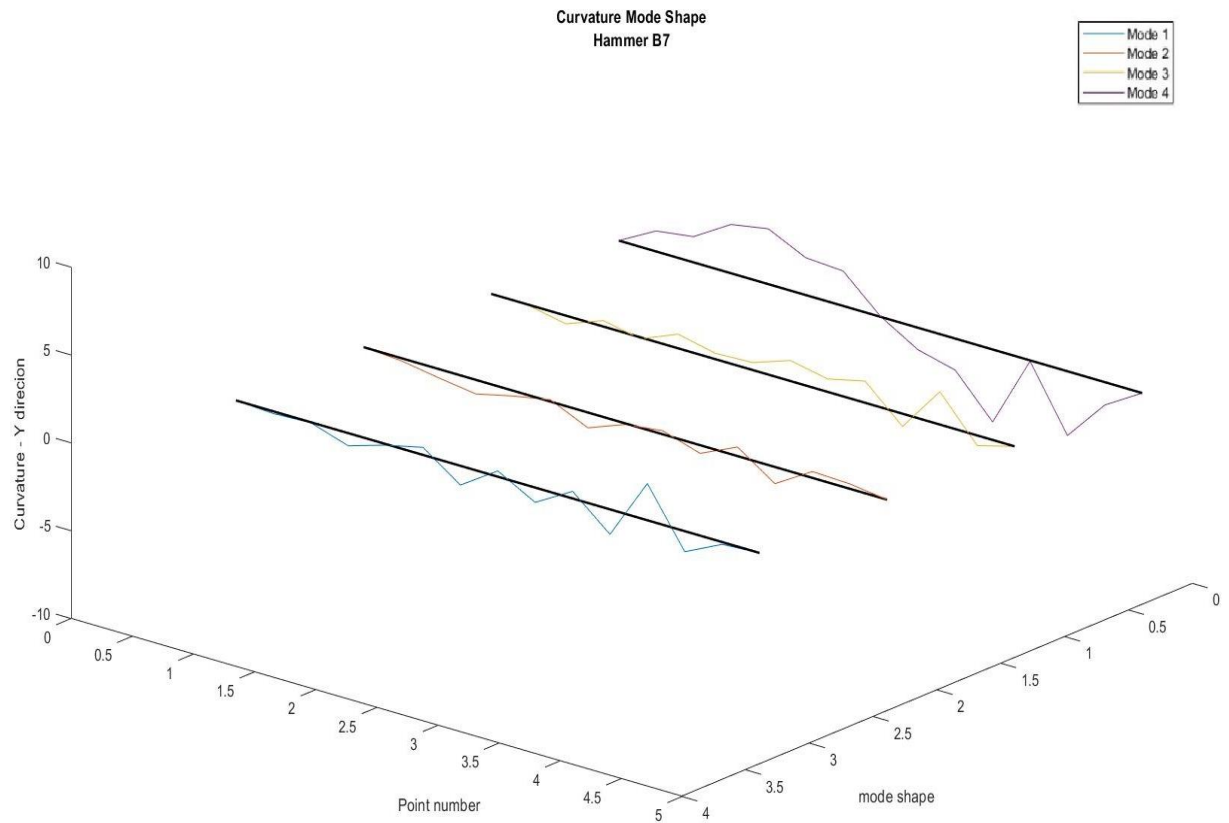


Fig. 25 Experimental curvature mode shape.

5.2 FEM

The structure that was modelled using the finite element software is a simply supported beam with double-T section which present a longitudinal length of 5m. It is characterized by a different thickness of the elements: 1 mm for the flanges and 1.5 mm for the web; the structure has small cantilevers at the extremities of 50mm.

5.2.1 Pre-processor

The geometry of the structure under examination has been realized through command codes written on a text file reported in the appendix. First, points were created by means of coordinates using parameters that allow to easily and automatically move from one model to another. The parameters used are shown in the following table:

Parameters	Values [m]	Description
L	5	Beam lenght
H	0,19	Beam height
B	0,2	Beam width
A	0,005	Length of the cantilever at the extremitie
d	3,65	Crack position
f	depends on model	Crack height
c	depends on model	Crack width

Table 10 Information on parameters.

After making the points, according to the above parameters, the lines and then the areas were created.

The different models tested are:

- Intact beam, without crack;
- Damaged beam with crack of 1 mm;
- Damaged beam with crack of 10 mm;
- Damaged beam with crack of 25 mm;
- Damaged beam with crack of 50 mm;

The damaged beams were modelled through a triangular opening in the web at the point of connection with the lower flange. with the same base and height ($f=c$); the position of the crack was inserted at a distance of 3.65 m from the left end of the beam and . This structural detail is shown in the image below:

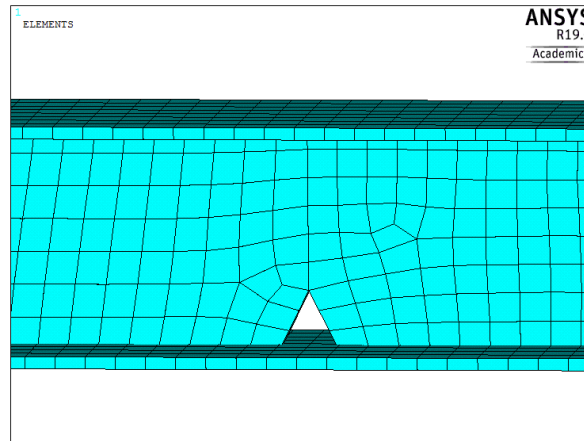


Table 11 Structural detail: example of triangular crack.

The material properties that have been inserted in the input data are shown in the following table:

Parameters	Values	Description
EX	8,50E+09	Elastic modulus in X direction
EY	2,85E+10	Elastic modulus in Y direction
EZ	8,50E+09	Elastic modulus in Z direction
PRXY	0,25	Poisson's ratio in XY plane
PRYZ	0,25	Poisson's ratio in YZ plane
PRXZ	0,12	Poisson's ratio in XZ plane
GXY	2,50E+09	Shear modulus in XY plane
GYX	2,50E+09	Shear modulus in YZ plane
GXZ	3,50E+09	Shear modulus in XZ plane
DENS	1734	Density

Table 12 Material properties input data.

The only element that has been used is the "shell281" element. Since the beam is characterized by different thicknesses between web and flanges, two sections have been created:

- Section 1: 10 mm for the flanges;
- Section 2: 15 mm for the web.

A quadrangular mesh (mapped) with a size of 0.025 m was used for all models, as follows:

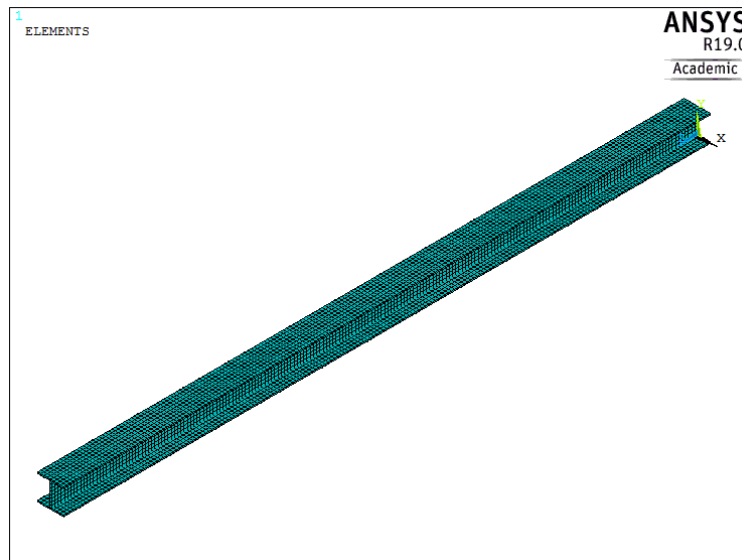


Fig. 26 Model of intact beam from Ansys.

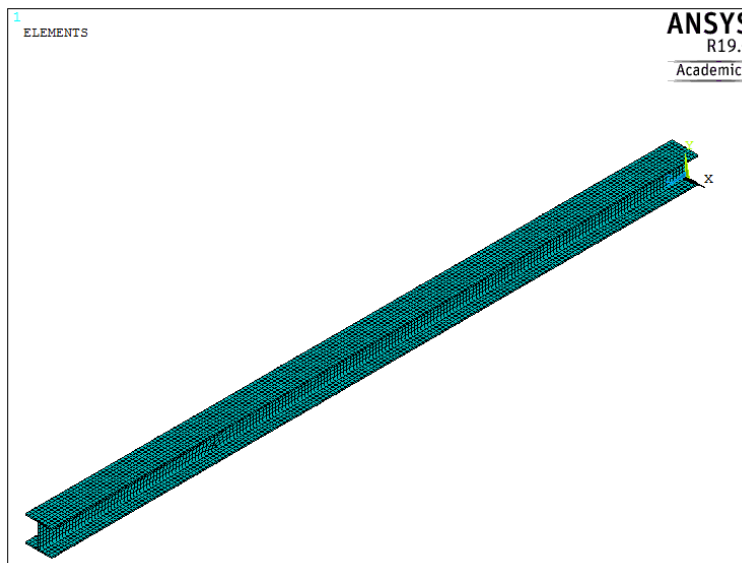


Fig. 27 Damaged beam from Ansys.

5.2.2 Post-Processor

Once the pre-processing operations have been completed, the finite element *modal analysis* is resolved. The graphs obtained from the modal analysis are shown as follows.

The data relative to the mode shapes has been obtained through the writing of a code that allows to generate a text file containing the displacements of modal shapes.

- Intact beam

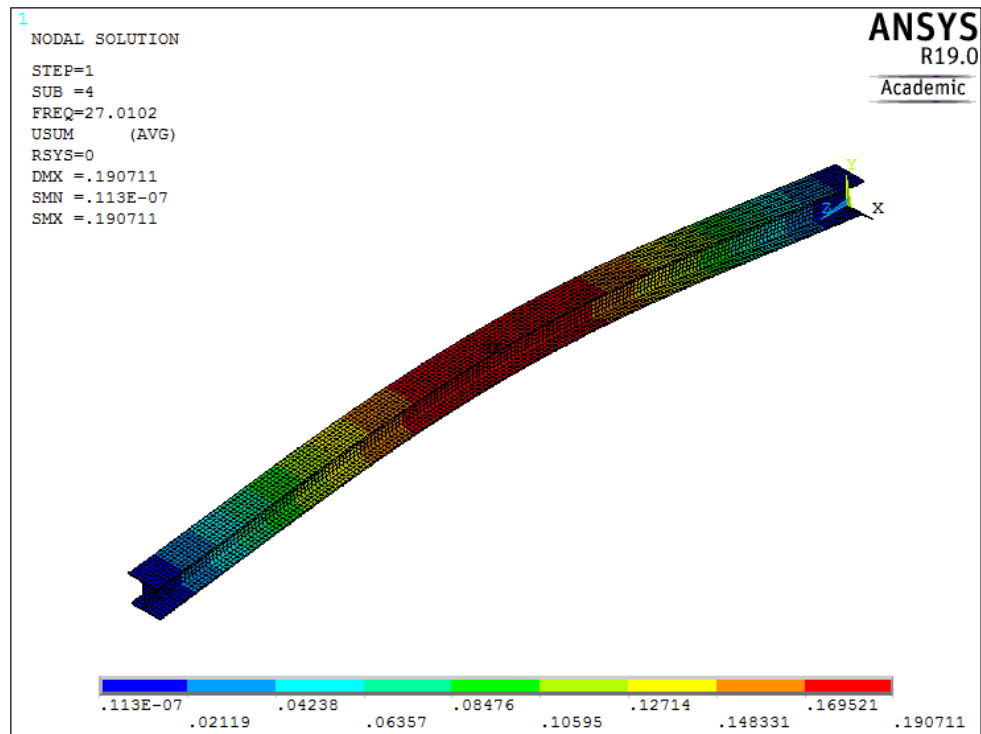


Fig. 28 Intact beam: mode shape 1 from Ansys.

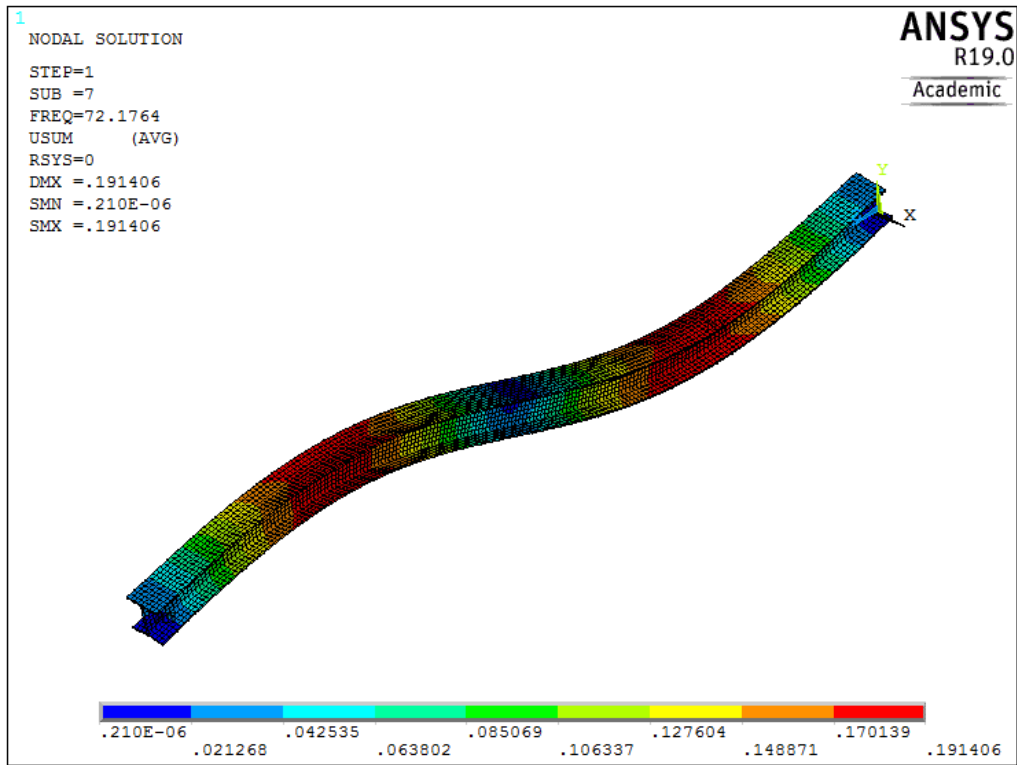


Fig. 29 Intact beam: mode shape 2 from Ansy.

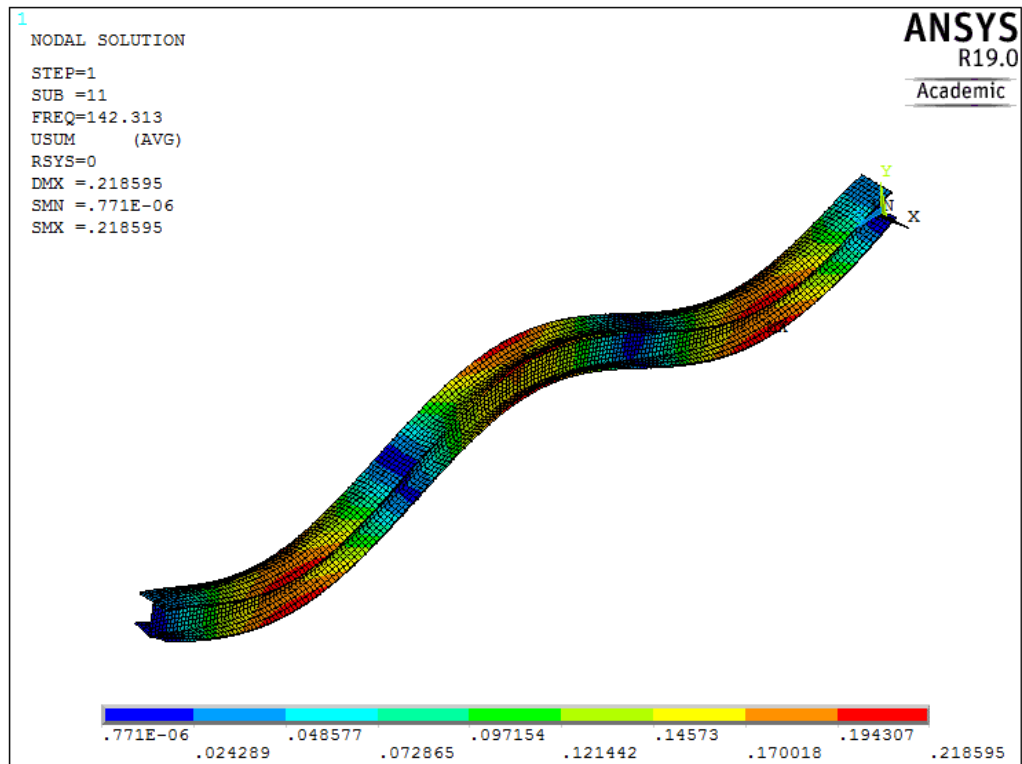


Fig. 30 Intact beam: mode shape 3 from Ansys.

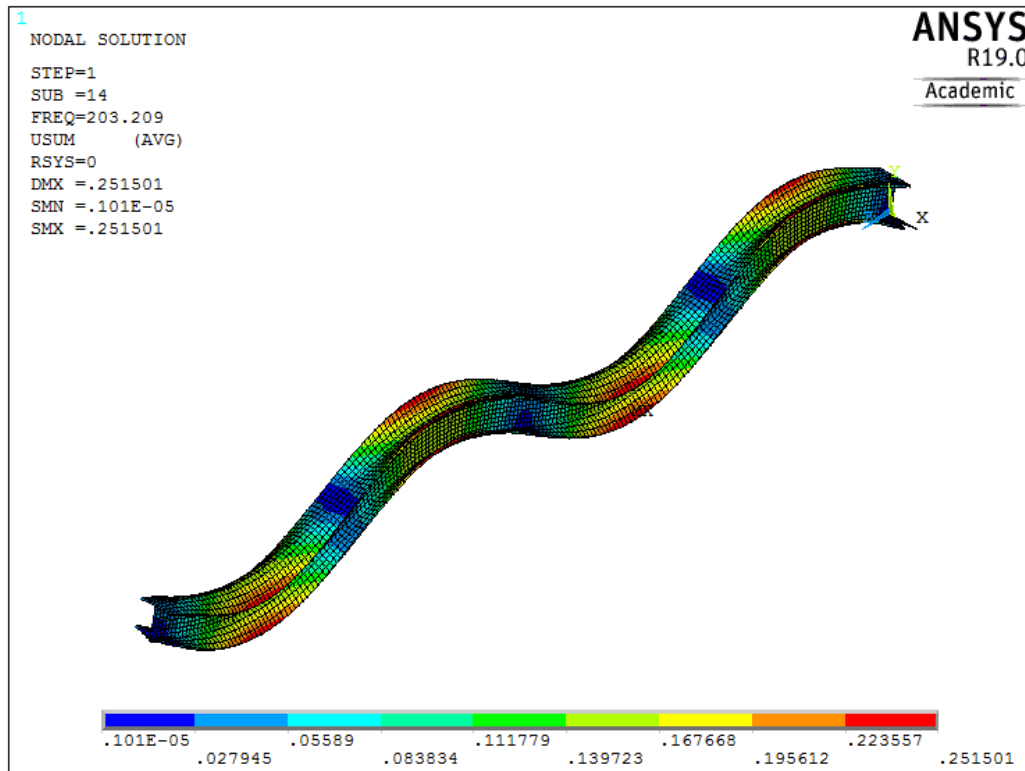


Fig. 31 Intact beam: mode shape 4 from Ansys.

- Damaged beam with crack of 1 mm

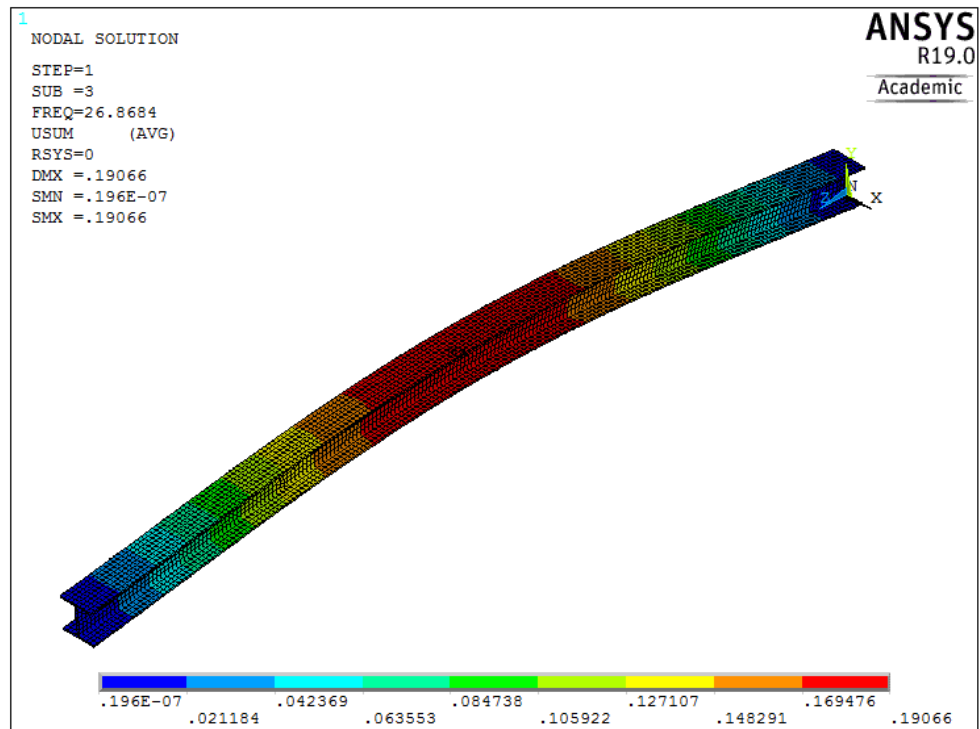


Fig. 32 Damaged beam with crack of 1 mm: mode shape 1 from Ansys.

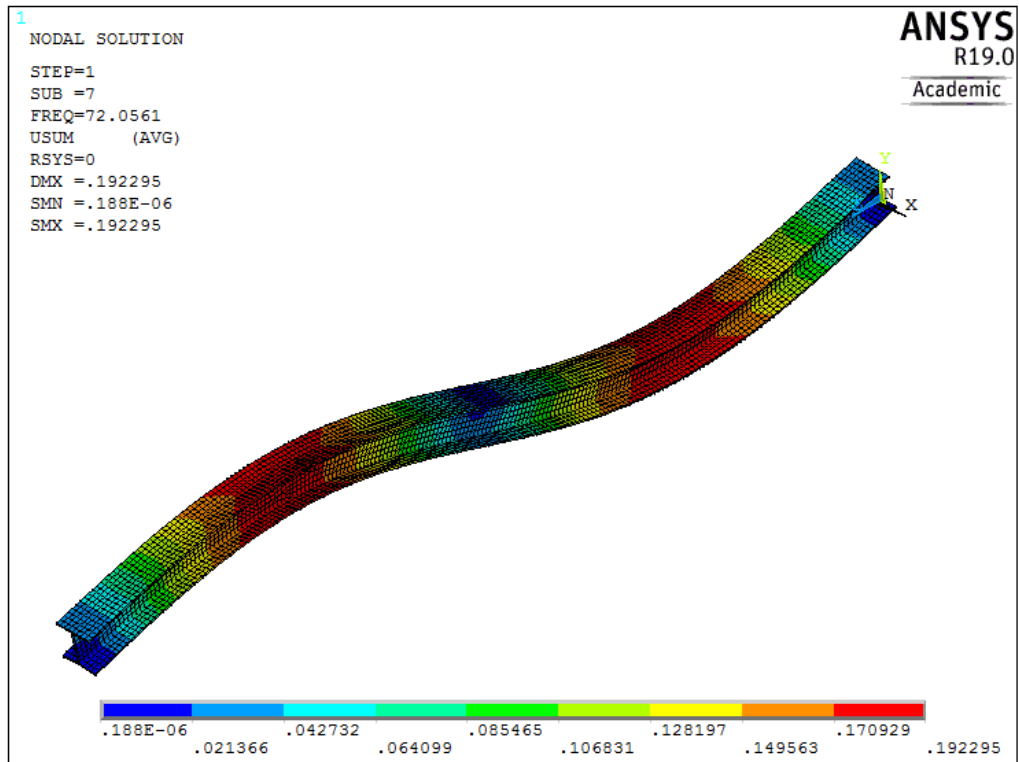


Fig. 33 Damaged beam with crack of 1 mm: mode shape 2 from Ansys.

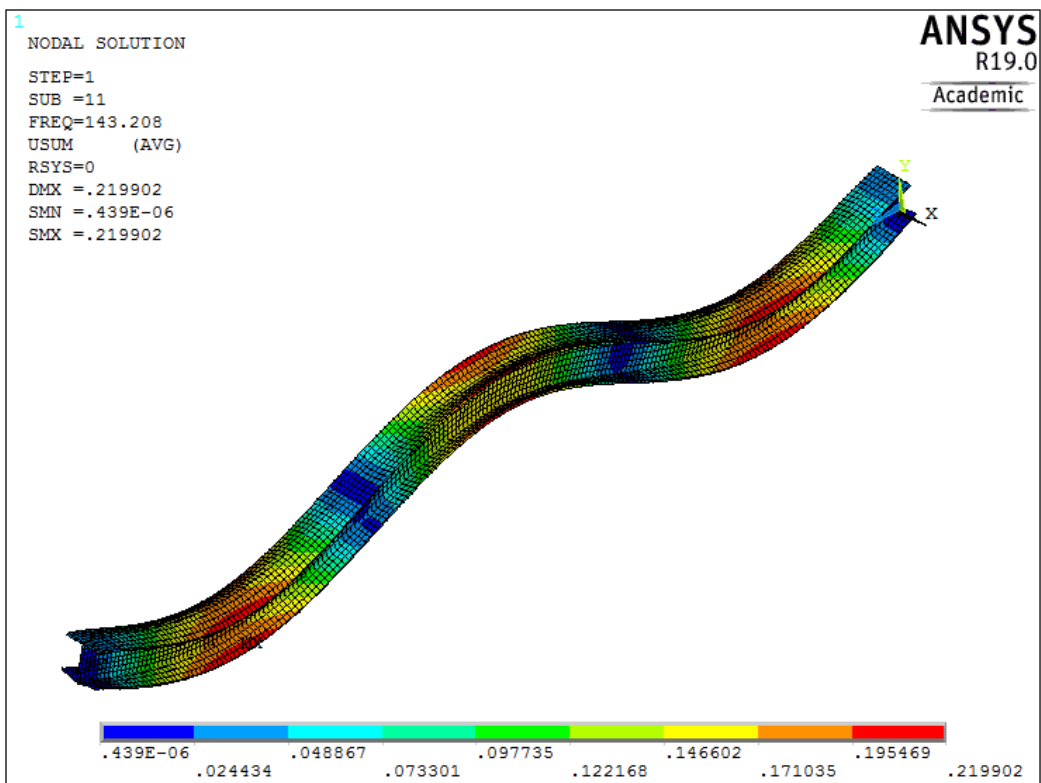


Fig. 34 Damaged beam with crack of 1 mm: mode shape 3 from Ansys.

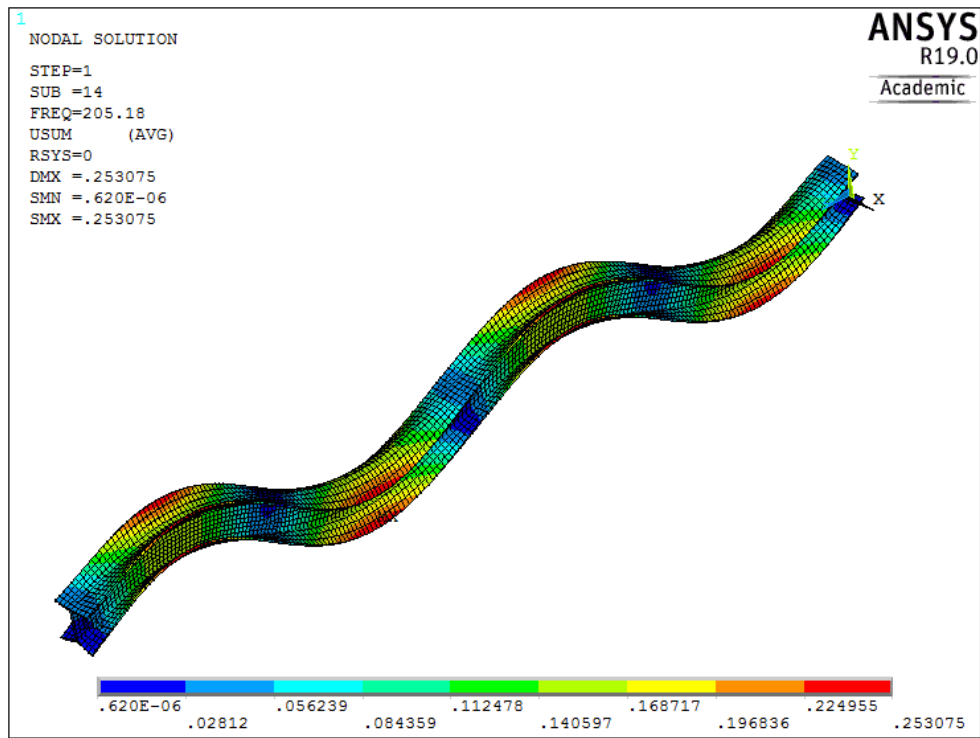


Fig. 35 Damaged beam with crack of 1 mm: mode shape 4 from Ansys.

- Damaged beam with crack of 10 mm

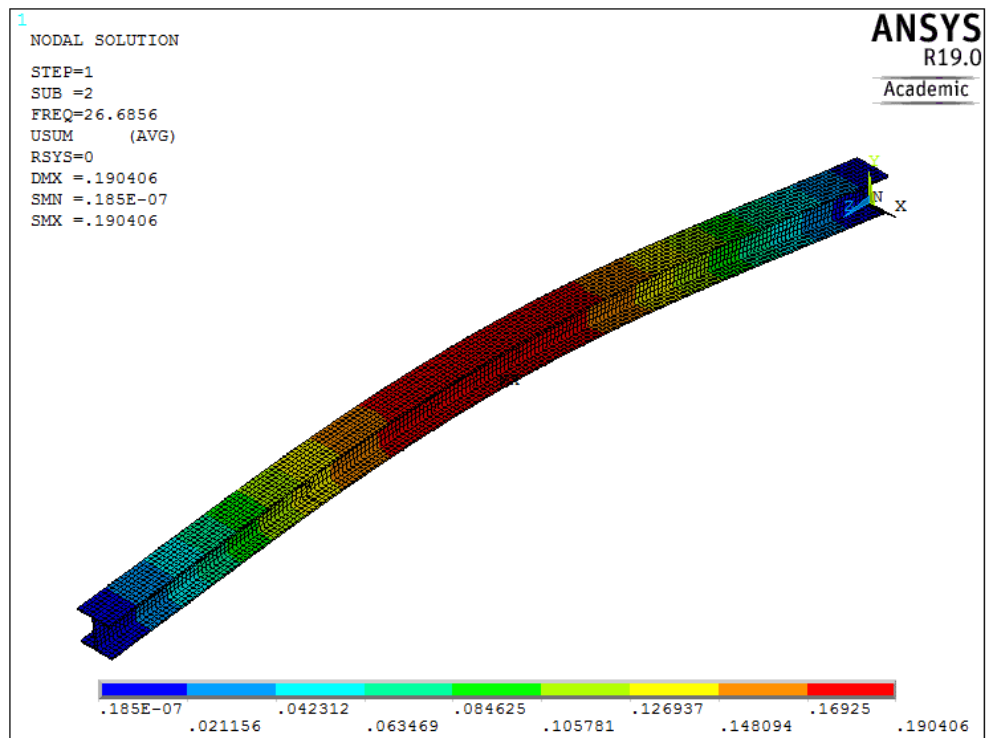


Fig. 36 Damaged beam with crack of 10 mm: mode shape 1 from Ansys.

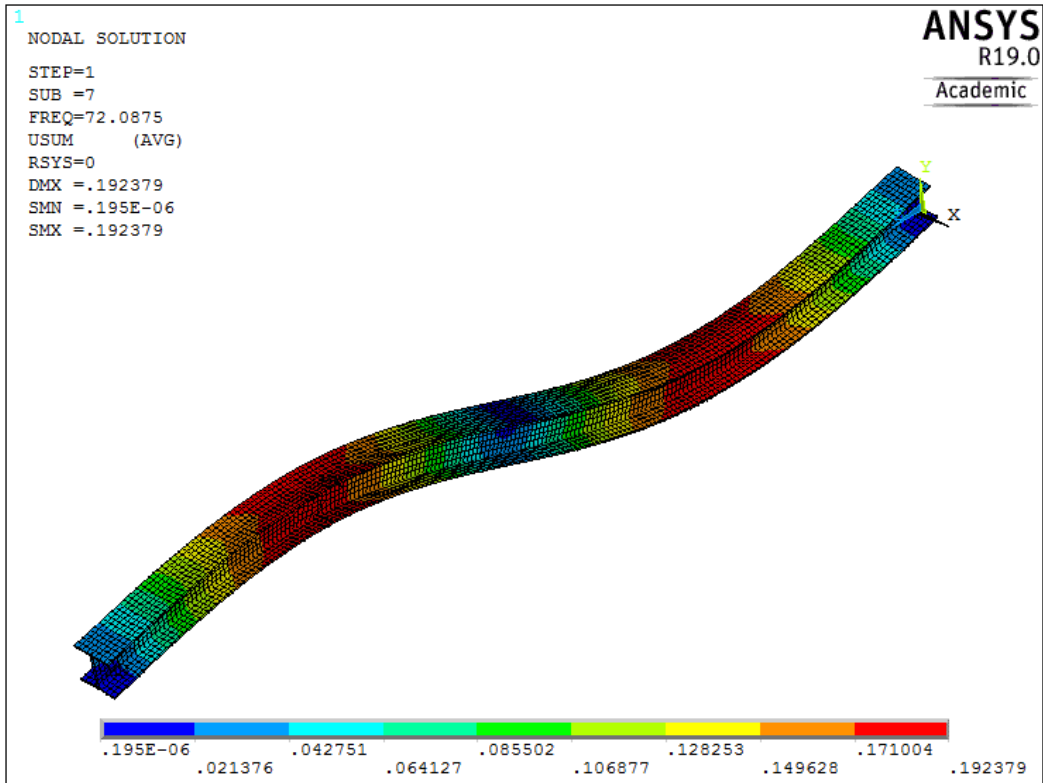


Fig. 37 Damaged beam with crack of 10 mm: mode shape 2 from Ansys.

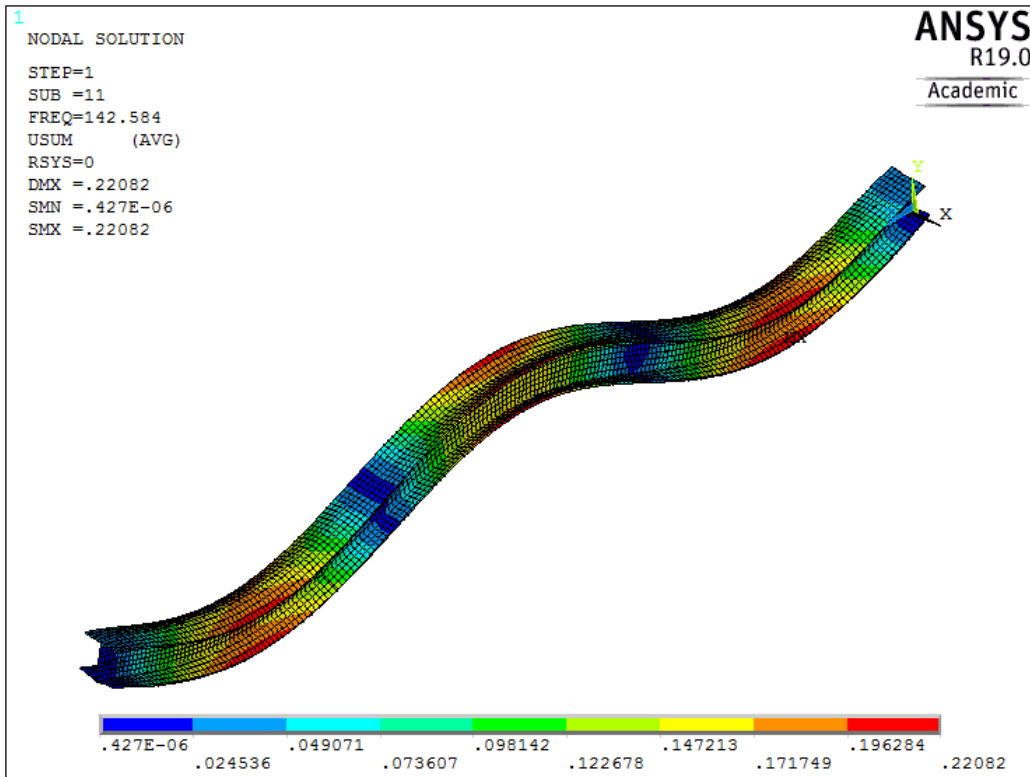


Fig. 38 Damaged beam with crack of 10 mm: mode shape 3 from Ansys.

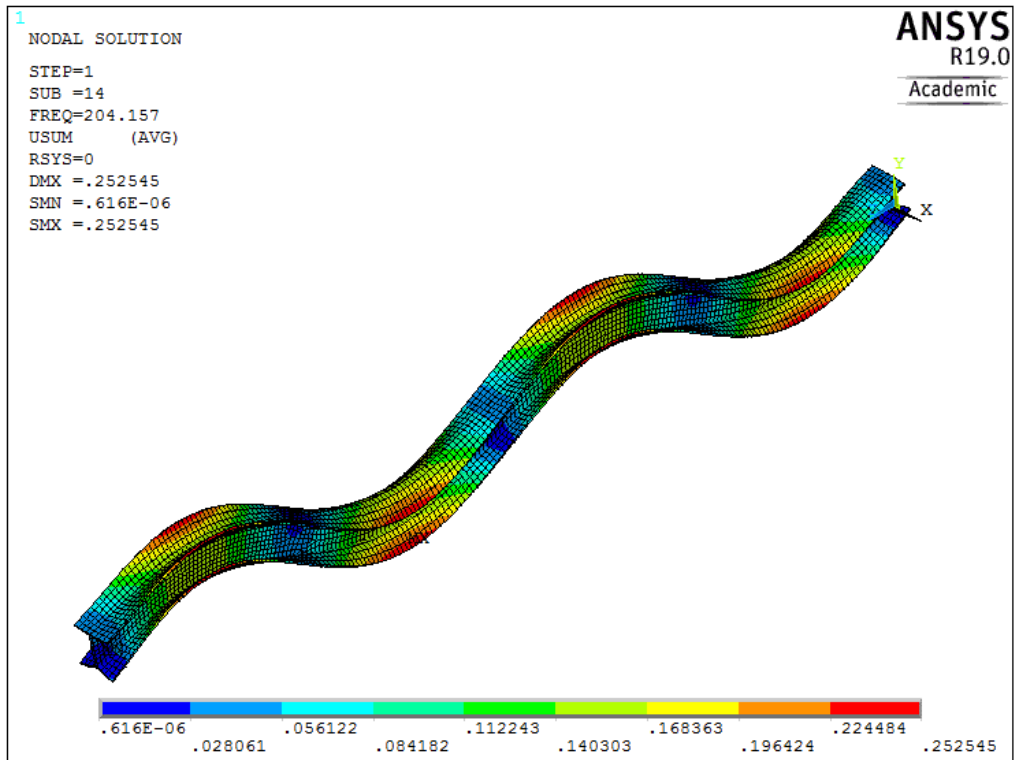


Fig. 39 Damaged beam with crack of 10 mm: mode shape 4 from Ansys.

- Damaged beam with crack of 25 mm

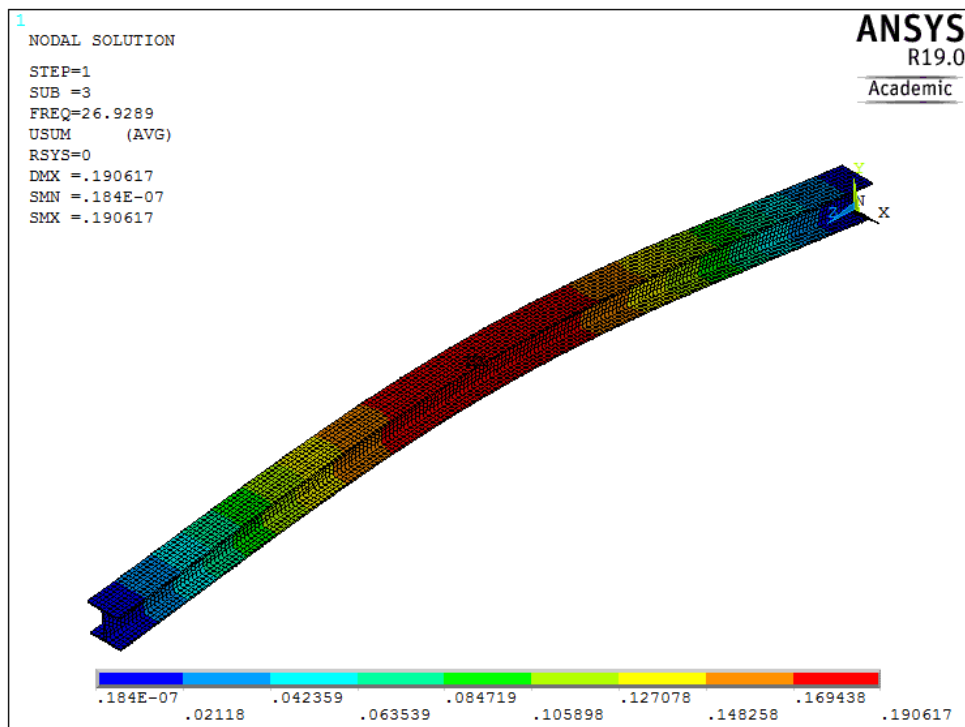


Fig. 40 Damaged beam with crack of 25 mm: mode shape 1 from Ansys.

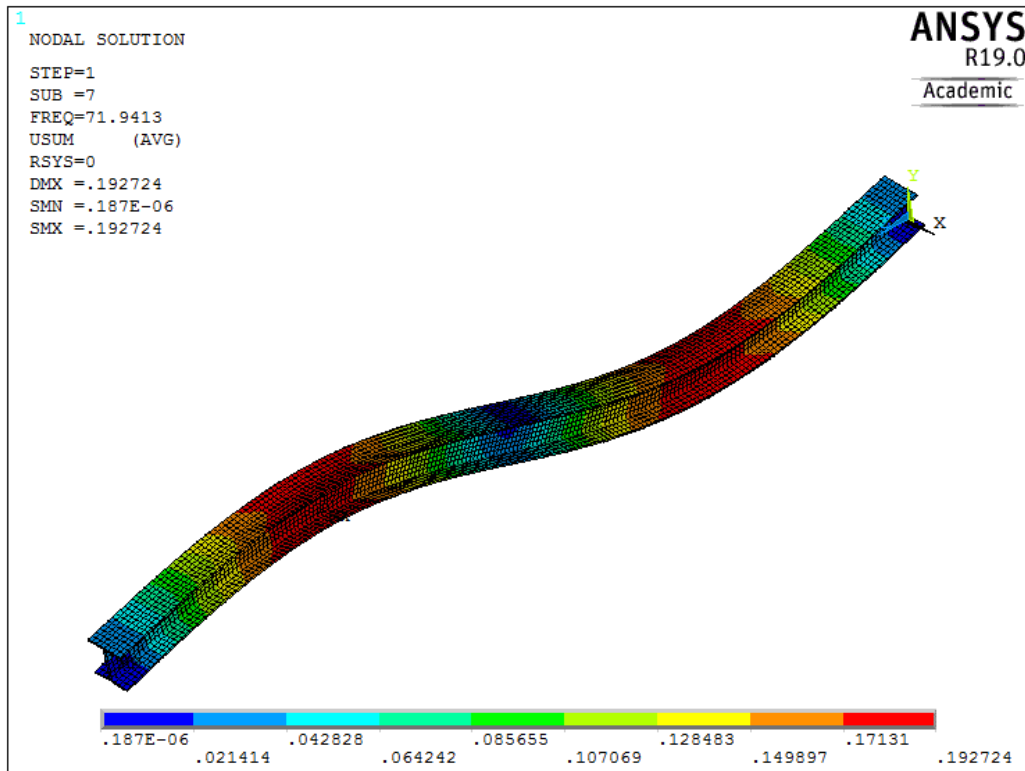


Fig. 41 Damaged beam with crack of 25 mm: mode shape 2 from Ansys.

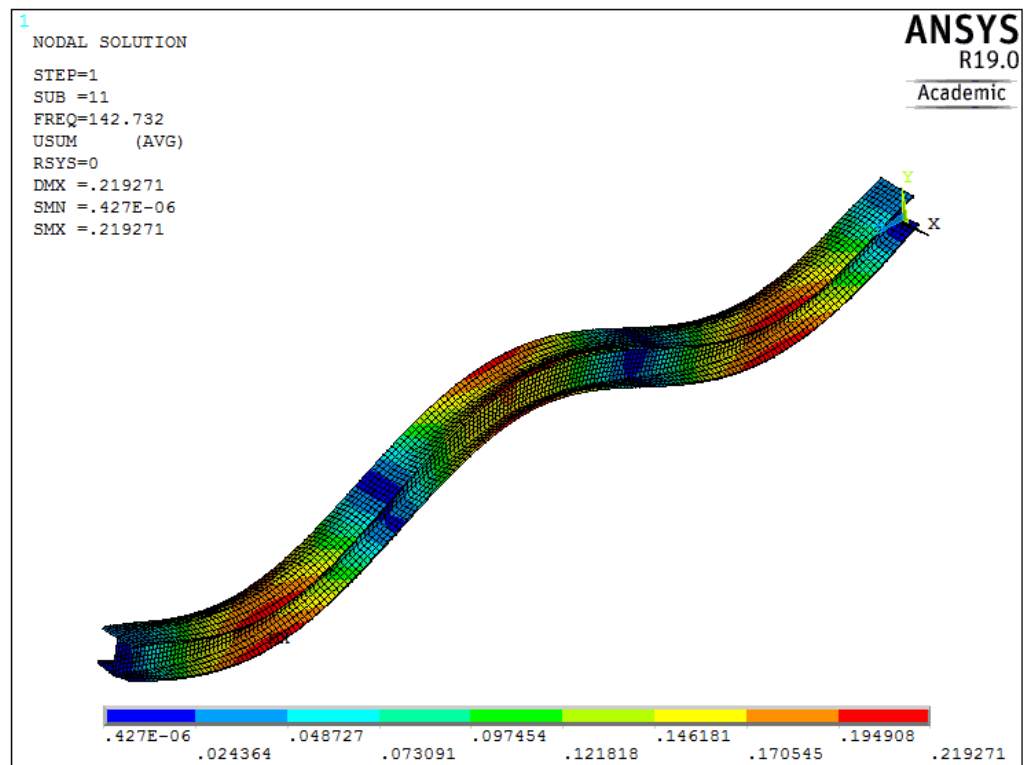


Fig. 42 Damaged beam with crack of 25 mm: mode shape 3 from Ansys.

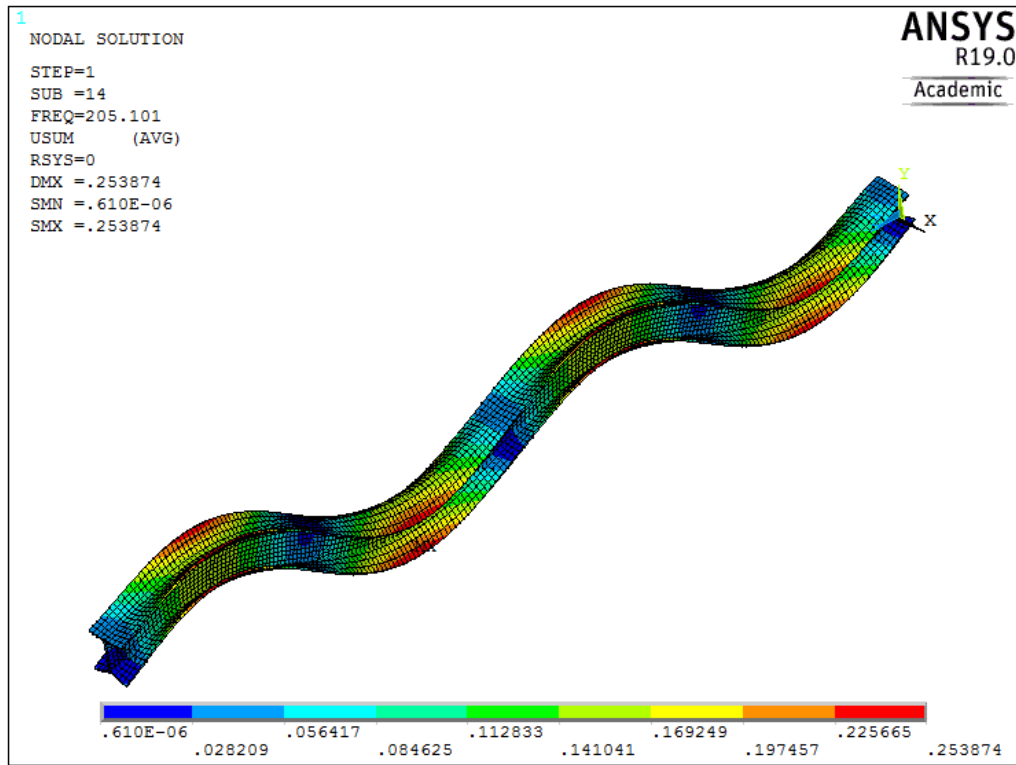


Fig. 43 Damaged beam with crack of 25 mm: mode shape 4 from Ansys.

- Damaged beam with crack of 50 mm

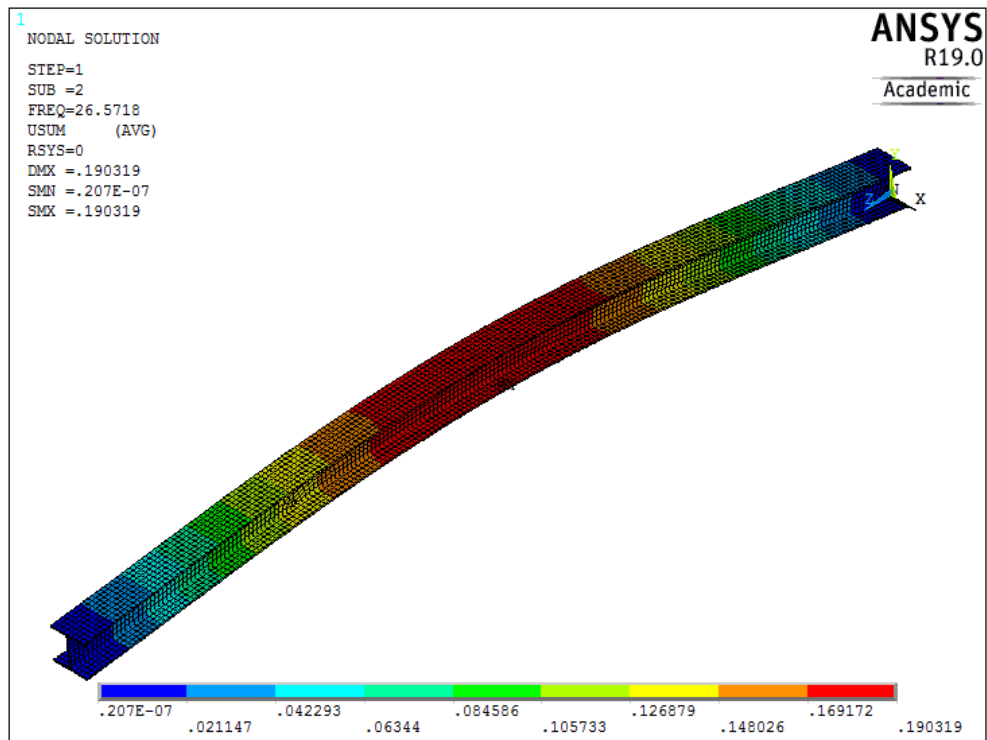


Fig. 44 Damaged beam with crack of 50 mm: mode shape 1 from Ansys.

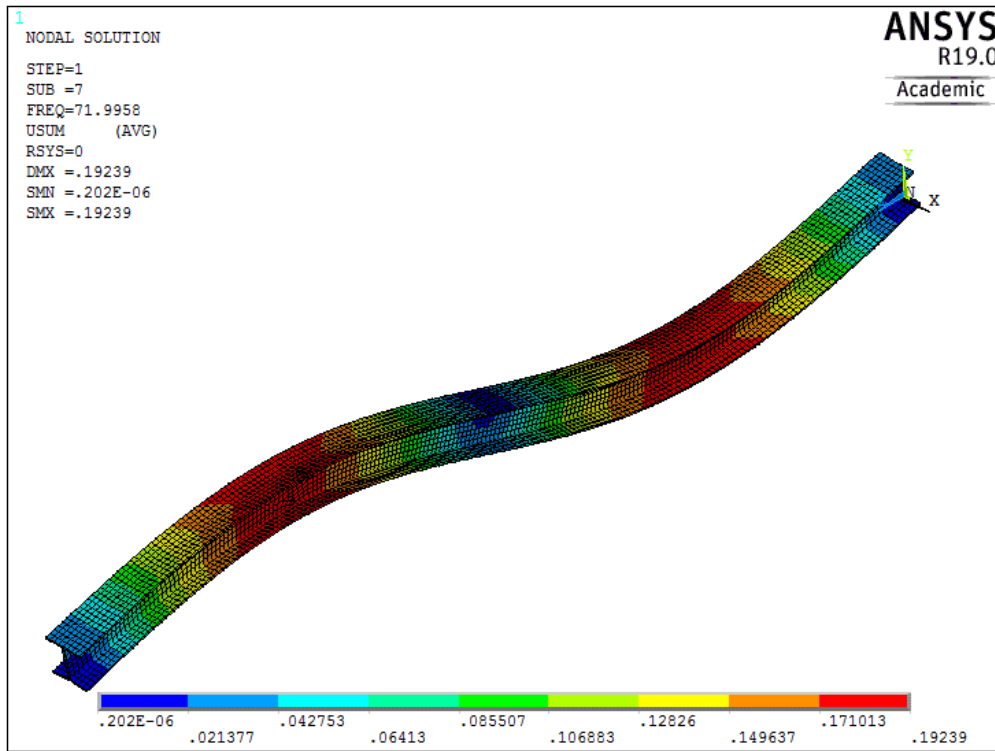


Fig. 45 Damaged beam with crack of 50 mm: mode shape 2 from Ansys.

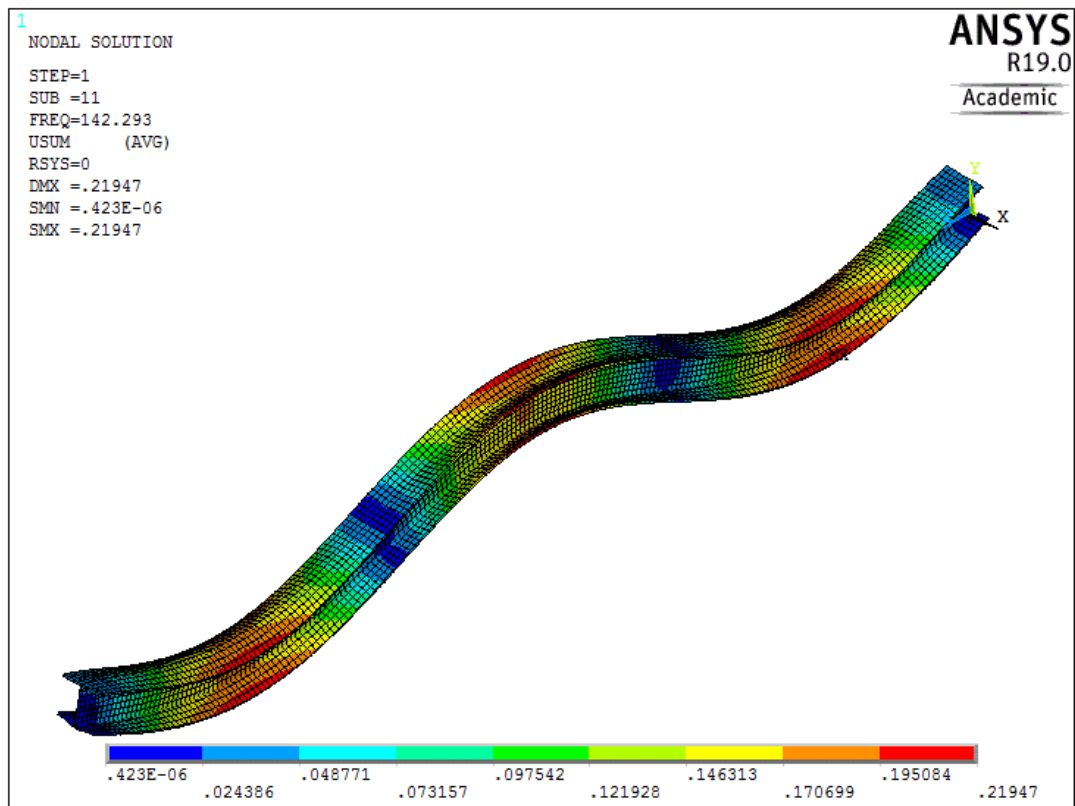


Fig. 46 Damaged beam with crack of 50 mm: mode shape 3 from Ansys.

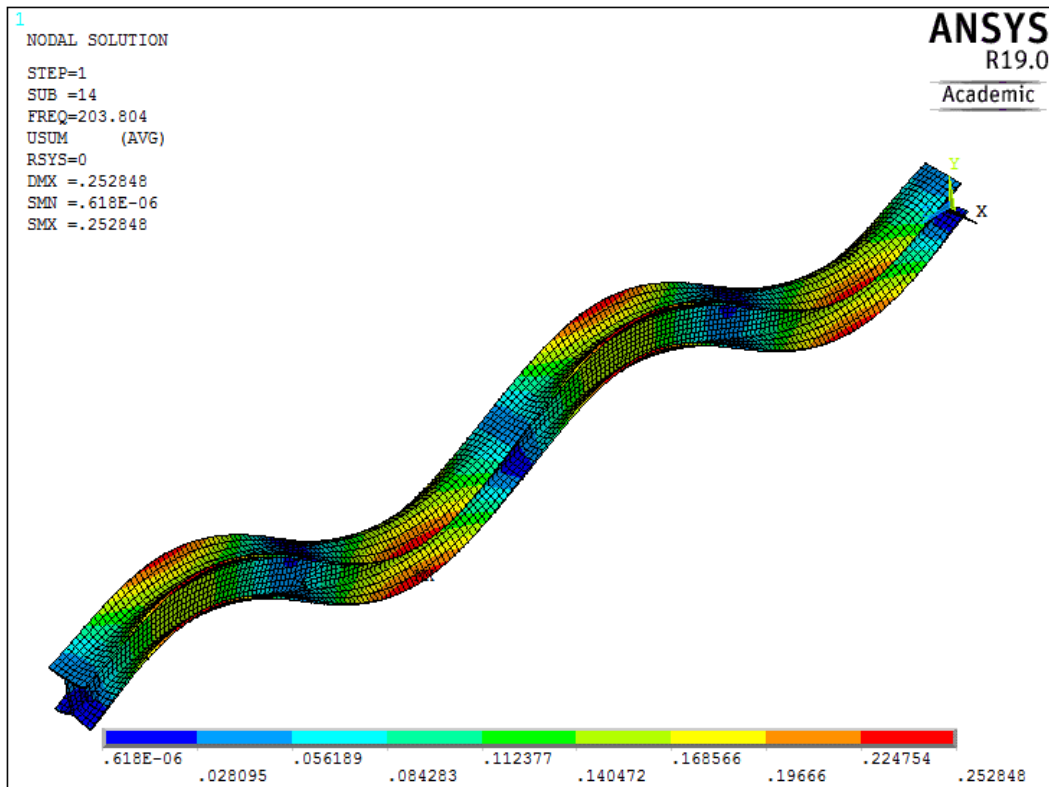


Fig. 47 Damaged beam with crack of 50 mm: mode shape 4 from Ansys.

All the mode shapes mentioned above have been processed, in the following paragraphs, using *Treed Gaussian Process* algorithm and *Curvature* method.

5.3 Curvature method on analytic models

The calculation of the curvatures has been carried out starting from the mode shapes obtained by Ansys software. The analytical formulation (number 42) has been expressed in the paragraph (3.2.2) on the method of curvatures.

To obtain the data of the mode shapes, from Ansys, data has been recorded from all the nodes present on the top flange with coordinates $X=0$ and $Y=0.19$; for a total of 401 nodes, therefore as if 401 accelerometers were available.

- Intact beam curvatures

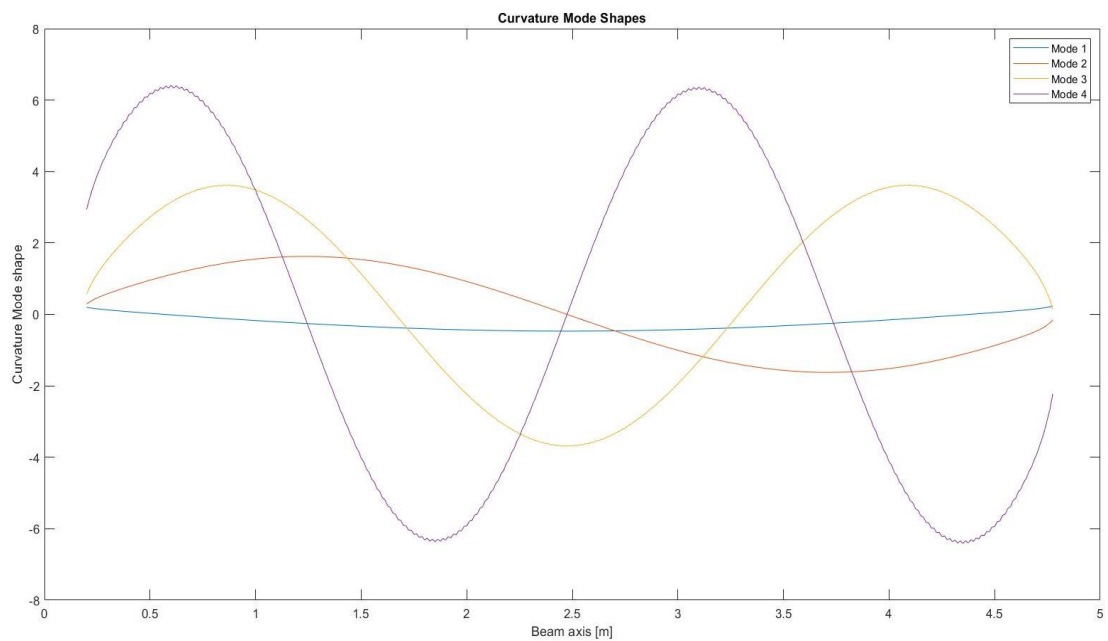


Fig. 48 Curvature Mode Shapes: intact beam.

These curves have been defined on 401 points.

- Damaged beam curvatures with crack of 1 mm

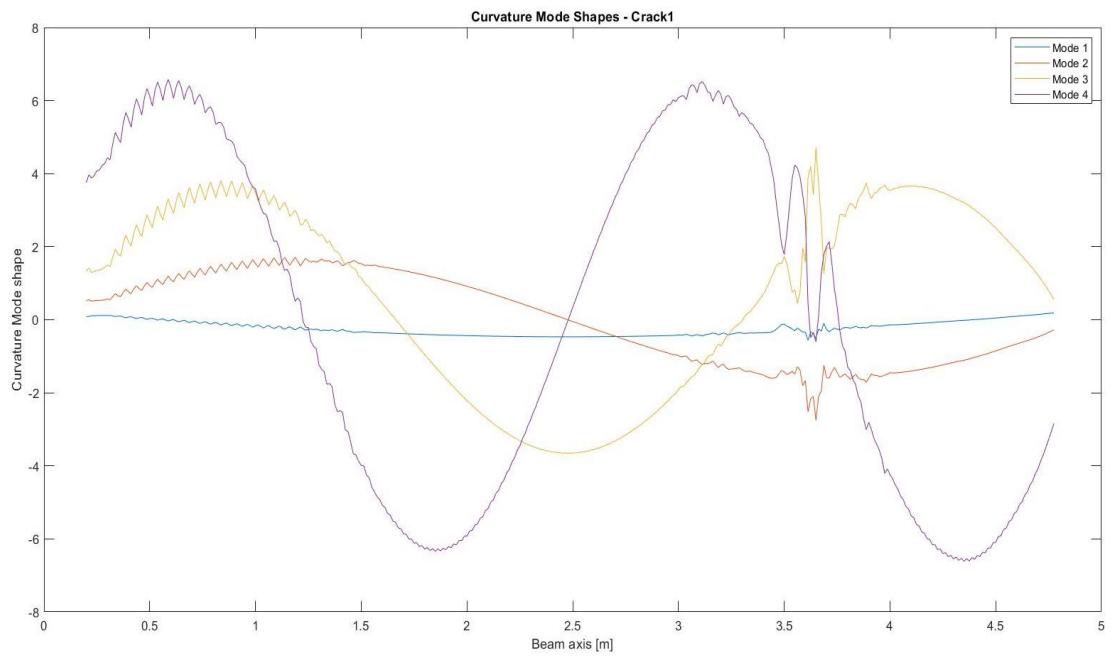


Fig. 49 Curvature Mode Shapes: damaged beam with crack of 1 mm.

- Damaged beam curvatures with crack of 10 mm

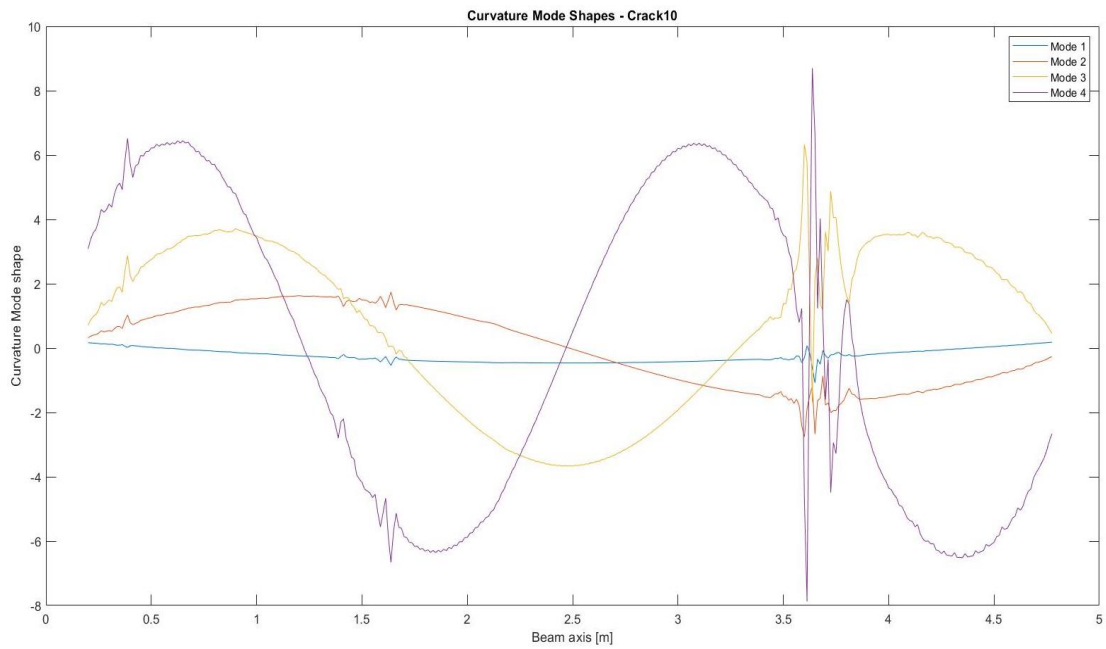


Fig. 50 Curvature Mode Shapes: damaged beam with crack of 10 mm.

- Damaged beam curvatures with crack of 25 mm

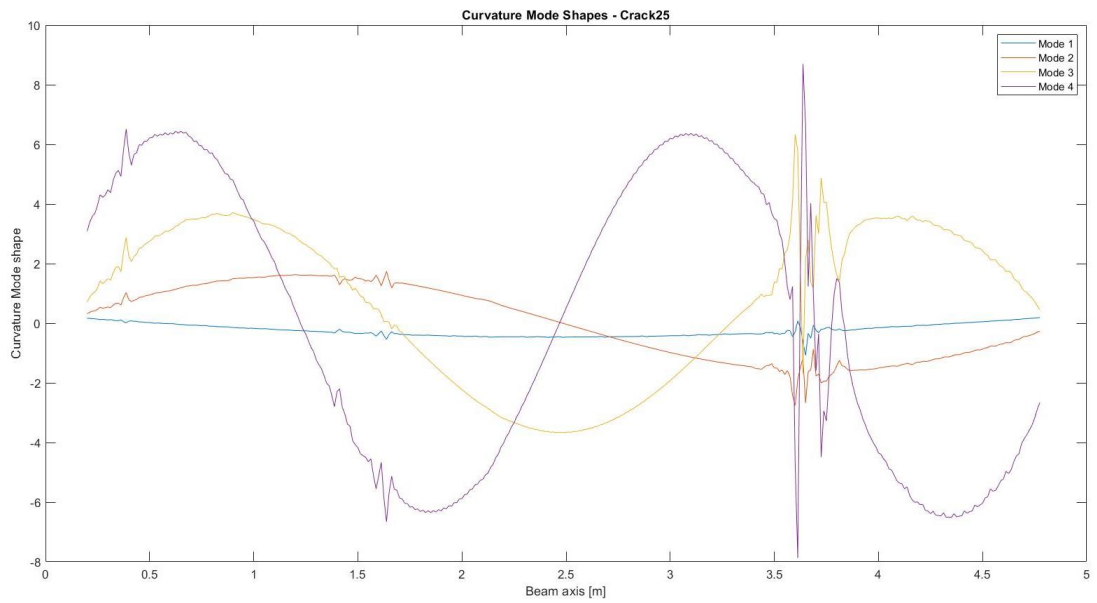


Fig. 51 Curvature Mode Shapes: damaged beam with crack of 25 mm.

- Damaged beam curvatures with crack of 50 mm

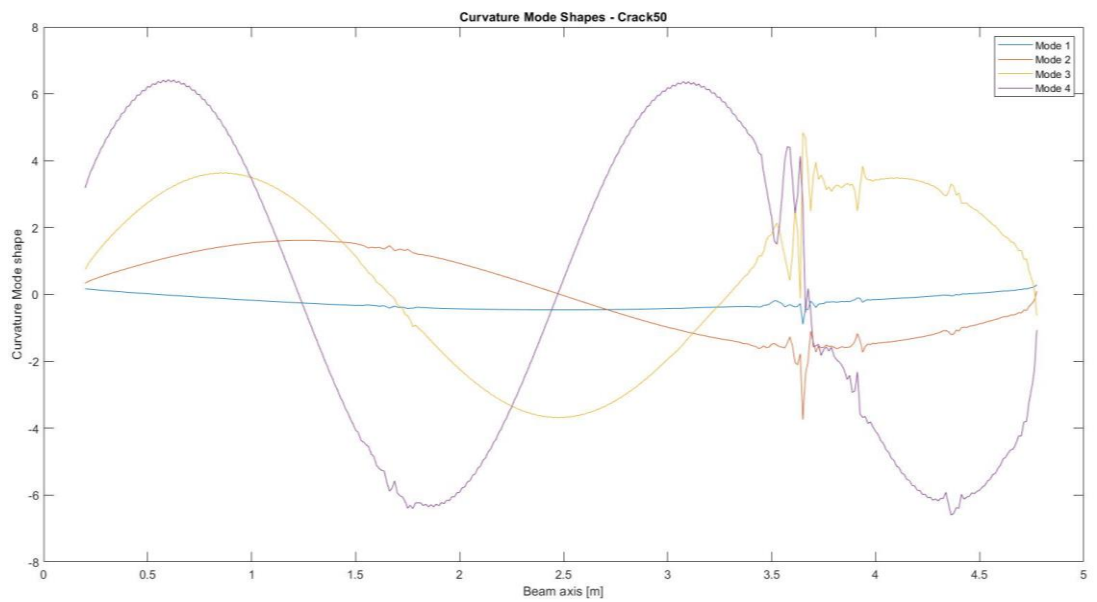


Fig. 52 Curvature Mode Shapes: damaged beam with crack of 50 mm.

Once the curvatures for all mode shapes were calculated, the differences between the cracked beam models and the intact beam model were calculated.

- Differences in curvatures between the intact beam model and cracked beam model with crack of 1 mm.

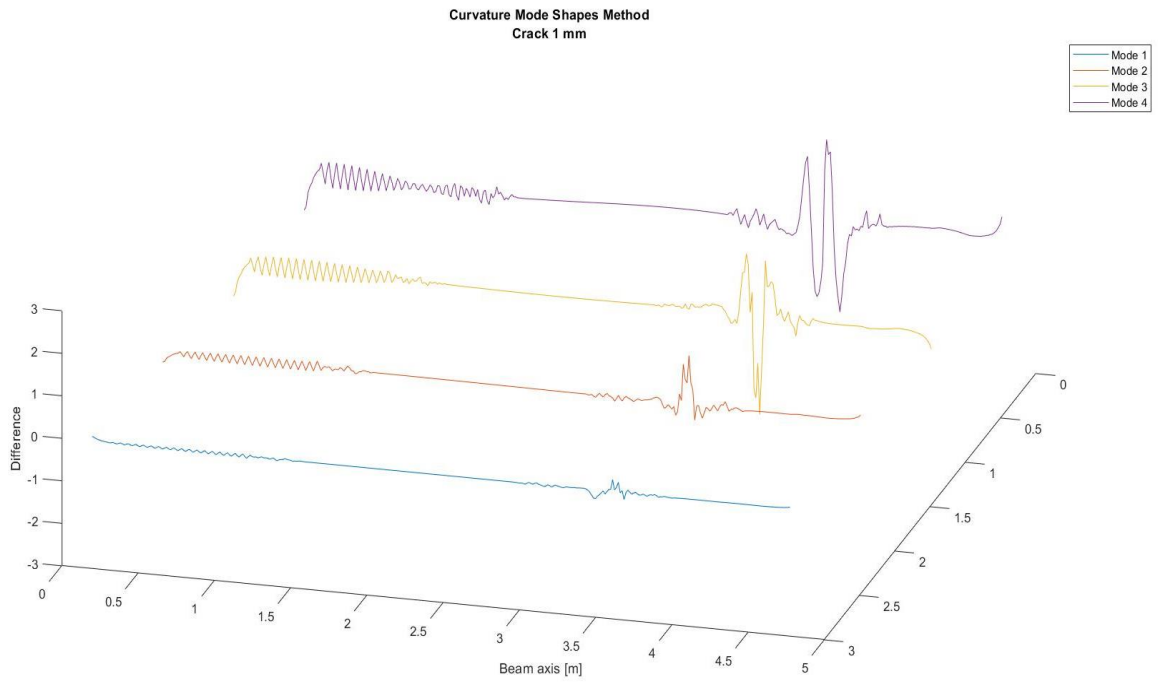


Fig. 53 Plot 3D: differences in curvatures for cracked beam model with crack of 1 mm.

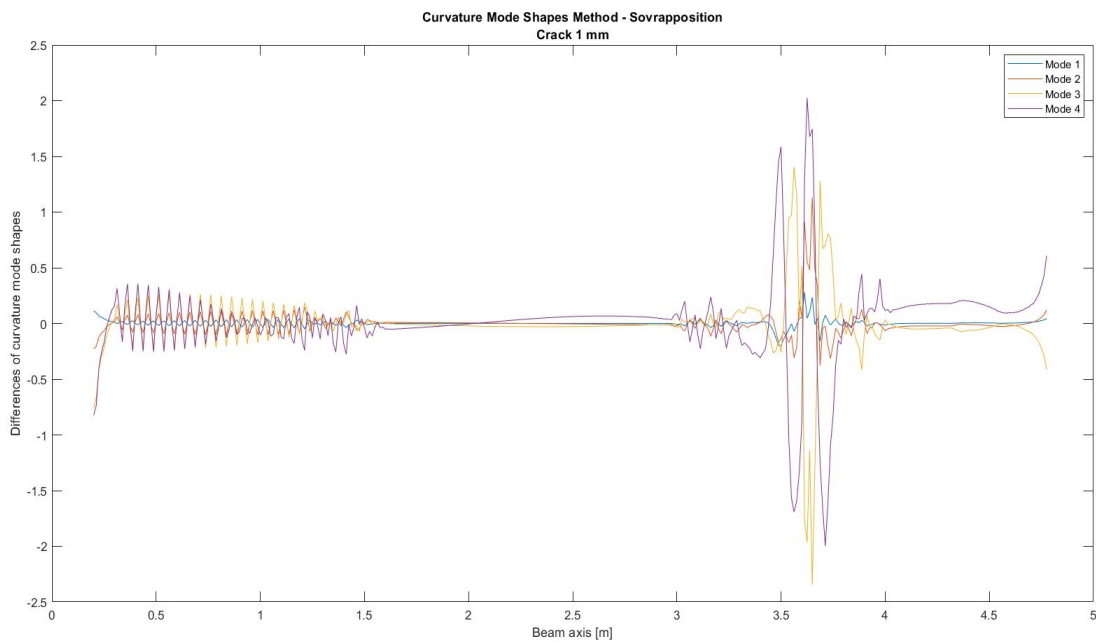


Fig. 54 Differences in curvatures for cracked beam model with crack of 1 mm.

- Differences in curvatures between the intact beam model and cracked beam model with crack of 10 mm.

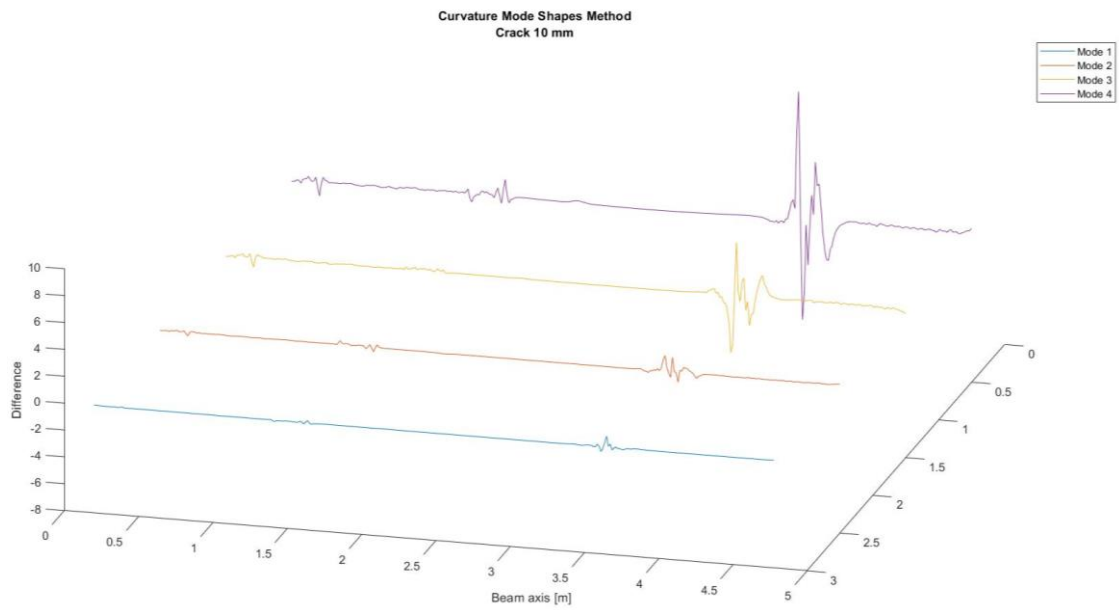


Fig. 55 Plot 3D: differences in curvatures for cracked beam model with crack of 10 mm.

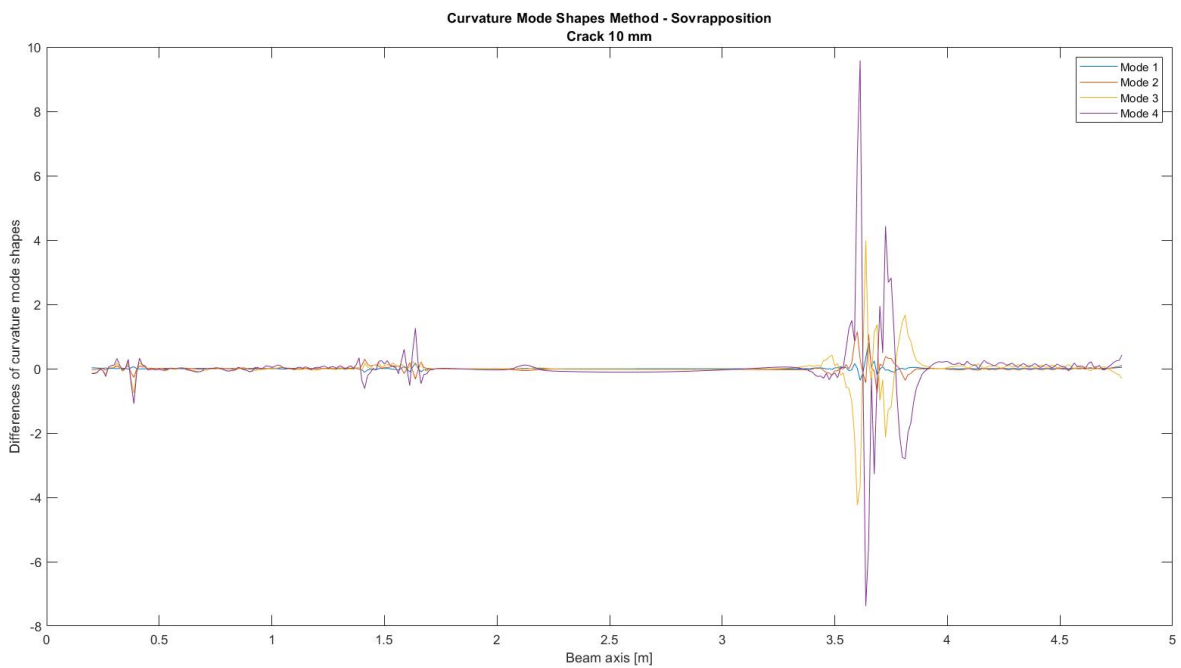


Fig. 56 Differences in curvatures for cracked beam model with crack of 10 mm.

- Differences in curvatures between the intact beam model and cracked beam model with crack of 25 mm.

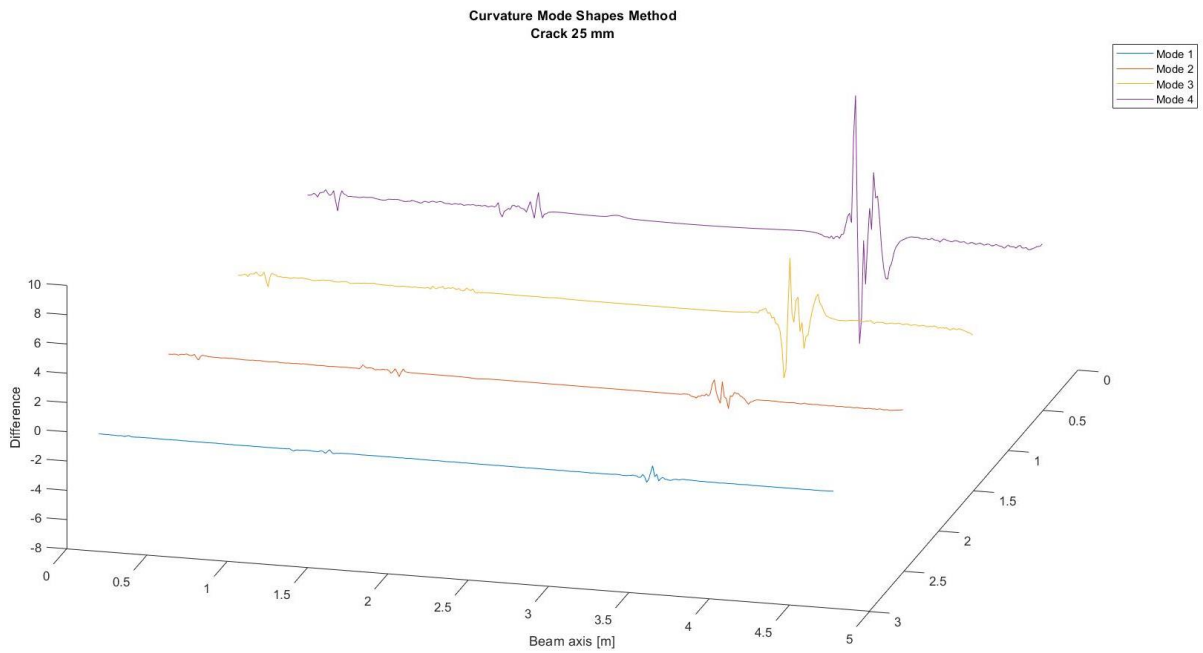


Fig. 57 Plot 3D: differences in curvatures for cracked beam model with crack of 25 mm.

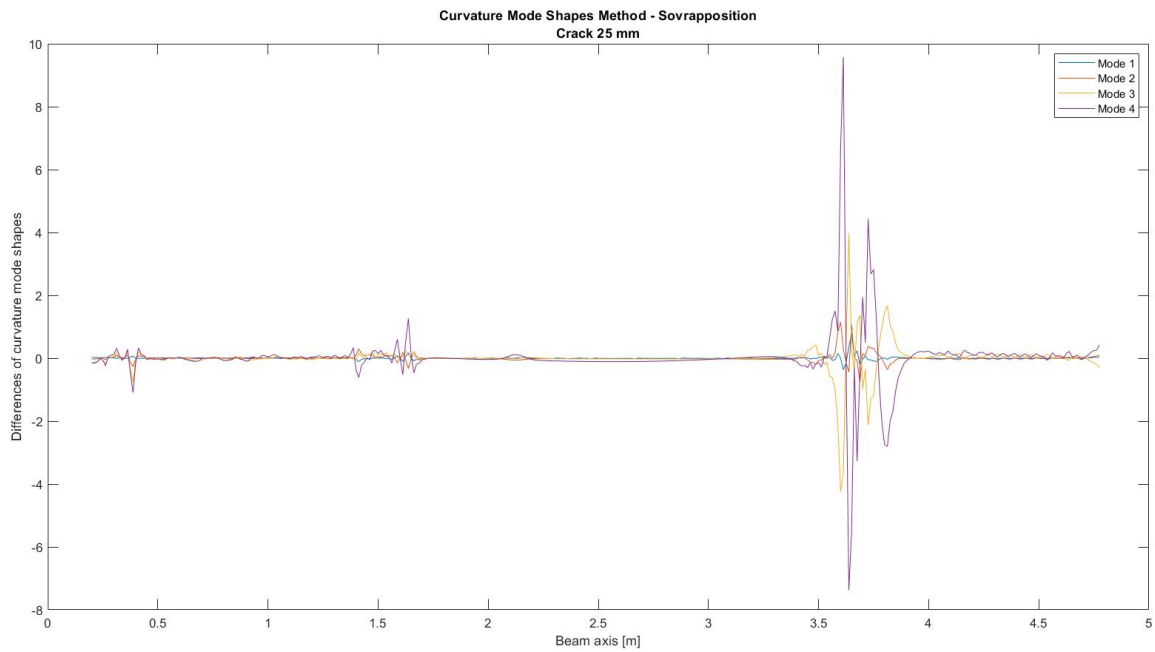


Fig. 58 Differences in curvatures for cracked beam model with crack of 25 mm.

- Differences in curvatures between the intact beam model and cracked beam model with crack of 50 mm.

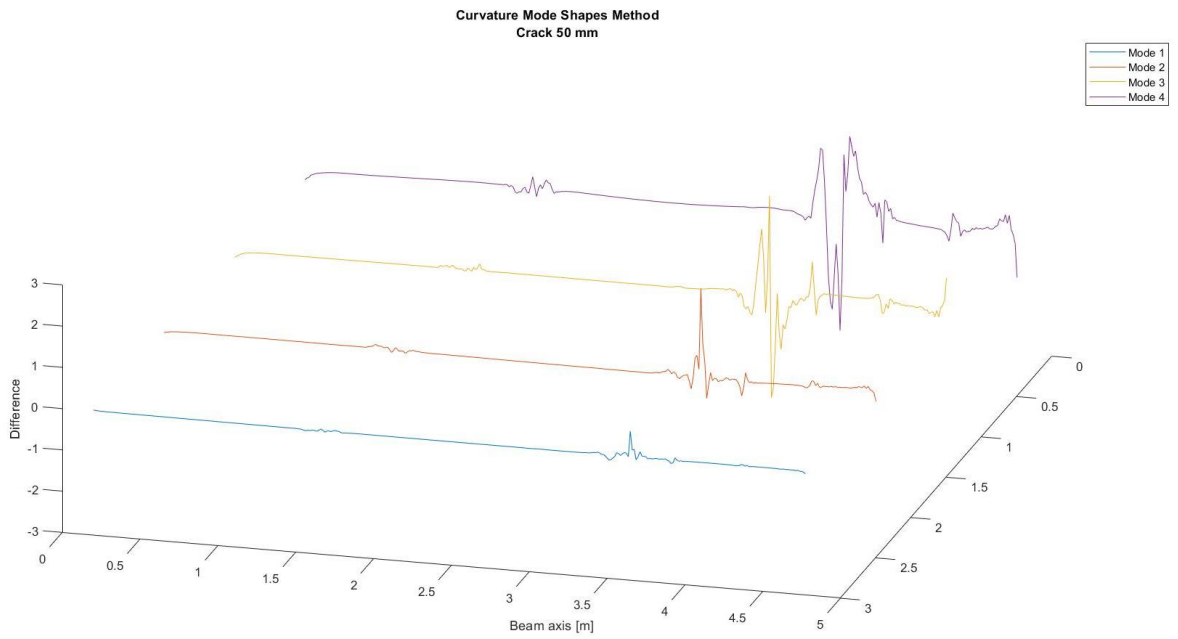


Fig. 59 Plot 3D: differences in curvatures for cracked beam model with crack of 50 mm.

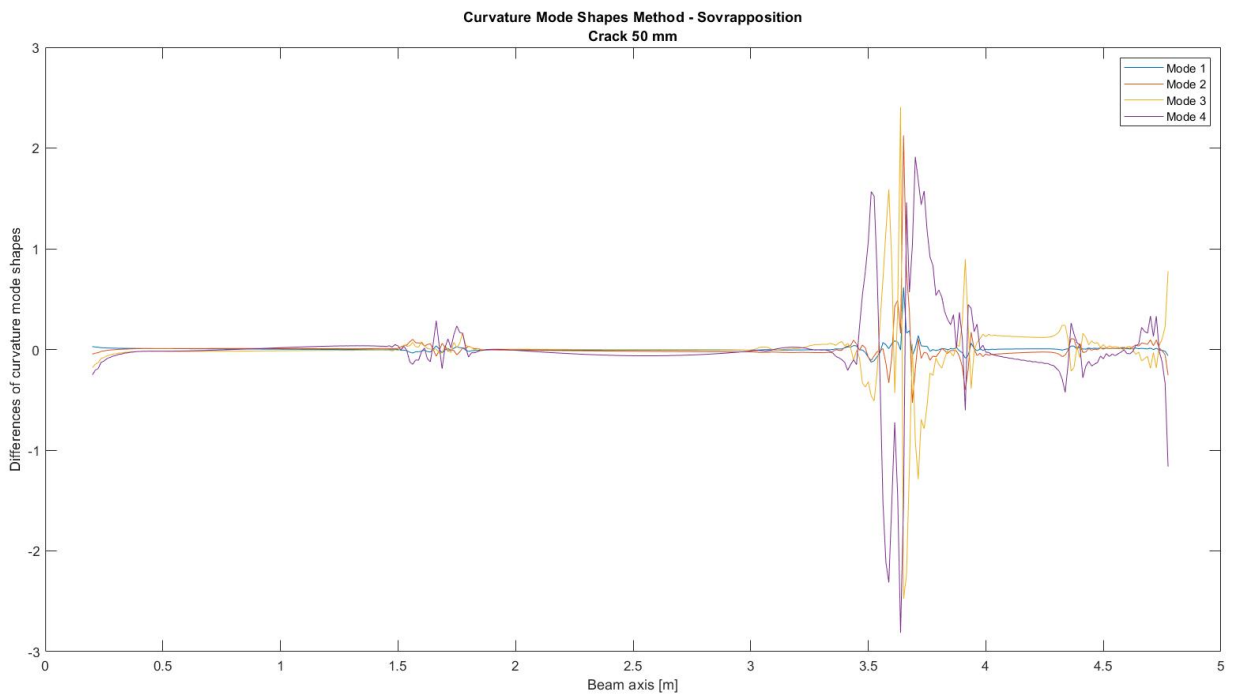


Fig. 60 Differences in curvatures for cracked beam model with crack of 1 mm.

The results obtained for the different crack sizes show that the curvature method is able to identify a precise area where a crack is present. The changes in the curvature mode shapes are localized in the area of damage. The previously reported results serve as support for subsequent tests.

In the next paragraph, the Treed Gaussian Process method will be used to localize the crack for both analytical and experimental data.

5.4 Treed Gaussian Process

The theoretical basis of the Treed Gaussian Process have been implemented in the R® software; analyses were carried out for both analytical and experimental data.

5.4.1 Analytical data

Before the analyses were carried out, all the data obtained in section 5.2.2 were dirtied with four type of noise of different intensities. This was done to make the simulation more real. Each eigenvector $\{\phi\}_i$ of the modal matrix has been normalised $\{\phi\}_{n,i}$ to its maximum value; instead the noise vector $\{R\}$ has been created on MatLab with the command 'randn' and then multiplied by 3 types of 'standard variation' std . The formulation is shown below:

$$\{\phi\}_{R,i,k} = \{\phi\}_{n,i} \cdot \{R\} \cdot std_k \quad (67)$$

Where:

$\{\phi\}_{n,i}$ is the normalised vector of the mode shape;

Index $i = 1,2,3,4$ refers to the mode shape;

Index $k = 1,2,3$ refers to the type of std .

The values associated with the std_k are represented in the table:

std_1	0,01
std_2	0,02
std_3	0,05

Table 13 Standard deviation values.

In conclusion, 48 mode shapes $\{\phi\}_{R_i,k}$ have been calculated and then, the corresponding curvatures were used in the TGP analysis. The following table summarises all 48 cases analysed.

Crack 1	Crack 10	Crack 25	Crack 50
1 st Curvature	1 st Curvature	1 st Curvature	1 st Curvature
std 1	std 1	std 1	std 1
std 2	std 2	std 2	std 2
std 3	std 3	std 3	std 3
2 nd Curvature	2 nd Curvature	2 nd Curvature	2 nd Curvature
std 1	std 1	std 1	std 1
std 2	std 2	std 2	std 2
std 3	std 3	std 3	std 3
3 th Curvature	3 th Curvature	3 th Curvature	3 th Curvature
std 1	std 1	std 1	std 1
std 2	std 2	std 2	std 2
std 3	std 3	std 3	std 3
4 th Curvature	4 th Curvature	4 th Curvature	4 th Curvature
std 1	std 1	std 1	std 1
std 2	std 2	std 2	std 2
std 3	std 3	std 3	std 3

Table 14 Summary table of modal analyses.

Once the modal forms were obtained with noise, the data was fed to the TGP method. To simplify the number of graphs, only the 1 mm and 50 mm crack results will be shown.

- CRACK 1 mm
- 1st Curvature

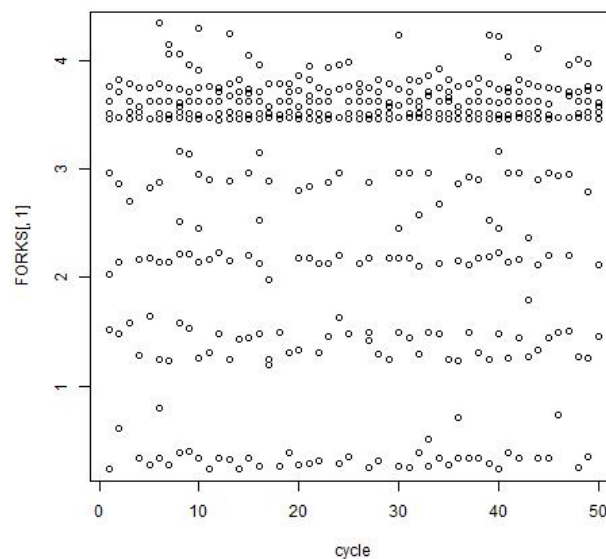


Fig. 61 Cycle – Crack detection, Crack 1 mm, mode-shape1-std1.

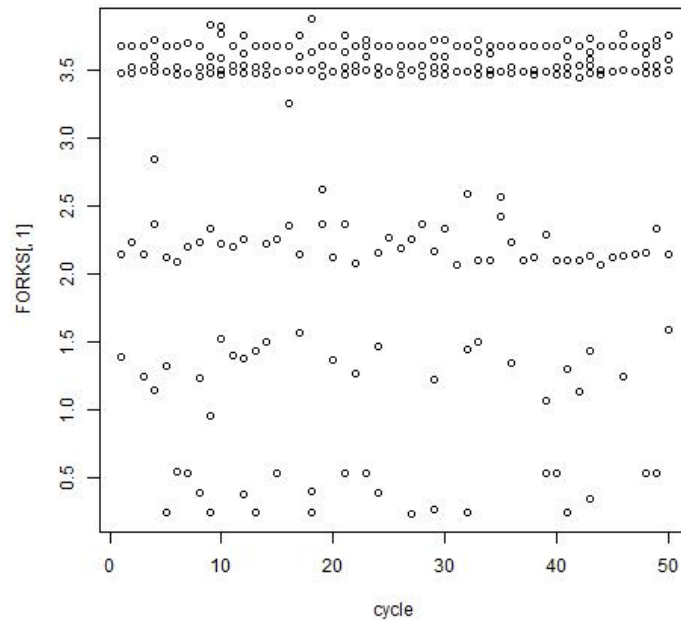


Fig. 62 Cycle – Crack detection, Crack 1 mm, mode-shape1-std3.

These two graphs show the position of the crack (in meters) on the y-axis and the number of cycles performed on the x-axis. It can be seen that there is a concentration of circles just near the crack (3.65 m). Two results obtained by the TGP are shown below:

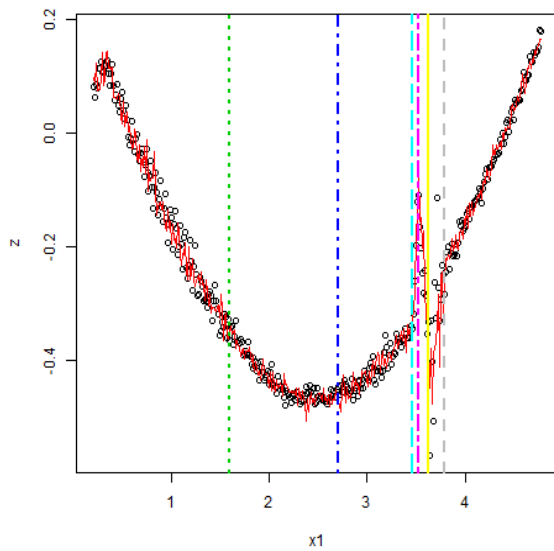


Fig. 64 First result of 50 cycles; Crack 1 mm;
mode-shape1-std1.

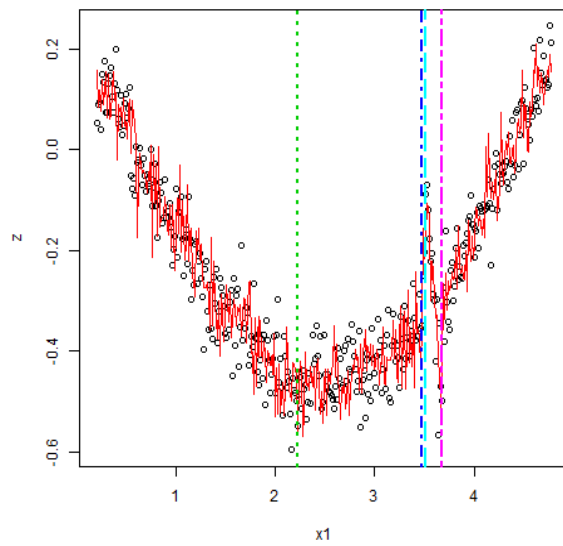


Fig. 63 First result of 50 cycles; Crack 1 mm;
mode-shape1-std3.

➤ 2nd Curvature

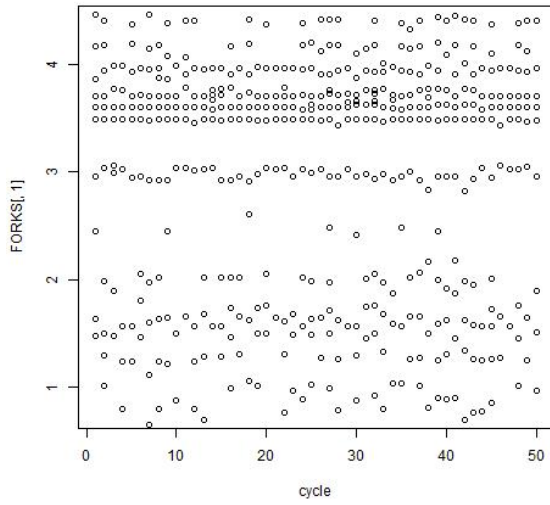


Fig. 66 Cycle – Crack detection, Crack 1 mm,
mode-shape2-std1.

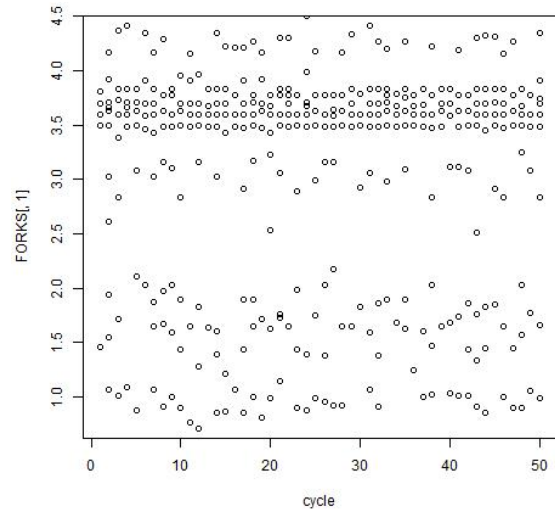


Fig. 65 Cycle – Crack detection, Crack 1 mm,
mode-shape2-std3.

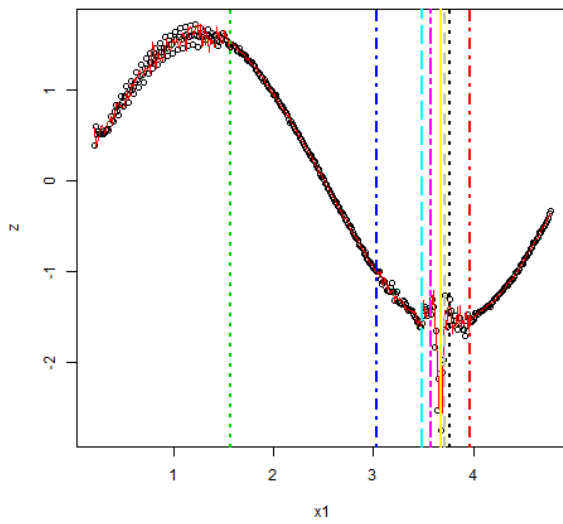


Fig. 68 First result of 50 cycles; Crack 1 mm;
mode-shape-2-std1

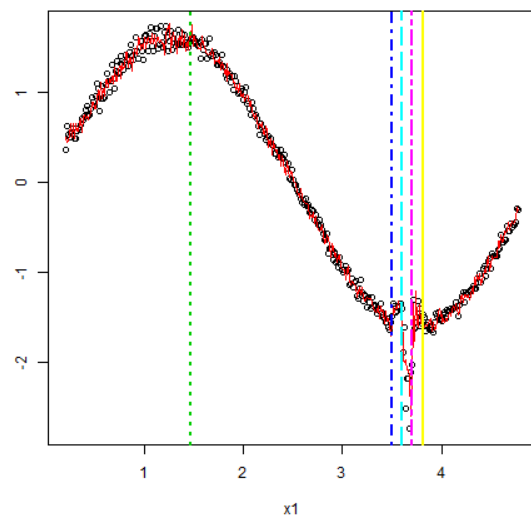


Fig. 67 First result of 50 cycles; Crack 1 mm;
mode-shape2-std3.

➤ 3th Curvature

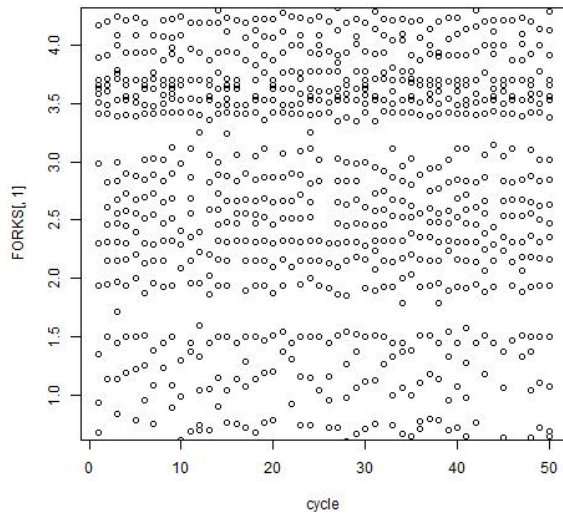


Fig. 70 Cycle – Crack detection, Crack 1 mm,

mode-shape3-std1

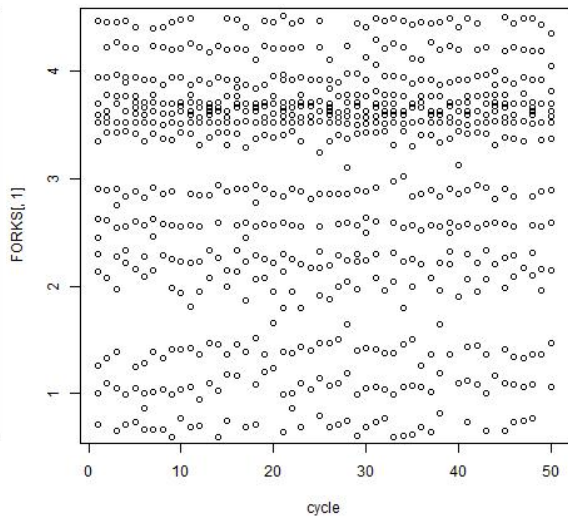


Fig. 69 Cycle – Crack detection, Crack 1 mm,

mode-shape3-std3.

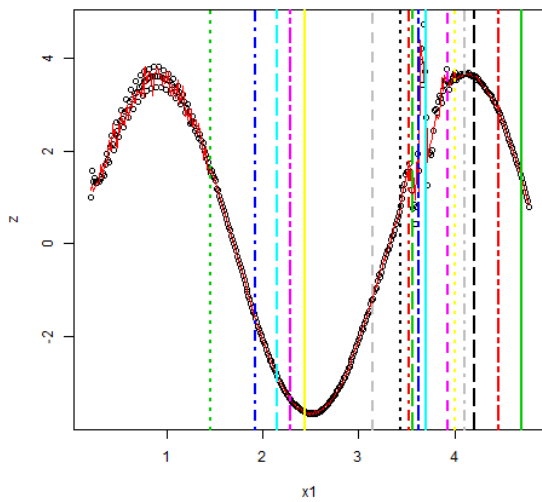


Fig. 72 First result of 50 cycles; Crack 1 mm;

mode-shape3-std1.

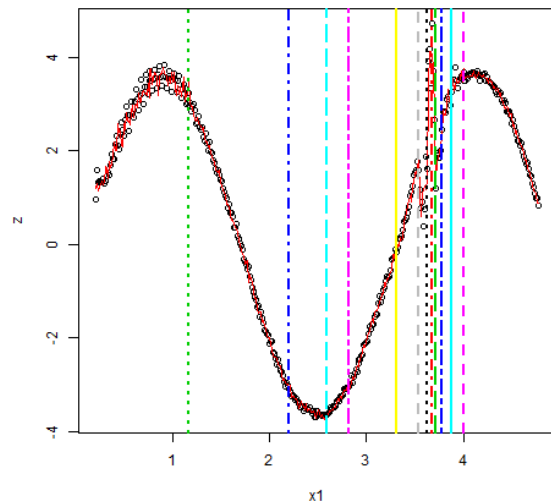


Fig. 71 First result of 50 cycles; Crack 1 mm;

mode-shape3-std3.

➤ 4th Curvature

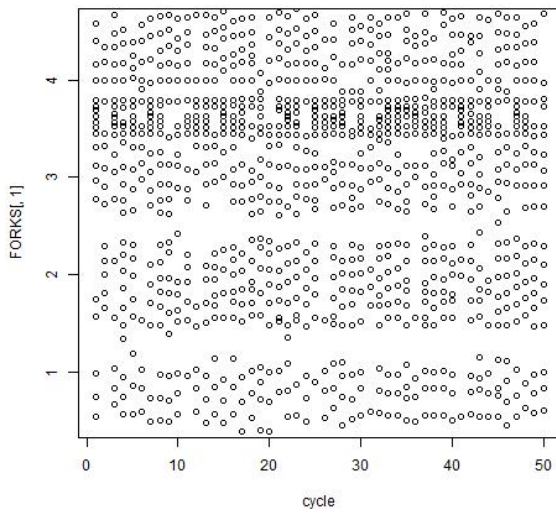


Fig. 74 Cycle – Crack detection, Crack 1 mm,
mode-shape4-std1.

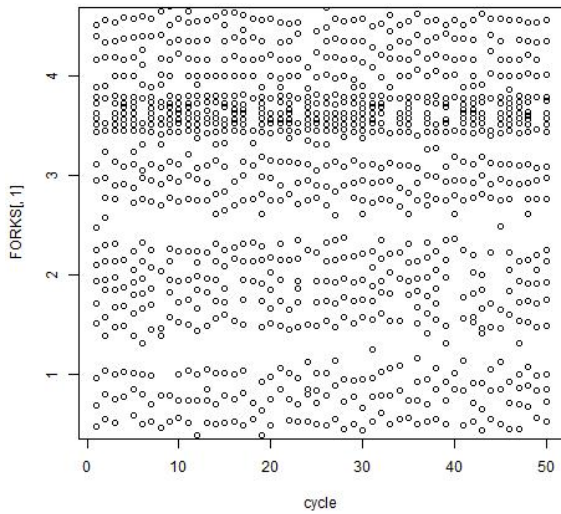


Fig. 73 Cycle – Crack detection, Crack 1 mm,
mode-shape4-std3.

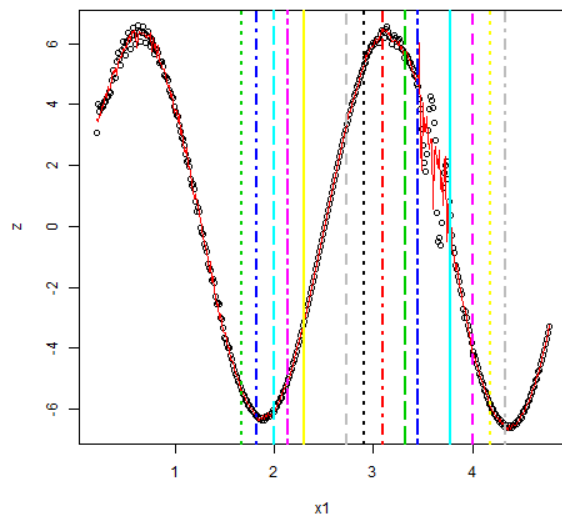


Fig. 75 First result of 50 cycles; Crack 1 mm;
mode-shape4-std1.

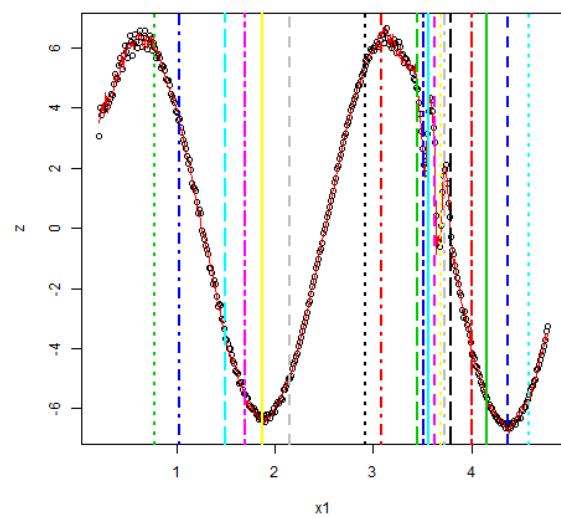


Fig. 76 First result of 50 cycles; Crack 1 mm;
mode-shape4-std3.

- CRACK 50 mm

➤ 1st Curvature

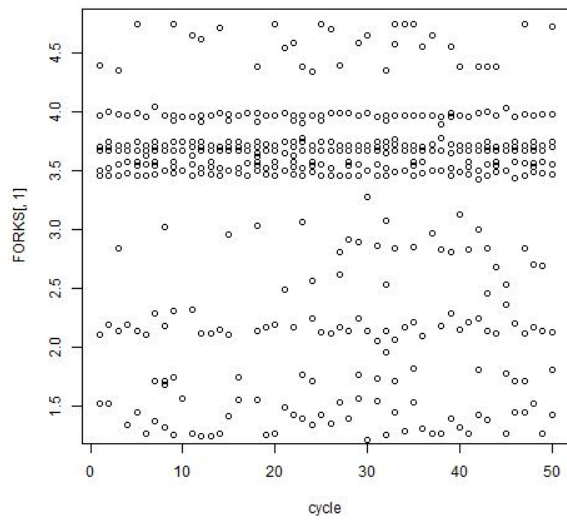


Fig. 78 Cycle – Crack detection, Crack 50 mm,
mode-shape1-std1.

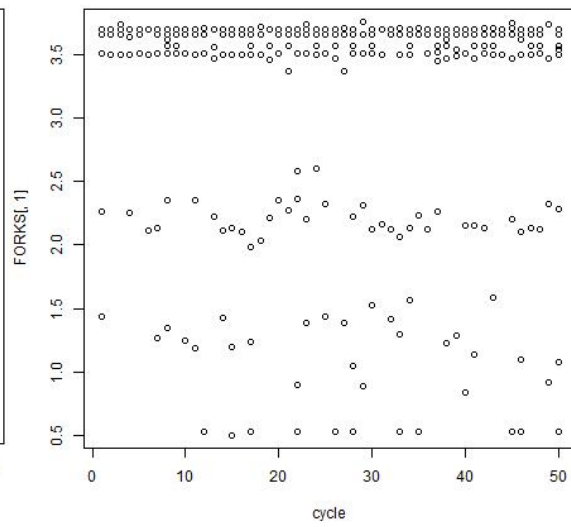


Fig. 77 Cycle – Crack detection, Crack 50 mm,
mode-shape1-std3.

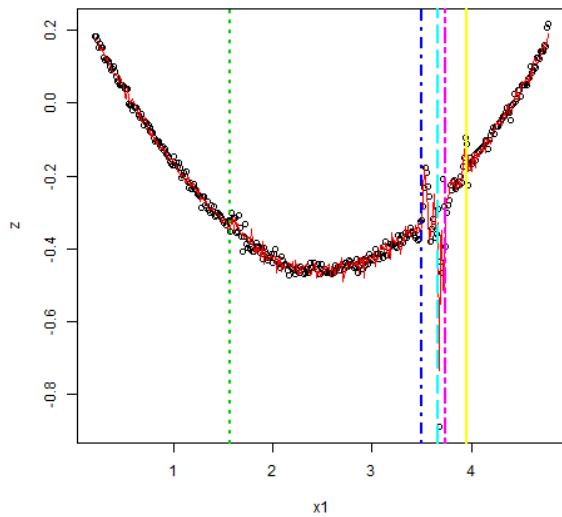


Fig. 79 First result of 50 cycles; Crack 50 mm;
mode-shape1-std1.

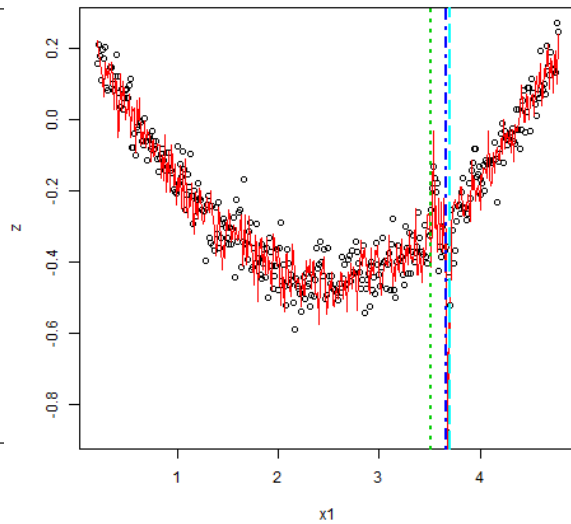


Fig. 80 First result of 50 cycles; Crack 50 mm; *mode-shape1-std3.*

➤ 2nd Curvature

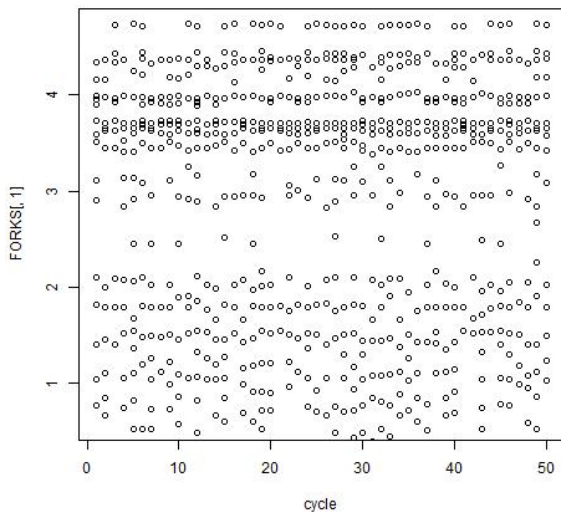


Fig. 81 Cycle – Crack detection, Crack 50 mm,
mode-shape2-std1.

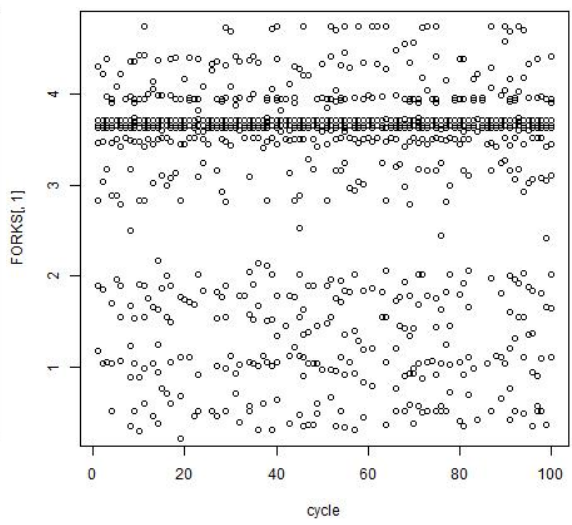


Fig. 82 Cycle – Crack detection, Crack 50 mm,
mode-shape2-std3.

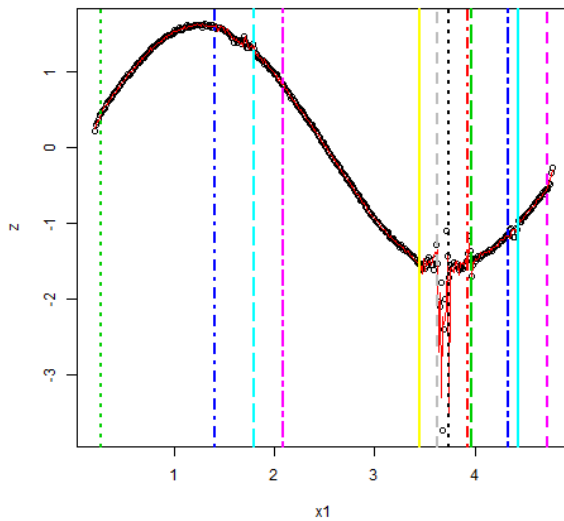


Fig. 84 First result of 50 cycles; Crack 50 mm;
mode-shape2-std1.

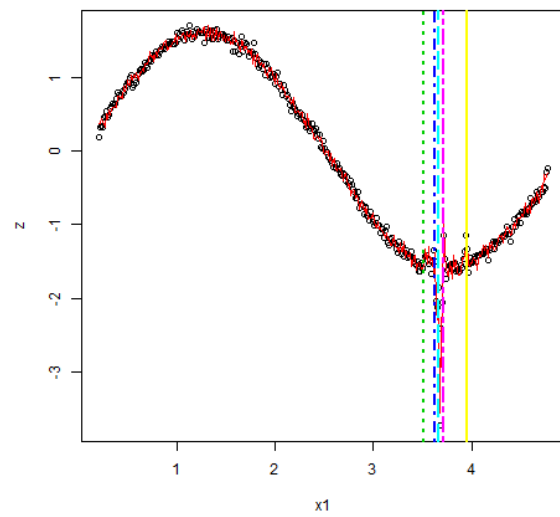


Fig. 83 First result of 50 cycles; Crack 50 mm;
mode-shape2-std3.

➤ 3th Curvature

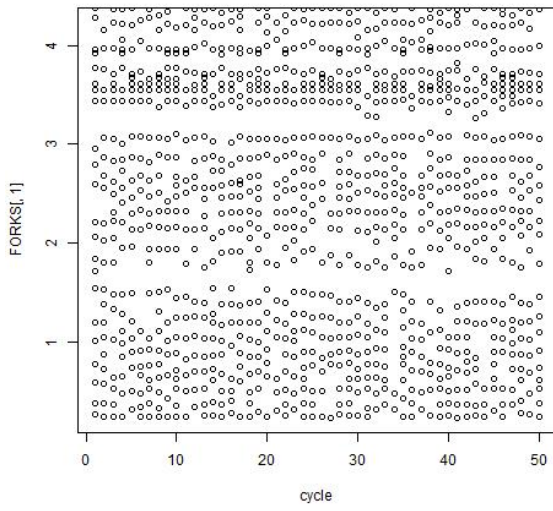


Fig. 86 Cycle – Crack detection, Crack 50 mm,
mode-shape3-std1.

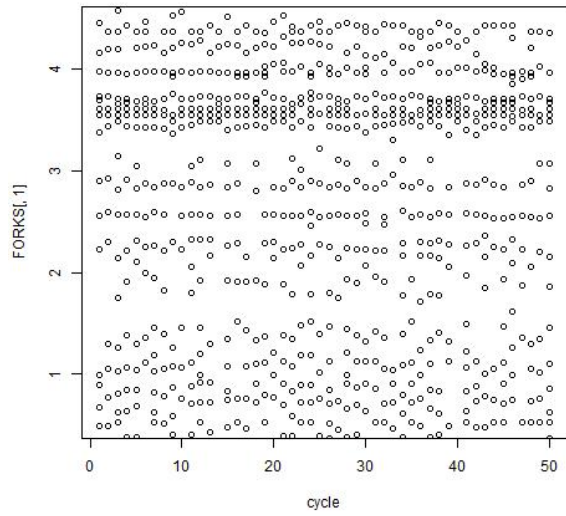


Fig. 85 Cycle – Crack detection, Crack 50 mm,
mode-shape3-std3

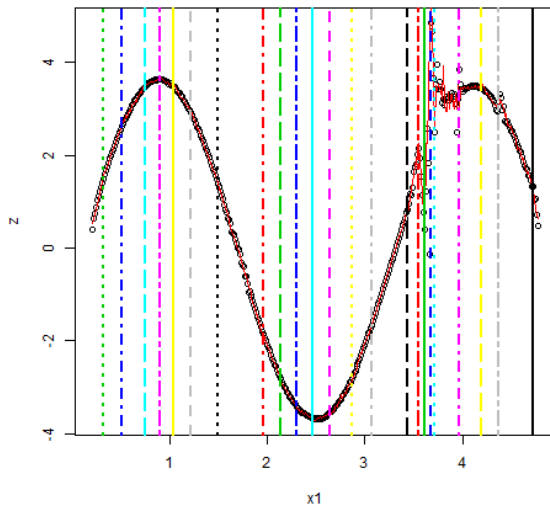


Fig. 88 First result of 50 cycles; Crack 50 mm;
mode-shape3-std1.

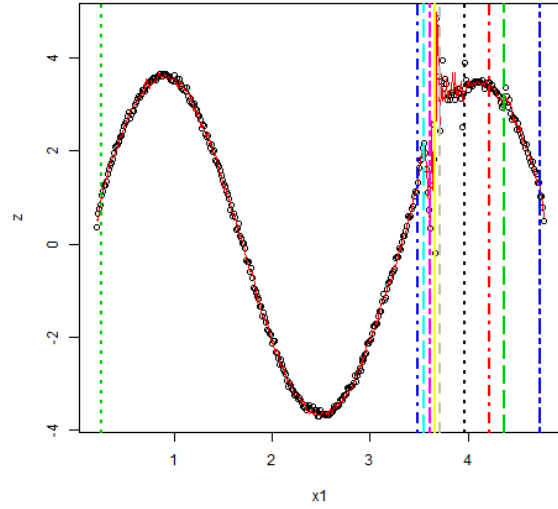


Fig. 87 First result of 50 cycles; Crack 50 mm;
mode-shape3-std3.

➤ 4th Curvature

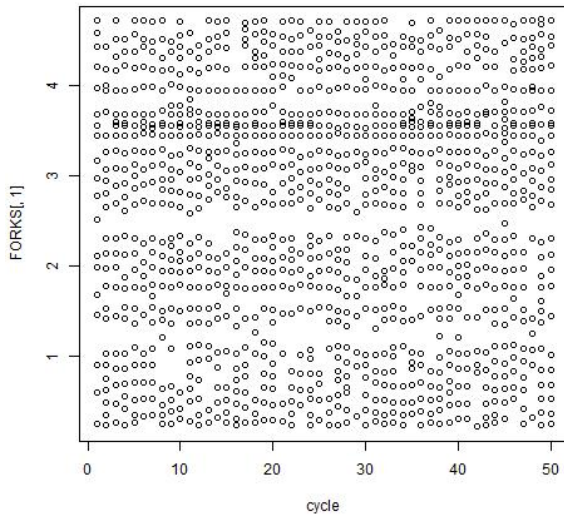


Fig. 90 Cycle – Crack detection, Crack 50 mm,
mode-shape4-std1.

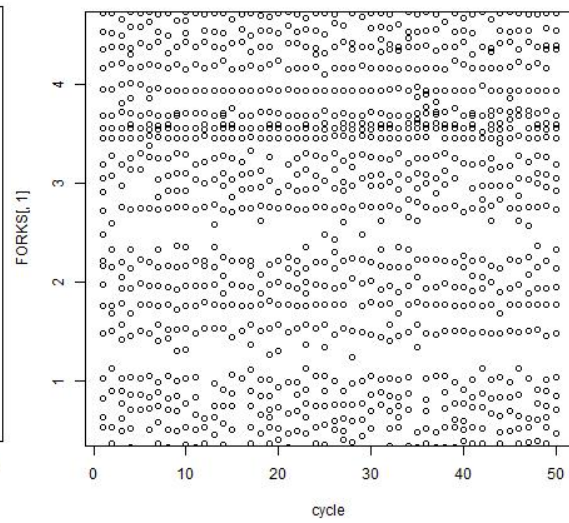


Fig. 89 Cycle – Crack detection, Crack 50 mm,
mode-shape4-std3.

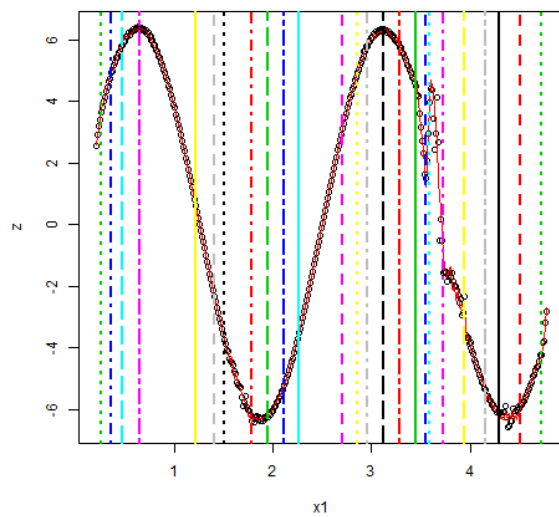


Fig. 92 First result of 50 cycles; Crack 50 mm;
mode-shape4-std1.

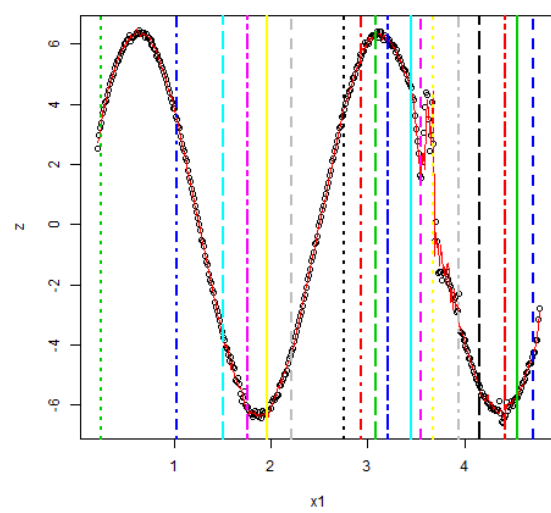


Fig. 91 First result of 50 cycles; Crack 50 mm;
mode-shape4-std3.

5.4.2 Experimental data

In the experimental case, it was decided to interpolate the data with a cubic function: pchip (Piecewise Cubic Hermite Interpolating Polynomial). This was done to create a continuous function with the aim of extracting more useful points for computational calculation on TGP algorithm. The number of points has therefore been increased from 15 (number of accelerometer present on the beam) to 401. Below, it can be seen that the function 'pchip' interpolates very well the 15 experimental points.

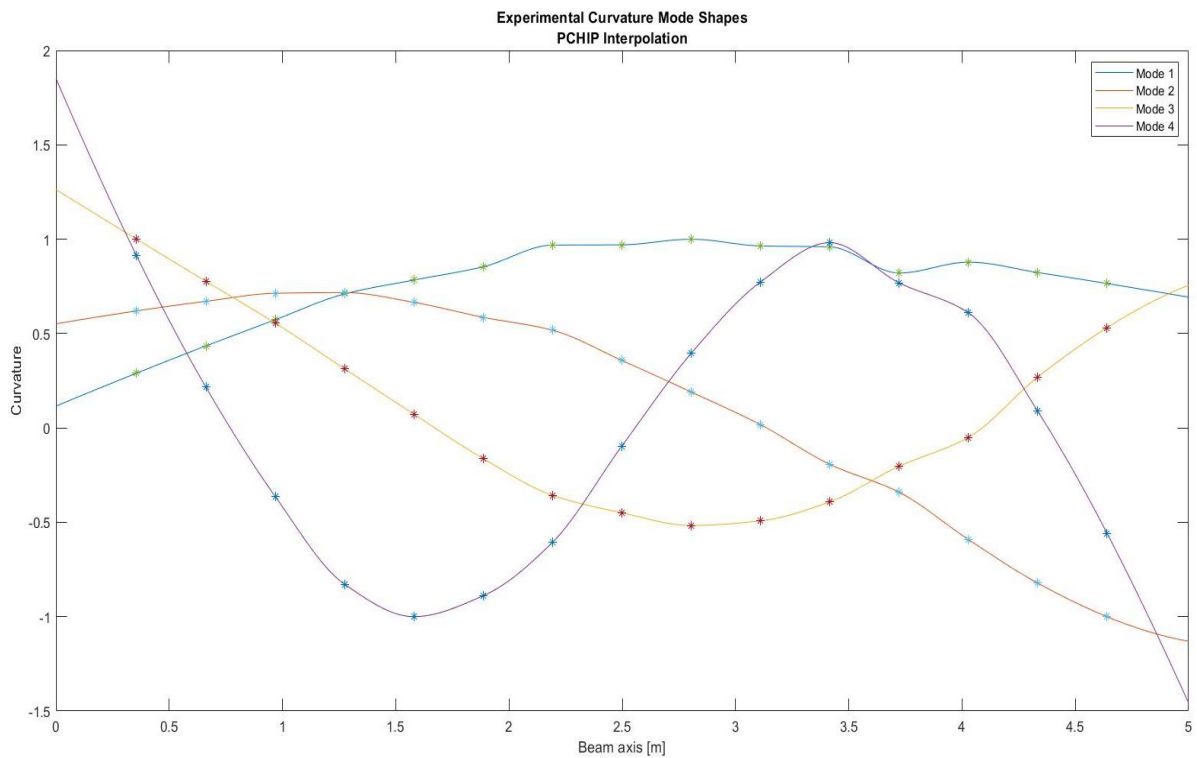


Fig. 93 Experimental mode shapes using pchip interpolation.

Once the continuous function is obtained, the modal displacements on 401 points are memorized at a constant step of 0.0125 m starting from the supports. Then on these data have been calculated the curvatures mode shape that are shown below.

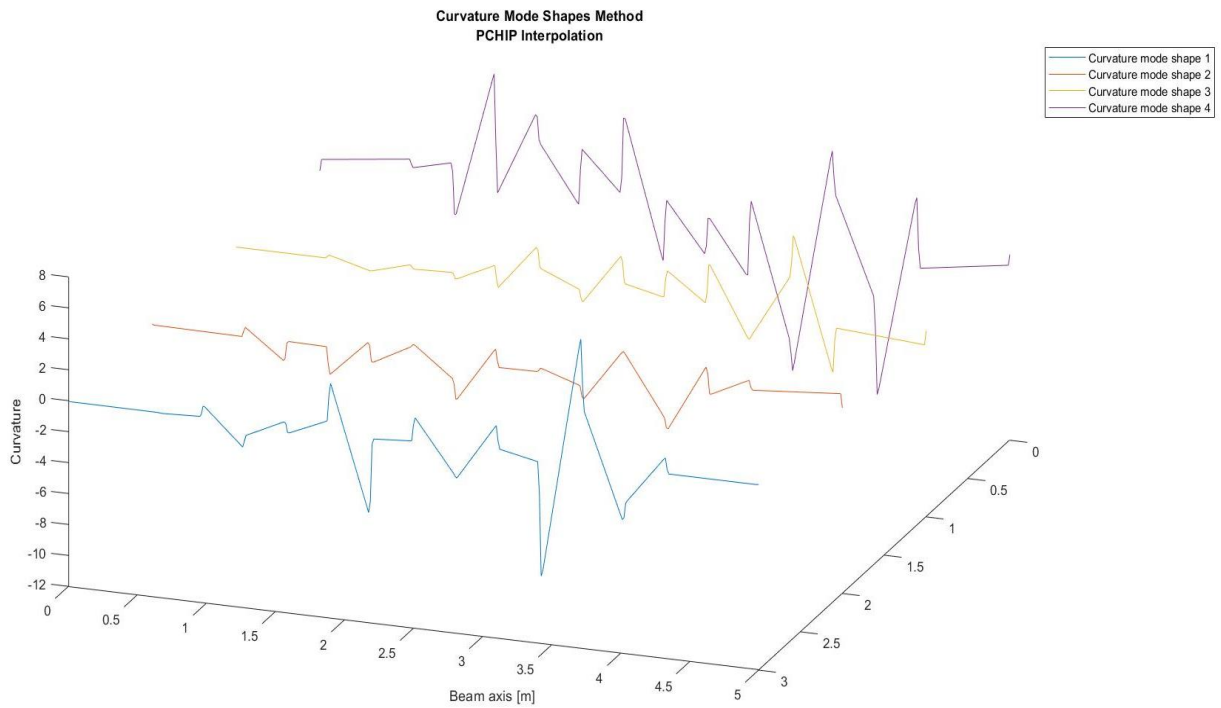


Fig. 94 Experimental curvature mode shapes using pchip interpolation.

The above curvatures were analysed using the TGP algorithm in R; the results obtained are reported as follows.

➤ 1st Curvature

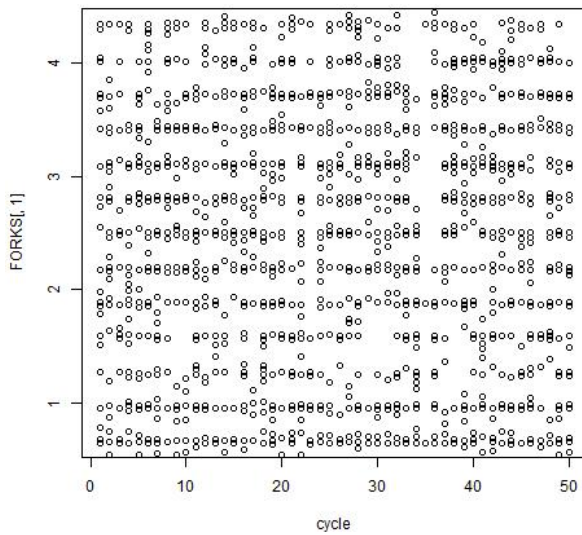


Fig. 96 Cycle – Crack detection, experimental data:

curvature mode shape 1.

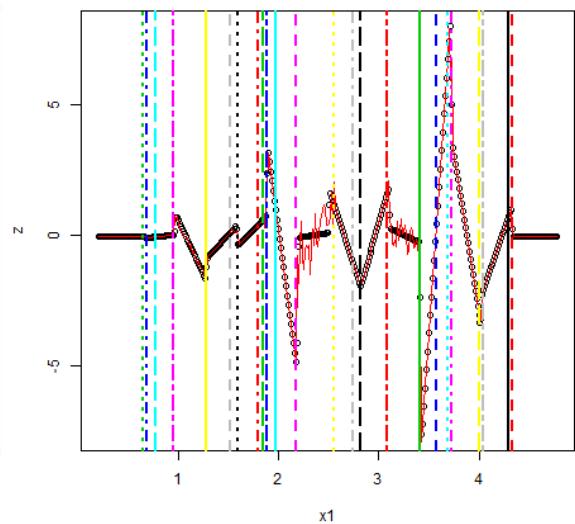


Fig. 95 First result of 50 cycles; Experimental data:

curvature mode shape 1.

➤ 2nd Curvature

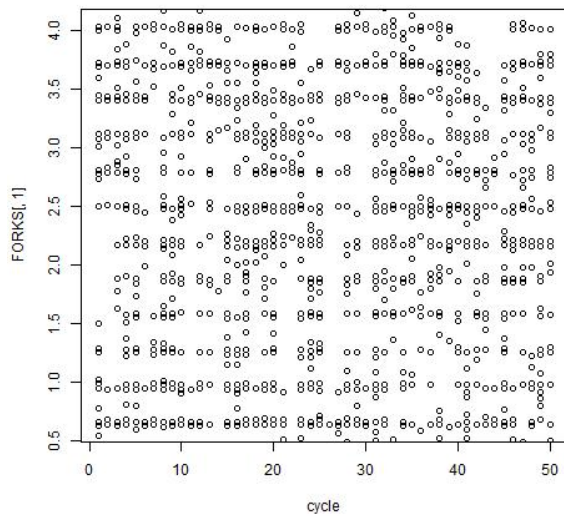


Fig. 97 Cycle – Crack detection, experimental data:

curvature mode shape 2.

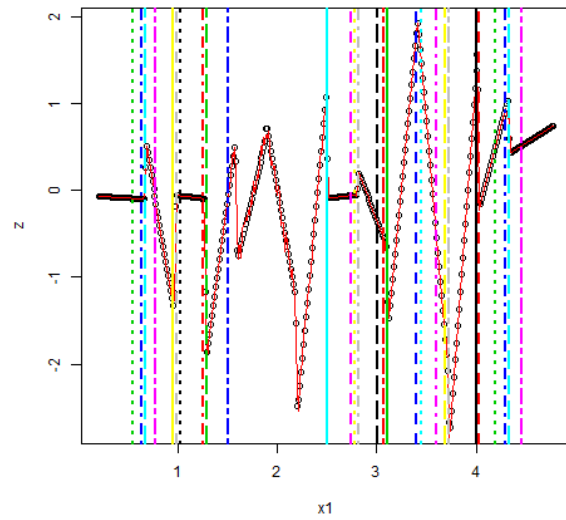


Fig. 98 First result of 50 cycles; Experimental data:

curvature mode shape 2.

➤ 3th Curvature

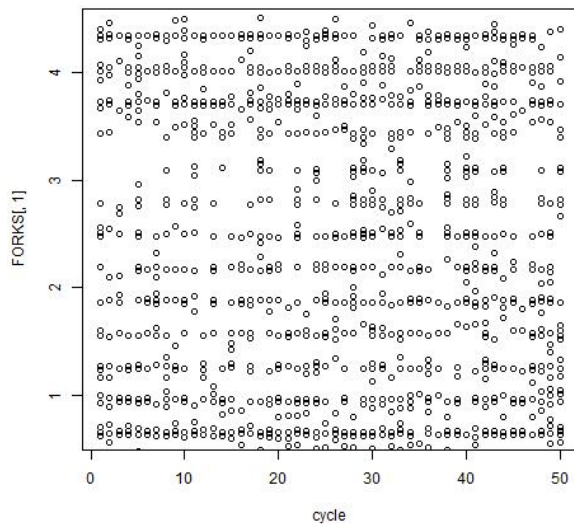


Fig. 100 Cycle – Crack detection, experimental data:

curvature mode shape 3.

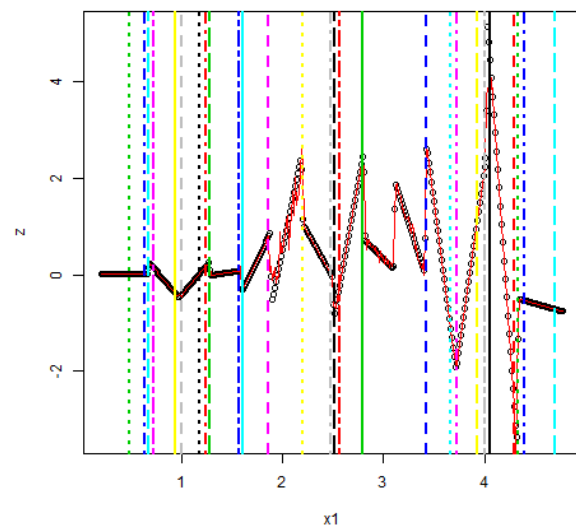


Fig. 99 First result of 50 cycles; Experimental data:

curvature mode shape 3.

➤ 4th Curvature

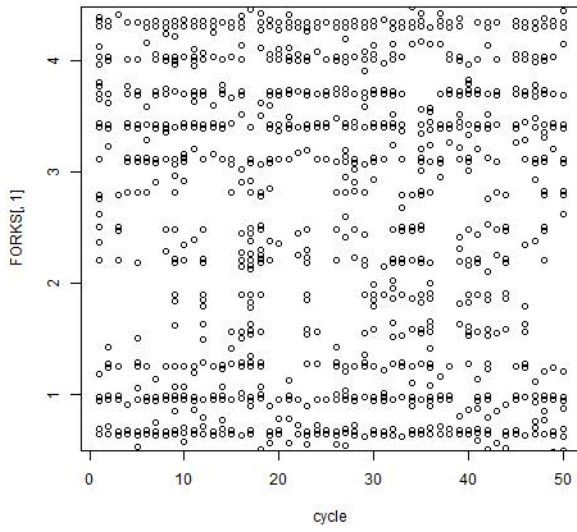


Fig. 101 Cycle – Crack detection, experimental data:
curvature mode shape 4.

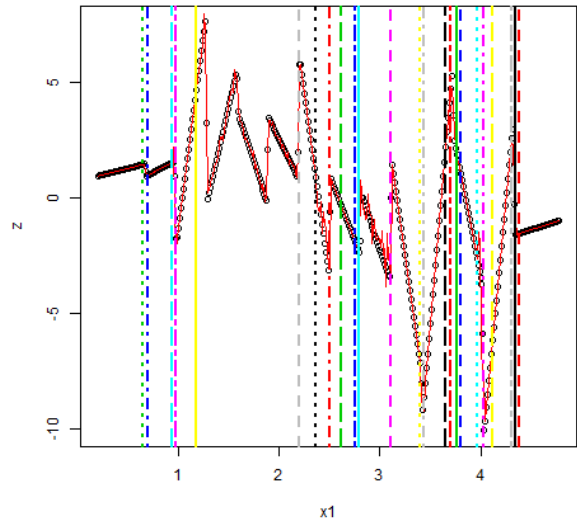


Fig. 102 First result of 50 cycles; Experimental data:
curvature mode shape 4.

6 CONCLUSION

Going back over the work done, it has been possible to derive the modal shapes through an experimental analysis. The work on experimental data was accompanied by work on analytical data.

Before using the Treed Gaussian Process method, the curvature method was applied to the FEM models to ensure that the models were created correctly.

From the results obtained on the analytical data it is clear that the "Treed Gaussian Process" method is able to identify and localize very well the crack on the structure when a large number of data is available (401). In the case of 401 data it is like having 401 fictitious accelerometers on the beam, therefore, a great deal of information can be obtained; the functions of modal forms and curvatures are more detailed and able to detect any structural imperfection.

From the results obtained on the analytical data using only 15 accelerometers, the TGP method provides results that are not reliable. This case was analyzed in order to compare the experimental results, which present only 15 accelerometers. The non-operation of the method is due to the lack of data, i.e. accelerometers.

With regard to the results obtained from the experimental data, the TGP method provides unreliable results. This is in line with the results obtained on FEM models using 15 accelerometers.

In conclusion, this work shows that the TGP method works well when you have a large amount of data available in order to derive very detailed modal forms; otherwise the method returns crack positions that are not traceable to reality. To learn more about a possible crack in the pultruded beam, it is therefore necessary to have several accelerometers.

BIBLIOGRAFIA

- [1] B. Goldsworthy, "Composites Visionary," *CompositesWorld*, 2003. [Online]. Available: <https://www.compositesworld.com/articles/brandt-goldsworthy-composites-visionary>.
- [2] G. B. a. S. Russo, "Free Vibrations of Pultred FRP Elements: Mechanical Characterization, Analysis and Applications," *JOURNAL OF COMPOSITES FOR CONSTRUCTION*, pp. 565-574, 2009.
- [3] T. a. J. T.T.Nguyen, "Influence of Boundary Conditions and geometric imperfections on Lateral-Torsional Resistance of a Pultred FRP I-beam by FEA," *Composite Structures*, 2013.
- [4] D. Ewins, "Modal Testing: Theory, Practice and Application," vol. 2, 2000.
- [5] J. J. a. S.Pappa, "An Eigensystem Realization Algorithm for Modal Parameter Identification and Model Reduction," *Giudance*, vol. 8, no. 5, pp. 620 - 627, 1985.
- [6] M. B. a. M. M. S. A. K. Pandey, "Damage detection from changes in curvature mode shapes," *Journal of Sound and Vibration*, pp. 321 - 332, 1991.
- [7] T. a. M.RICHARDSON, "Fault detection in structures from changes in their modal parameters," *Proceedings of the 7th International Modal Analysis Conference*, vol. 1, pp. 87-94, 1989.
- [8] N. a. D.J.EWINS, "Spatial correlation of mode shape, the Co-ordinate Modal Assurance Criterion (COMAC)," *Proceedings of the 6th International Modal Analysis Conference*, vol. 1, pp. 690-695, 1988.
- [9] P. a. R.D.ADAMS, "The location of defects in structures from measurements of natural frequencies," *Journal of Strain Analysis*, vol. 14, no. 2, pp. 49-57, 1979.
- [10] C. a. K. M.Civera, "Detention of Cracks in Beams using Treed Gaussian Processes," *Structural Health Monitoring & Damage Detection*, vol. 7, pp. 85-97, 2017.

- [11] C. a. C. Williams, "Gaussian Process for Machine Learning," *The MIT Press*, 2006.
- [12] C. a. M. J.J. Hensman, "Detecting mode-shape discontinuities without differentiating examining a Gaussian process approach," *Proceedings of 9th International Conference in Damage Assessment (DAMAS 2011)*, 2011.
- [13] E. G. a. R. M. H.A. Chipman, "Bayesian treed models.," *Journal of the American Statistical Association*, pp. 935-948, 1998.
- [14] R.B. Gramacy, "Bayesian Treed Gaussian Process Models," *PhD thesis, University of California*, 2005.

ANSYS CODE

❖ Intact Beam

FINISH

/CLEAR

/FILNAME,TraveH

/PREP7

/VIEW,1,1,1,1

!Definire la proprietà geometriche

L=5

!lunghezza della trave

H=0.19

!altezza della trave (linea media)

B=0.2

!larghezza della trave

A=0.05

!distanza tra l'estremità e l'appoggio

!Definire i punti della struttura.

K,1,0,0,0

K,2,B/2,0,0

K,3,B/2,0,L

K,4,0,0,L

K,5,-B/2,0,5

K,6,-B/2,0,0

K,7,0,H,0

K,8,B/2,H,0

K,9,B/2,H,L

K,10,0,H,L

K,11,-B/2,H,L

K,12,-B/2,H,0

K,13,B/2,0,A

K,14,0,0,A

K,15,-B/2,0,A

K,16,B/2,0,L-A

K,17,0,0,L-A

K,18,-B/2,0,L-A
K,19,B/2,H,A
K,20,0,H,A
K,21,-B/2,H,A
K,22,B/2,H,L-A
K,23,0,H,L-A
K,24,-B/2,H,L-A

!Definire le linee tra i punti

LSTR,1,2
LSTR,1,6
LSTR,14,13
LSTR,14,15
LSTR,17,16
LSTR,17,18
LSTR,4,3
LSTR,4,5
LSTR,2,13
LSTR,1,14
LSTR,6,15
LSTR,13,16
LSTR,14,17
LSTR,15,18
LSTR,16,3
LSTR,17,4
LSTR,18,5
LSTR,1,7
LSTR,14,20
LSTR,17,23
LSTR,4,10
LSTR,7,8
LSTR,7,12
LSTR,20,19
LSTR,20,21

LSTR,23,22
LSTR,23,24
LSTR,10,9
LSTR,10,11
LSTR,8,19
LSTR,7,20
LSTR,12,21
LSTR,19,22
LSTR,20,23
LSTR,21,24
LSTR,22,9
LSTR,23,10
LSTR,24,11

!Definire le aree (flangia e anima).

AL,1,9,3,10
AL,2,10,4,11
AL,3,12,5,13
AL,4,13,6,14
AL,5,15,7,16
AL,6,16,8,17
AL,22,30,24,31
AL,23,31,25,32
AL,24,33,26,34
AL,25,34,27,35
AL,26,36,28,37
AL,27,37,29,38
AL,18,10,19,31
AL,19,13,20,34
AL,20,16,21,37

!Definire le proprietà meccaniche del materiale.

MP,EZ,1,8.5e9 !moduli elastici.
MP,EX,1,8.5e9

MP,EY,1,28.5e9
MP,GXY,1,2.5e9 !moduli di elasticità a taglio.
MP,GXZ,1,3.5e9
MP,GYZ,1,2.5e9
MP,PRXZ,1,0.12 !coefficienti di Poisson.
MP,PRYZ,1,0.25
MP,PRXY,1,0.25
MP,DENS,1,1734 !Densità.

MP,EZ,2,8.5e9 !moduli elastici.
MP,EX,2,8.5e9
MP,EY,2,28.5e9
MP,GXY,2,2.5e9 !moduli di elasticità a taglio.
MP,GXZ,2,3.5e9
MP,GYZ,2,2.5e9
MP,PRXZ,2,0.12 !coefficienti di Poisson.
MP,PRYZ,2,0.25
MP,PRXY,2,0.25
MP,DENS,2,1734 !Densità.

!definire il tipo di elemento.

ET,1,SHELL281

!sezione della flangia 10mm.

SECTYPE,1,SHELL281

SECDATA,0.010,1

!sezione dell'anima 15mm.

SECTYPE,2,SHELL281

SECDATA,0.015,2

!Creare la mesh nelle flange.

ASEL,S,AREA,,1

ASEL,A,AREA,,2

ASEL,A,AREA,,3

```
ASEL,A,AREA,,4
ASEL,A,AREA,,5
ASEL,A,AREA,,6
ASEL,A,AREA,,7
ASEL,A,AREA,,8
ASEL,A,AREA,,9
ASEL,A,AREA,,10
ASEL,A,AREA,,11
ASEL,A,AREA,,12
AATT,1,,1,,1
ESIZE,0.025
AMESH,1,12
!Creare la mesh nell'anima.
ASEL,S,AREA,,13
ASEL,a,AREA,,14
ASEL,a,AREA,,15
AATT,2,,1,,2
ESIZE,0.025
AMESH,13,15

!Vincoli.
LSEL,S,LINE,,3,4
LSEL,A,LINE,,5,6
!Definire DOF alle linee.
DL,ALL,,UY,0
DL,ALL,,UZ,0
DL,ALL,,UX,0
DL,ALL,,ROTZ,0

/ESHAPE,1
EPLT

!Soluzione
/SOLU
```

```
!Analisi modale
ANTYPE,MODAL
MODOPT,LANB,20
SOLVE
```

❖ Damaged beam with crack of 1 mm

```
FINISH
/CLEAR
/FILNAME,TraveH
/PREP7
/VIEW,1,1,1,1
```

!Definire la Proprietà Geometriche.

L=5	!lunghezza della trave
H=0.19	!altezza della trave (linea media)
B=0.2	!larghezza della trave
A=0.05	!distanza tra l'estremità e l'appoggio
d=3.65	!distanza dall'origine al crack
f=0.001	!altezza crack
C=0.001	!larghezza crack

!Definire i punti della struttura.

```
K,1,0,0,0
K,2,B/2,0,0
K,3,B/2,0,L
K,4,0,0,L
K,5,-B/2,0,5
K,6,-B/2,0,0
K,7,0,H,0
K,8,B/2,H,0
K,9,B/2,H,L
K,10,0,H,L
K,11,-B/2,H,L
```

K,12,-B/2,H,0
K,13,B/2,0,A
K,14,0,0,A
K,15,-B/2,0,A
K,16,B/2,0,L-A
K,17,0,0,L-A
K,18,-B/2,0,L-A
K,19,B/2,H,A
K,20,0,H,A
K,21,-B/2,H,A
K,22,B/2,H,L-A
K,23,0,H,L-A
K,24,-B/2,H,L-A
!Damage points
K,25,B/2,0,d-c/2
K,26,0,0,d-c/2
K,27,-B/2,0,d-c/2
K,28,B/2,0,d+c/2
K,29,0,0,d+c/2
K,30,-B/2,0,d+c/2
K,31,0,H,d
K,32,0,f,d
K,33,B/2,H,d
K,34,-B/2,H,d

!Definire le linee tra i punti

LSTR,1,2
LSTR,1,6
LSTR,14,13
LSTR,14,15
LSTR,26,25
LSTR,26,27
LSTR,29,28
LSTR,29,30

LSTR,17,16
LSTR,17,18
LSTR,4,3
LSTR,4,5
LSTR,2,13
LSTR,1,14
LSTR,6,15
LSTR,13,25
LSTR,14,26
LSTR,15,27
LSTR,25,28
LSTR,26,29
LSTR,27,30
LSTR,28,16
LSTR,29,17
LSTR,30,18
LSTR,16,3
LSTR,17,4
LSTR,18,5
LSTR,1,7
LSTR,14,20
LSTR,32,31
LSTR,26,32
LSTR,29,32
LSTR,17,23
LSTR,4,10
LSTR,7,8
LSTR,7,12
LSTR,20,19
LSTR,20,21
LSTR,31,33
LSTR,31,34
LSTR,23,22
LSTR,23,24

LSTR,10,9
LSTR,10,11
LSTR,8,19
LSTR,7,20
LSTR,12,21
LSTR,19,33
LSTR,20,31
LSTR,21,34
LSTR,33,22
LSTR,31,23
LSTR,34,24
LSTR,22,9
LSTR,23,10
LSTR,24,11

!Definire le aree (flangia e anima).

AL,1,13,3,14
AL,2,14,4,15
AL,3,16,5,17
AL,4,17,6,18
AL,5,19,7,20
AL,6,20,8,21
AL,7,22,9,23
AL,8,23,10,24
AL,9,25,11,26
AL,10,26,12,27
AL,35,45,37,46
AL,36,46,38,47
AL,37,48,39,49
AL,38,49,40,50
AL,39,51,41,52
AL,40,52,42,53
AL,41,54,43,55
AL,42,55,44,56

AL,28,46,29,14
AL,29,49,30,31,17
AL,30,52,33,23,32
AL,33,55,34,26

!Definire le proprietà meccaniche del materiale.

MP,EZ,1,8.5e9 !moduli elastici.
MP,EX,1,8.5e9
MP,EY,1,28.5e9
MP,GXY,1,2.5e9 !moduli di elasticità a taglio.
MP,GXZ,1,3.5e9
MP,GYZ,1,2.5e9
MP,PRXZ,1,0.12 !coefficienti di Poisson.
MP,PRYZ,1,0.25
MP,PRXY,1,0.25
MP,DENS,1,1734 !Densità.

MP,EZ,2,8.5e9 !moduli elastici.
MP,EX,2,8.5e9
MP,EY,2,28.5e9
MP,GXY,2,2.5e9 !moduli di elasticità a taglio.
MP,GXZ,2,3.5e9
MP,GYZ,2,2.5e9
MP,PRXZ,2,0.12 !coefficienti di Poisson.
MP,PRYZ,2,0.25
MP,PRXY,2,0.25
MP,DENS,2,1734 !Densità.

!definire il tipo di elemento.

ET,1,SHELL281

!sezione della flangia 10mm.

SECTYPE,1,SHELL281

SECDATA,0.010,1

!sezione dell'anima 15mm.

SECTYPE,2,SHELL281

SECDATA,0.015,2

!Creare la mesh nelle flange.

ASEL,S,AREA,,1

ASEL,A,AREA,,2

ASEL,A,AREA,,3

ASEL,A,AREA,,4

ASEL,A,AREA,,5

ASEL,A,AREA,,6

ASEL,A,AREA,,7

ASEL,A,AREA,,8

ASEL,A,AREA,,9

ASEL,A,AREA,,10

ASEL,A,AREA,,11

ASEL,A,AREA,,12

ASEL,A,AREA,,13

ASEL,A,AREA,,14

ASEL,A,AREA,,15

ASEL,A,AREA,,16

ASEL,A,AREA,,17

ASEL,A,AREA,,18

AATT,1,,1,,1

ESIZE,0.025

AMESH,1,18

!Creare la mesh nell'anima.

ASEL,S,AREA,,19

ASEL,A,AREA,,20

ASEL,A,AREA,,21

ASEL,A,AREA,,22

AATT,2,,1,,2

ESIZE,0.025

AMESH,19,22

```
!Vincoli.  
LSEL,S,LINE,,3,4  
LSEL,A,LINE,,9,10  
!Definire DOF alle linee.  
DL,ALL,,UY,0  
DL,ALL,,UZ,0  
DL,ALL,,UX,0  
DL,ALL,,ROTZ,0
```

```
/ESHAPE,1  
EPLOT
```

```
!Soluzione  
/SOLU  
!Analisi modale  
ANTYPE,MODAL  
MODOPT,LANB,20  
SOLVE
```